

NASA TECHNICAL NOTE



NASA TN D-4610

C.1

NASA TN D-4610



LOAN COPY: RETURN TO  
AFWL (WLIL-2)  
KIRTLAND AFB, N MEX

**AERODYNAMIC CHARACTERISTICS OF  
A LARGE-SCALE MODEL WITH AN  
UNSWEEP WING AND AUGMENTED JET FLAP**

*by*

*David G. Koenig and Victor R. Corsiglia*

*Ames Research Center*

*Moffett Field, Calif.*

*and*

*Joseph P. Morelli*

*Army Aeronautical Research Laboratory*

*Moffett Field, Calif.*



NATIONAL AERONAUTICS AND SPACE ADMINISTRATION • WASHINGTON, D. C. • JUNE 1968



AERODYNAMIC CHARACTERISTICS OF A LARGE-SCALE MODEL WITH  
AN UNSWEPT WING AND AUGMENTED JET FLAP

By David G. Koenig and Victor R. Corsiglia

Ames Research Center  
Moffett Field, Calif.

and

Joseph P. Morelli

Army Aeronautical Research Laboratory  
Moffett Field, Calif.

NATIONAL AERONAUTICS AND SPACE ADMINISTRATION

---

For sale by the Clearinghouse for Federal Scientific and Technical Information  
Springfield, Virginia 22151 - CFSTI price \$3.00

# AERODYNAMIC CHARACTERISTICS OF A LARGE-SCALE MODEL WITH

## AN UNSWEPT WING AND AUGMENTED JET FLAP

By David G. Koenig and Victor R. Corsiglia  
Ames Research Center

and

Joseph P. Morelli  
Army Aeronautical Research Laboratory

### SUMMARY

An investigation was made to determine the aerodynamic characteristics of a complete model equipped with an augmented jet flap. The augmented jet flap is a jet flap with the primary jet thrust increased by means of an ejector system installed in the wing trailing-edge flap. The flap was installed on the inboard part of the wing, and blown ailerons were installed on the outboard part. Tests were made with and without the horizontal tail at zero airspeed and at a dynamic pressure of 8 psf corresponding to a Reynolds number of  $3.0 \times 10^6$ .

The measured thrust of the augmented jet flap was about 1.42 times that of the measured primary jet for flap deflections of  $60^\circ$  and  $70^\circ$  and 1.25 times the isentropic jet thrust. This ratio did not significantly decrease at forward speed. A maximum lift coefficient of 6 was measured for a jet coefficient of 1.30 when the model was equipped with full-span leading-edge slats. Symmetrical aileron deflection and flap boundary-layer control were effective in producing lift increments at model attitudes below that for wing stall. With the horizontal tail installed, the variation of pitching moment with angle of attack was stable up to and including wing stall. Comparisons with jet flap test results on the basis of the same static thrust output of the systems indicated that the present augmented-jet flap configuration produced slightly higher lift increments and had more forward center-of-pressure locations. For the same isotropic primary thrust, the augmented jet flap produced 50 percent more jet force and 22 percent more lift than the jet flap.

### INTRODUCTION

The jet flap has been considered in several forms for integration into the lift propulsion systems of STOL turbojet or turbofan aircraft. Most of the designs have high-velocity-jet sheets expelled either at the wing trailing edge or over the top of a trailing-edge flap. Wind-tunnel studies of some of these designs are reported in references 1 through 4. Integration of the jet flap into aircraft designs has been difficult because of problems in delivering sufficient gas flow to the wing trailing edge to achieve the needed

jet thrust. Another difficulty with the jet flap is that large nose-down pitching moments result when the jet is expelled near the wing trailing edge.

The augmented jet flap or augmentor wing was proposed in reference 5 as an improvement over the basic jet flap in the sense that higher jet thrusts and less negative pitching moments would result. In this concept, the thrust of the primary jet is augmented by an ejector system combined with the trailing-edge flap. The design and possible applications are discussed in reference 5.

In order to determine the aerodynamic characteristics of the augmented jet flap at high Reynolds number, a large-scale model was built and tested in the Ames 40- by 80-Foot Wind Tunnel. The wing of the model was unswept, and the augmentor wing section extended 60 percent of the span. The compressed air for the augmentor was supplied by axial flow compressors with turbines driven by the exhaust gas of a jet engine. Static tests and wind-tunnel tests out of ground effect were made for flap angles from 30° to 100°. At augmentor flap angles of 60° and 100°, the model was tested with a high-positioned horizontal tail. The investigations included the effects of sideslip and differential aileron deflection.

#### NOTATION

a	gap between the upper jet-augmentor door and the upper surface of the wing (see fig. 2(b)), in.
A	augmentation ratio of the jet augmentor, $\frac{J_A}{J_I}$ , $\frac{J_P}{J_I}$ , or $\frac{J_A}{J_P}$
AR	wing aspect ratio, $\frac{b^2}{S}$
b	wing span, ft
c	wing chord, ft
$\bar{c}$	mean aerodynamic chord, ft
$c_f$	flap chord, ft
$c_r$	wing root chord, ft
$C_D$	drag coefficient, $\frac{\text{drag}}{qS}$
$C_{Dm}$	total momentum drag coefficient due to gas generator and compressor gas flow
$C_J$	jet force coefficient, or total jet force coefficient, $C_{J_A} + C_{\mu_f} + C_{\mu_a}$ , $\frac{\text{jet reaction force}}{qS}$

$C_L$	rolling-moment coefficient with reference to stability axes, $\frac{\text{rolling moment}}{qSb}$
$C_L$	lift coefficient, $\frac{\text{lift}}{qS}$
$C_{LAERO}$	$C_L$ less vertical thrust component, $C_L - C_{JA} \sin(\alpha + \theta) - C_{\mu_f} \sin(\alpha + \delta_f) - C_{\mu_a} \sin(\alpha + \delta_a)$
$C_{L\delta_A}$	flap lift effectiveness parameter for the augmented jet flap and the jet flap, respectively, obtained from linear theory for $E = 1$
$C_{L\delta_J}$	
$\Delta C_L$	flap lift increment, $C_L - (C_L, \alpha = 0, \theta = 0, C_J = 0)$
$C_m$	pitching-moment coefficient, $\frac{\text{pitching moment}}{qSc_r}$ ; moment center located at the $\frac{c_r}{4}$ point
$C_n$	yawing-moment coefficient, $\frac{\text{yawing moment}}{qSb}$
$C_T$	tail-pipe thrust coefficient, $\frac{\text{tail-pipe thrust}}{qS}$
$C_y$	side-force coefficient with reference to wind axes, $\frac{\text{side force}}{qS}$
$C_{\mu_a}$	aileron blowing coefficient, $\frac{\text{nozzle reaction force}}{qS}$
$C_{\mu_f}$	flap blowing coefficient, $\frac{\text{nozzle reaction force}}{qS}$
$d$	gap between lower augmentor door and flap lower surface (see fig. 2(b)), in.
$E$	flap chord ratio, $\frac{c_f}{c}$
$i_t$	horizontal-tail incidence, positive with trailing edge down, deg
$J$	jet force, evaluated at $V_\infty = 0$ , lb
$J_p$	jet reaction force evaluated at $V_\infty = 0$ with the upper door and flap removed, lb
$l$	distance from the $\frac{c_r}{4}$ point on the wing to $\frac{\bar{c}}{4}$ point on the hori- zontal tail, ft
$m_j$	mass rate of flow through the primary nozzle of the jet augmentor measured as compressor output less aileron flow, slugs/sec
$p_d$	augmentor-duct total pressure (see fig. 2(g)), lb/sq ft
$p_\infty$	free-stream static pressure, lb/sq ft

q	free-stream dynamic pressure, lb/sq ft
S	wing area, sq ft
S <sub>F</sub>	portion of the wing area included by the jet flap installation, sq ft
S <sub>t</sub>	area of the horizontal tail, sq ft
t	wing maximum thickness
T <sub>d</sub>	duct total temperature, °R
T <sub>∞</sub>	free-stream total temperature, °R
V <sub>J</sub>	local velocity at augmentor exhaust, ft/sec
V <sub>t</sub>	horizontal tail volume coefficient $\left(\frac{l}{c_r}\right)\left(\frac{S_t}{s}\right)$
V <sub>∞</sub>	free-stream velocity, ft/sec
w	weight rate of flow, lb/sec
$\bar{x}_{cp}$	location of the center of pressure in wing chords with respect to the wing leading edge
y	distance outboard from the model plane of symmetry, ft
z	distance above the moment center measured perpendicular to the extended wing chord plane, ft
α	model angle of attack, deg
β	angle of sideslip, deg
δ <sub>a</sub>	aileron deflection; (δ <sub>aL</sub> /δ <sub>aR</sub> = 60/80 means left aileron at 60° and right aileron at 80°) positive with trailing edge down, deg
Δδ <sub>a</sub>	(right aileron deflection) - (left aileron deflection)
δ <sub>d</sub>	lower-door deflection, positive with trailing edge down, deg
δ <sub>e</sub>	elevator deflection, positive with trailing edge down, deg
δ <sub>f</sub>	flap deflection (see fig. 2(b)) positive with trailing edge down, deg
ε	downwash at the horizontal-tail position (along the 50 percent tail chord line), deg
η	dimensionless spanwise location, $\frac{2y}{b}$

$\theta$  augmented jet force angle or jet angle evaluated for the present investigation on the static test stand with reference to the wing chord plane, deg

#### Configuration Notation

D lower door extension (see fig. 2(b))  
E end plates on the outboard edge of the jet augmentor (see fig. 1(f))  
F fences on top of the wing near the wing-fuselage juncture (see fig. 1(f))

#### Subscripts

a aileron  
A augmented jet flap  
d duct or lower door  
f flap  
I isentropic conditions  
J jet, jet flap  
L lift or left side  
R right side  
u uncorrected  
 $\infty$  free stream

#### MODEL AND APPARATUS

Figures 1(a) through (e) show the model mounted in the wind tunnel and on the static test stand.

#### Basic Model

Geometric data for the model are presented in table I and sketches of the model are shown in figure 2. When the horizontal tail was not used, it was replaced with a rake having five directional pitot tubes. The wing was equipped with a full-span, fixed, leading-edge slat (see fig. 2(c)).

## Blowing Systems

The model was equipped with three blowing systems: the jet augmentor, trailing-edge-flap BLC, and aileron BLC. Air supply for the augmentor and aileron duct systems was provided by the load compressor unit shown in figure 2(f). The flap BLC primary air was supplied by the J-85 compressor bleed. The load compressors were modified Viper engines driven by hot gases from a J-85 gas turbine engine. These hot gases exhausted out the Viper tail pipes. The augmentor, aileron BLC and flap BLC ducts are shown in figure 2(g). Typical variations of airflow quantity and temperature measured in the augmentor duct are shown in figure 3. Total pressure loss in the augmentor ducts between the load compressor and the primary nozzle was below 4 percent for most test conditions.

Jet augmentor.- The jet augmentor was an ejector system with the forward wall formed by the wing, fixed vane, and lower door as shown in figure 2(d). The rear wall was formed by the upper door and trailing-edge flap. Primary air from the load compressor was ejected into the augmentor which pumped in secondary air from the wing upper surface and from the lower surface through the two slots formed by the nozzle, fixed vane, and lower door. The mixed jet was ejected downward between the flap and lower door. The present system was designed for most efficient operation for a flap deflection of about  $65^\circ$ .

For given flap deflections,  $\delta_f$ , the inlet and exit gaps, a and d (see fig. 2(b) section A-A) were varied remotely. The upper door lip could be varied independently of the upper door to maintain unseparated flow at the leading edge. During most of the tests the lip was fixed at a  $5^\circ$  deflection as shown in figure 2(d). The force output of the augmentor was varied during the tests by the adjustment of the throttle setting of the gas generator.

For the static tests, inlet fairings were installed on the lip and side of the augmentor to reduce the stall inside the augmentor lip (see fig. 1(e)).

Flap BLC.- Compressor bleed air was ducted to the flap BLC nozzles as shown in figure 2(g). The nozzles were part of an ejector system with the secondary air entering through openings in the upper door lip (see figs. 1(e) and 2(d)) and flowing down inside the upper door to the mixing chamber. Flap BLC flow quantities were varied for a constant augmentor output by coordinating the J-85 throttle and compressor bleed valve.

For  $\delta_f = 100^\circ$ , flap construction was such that a spanwise slot on the flap knee behind the BLC nozzle was unported. (See fig. 2(d).) The slot was 1 inch wide and the BLC jet sheet had to cross it before impinging on the surface of the flap radius.

Aileron BLC.- As shown in figure 2(g), the aileron BLC system was fed through the forward air-supply duct of the jet augmentor. Aileron blowing was therefore coupled with the augmentor output and was never varied independently. Airflow to the ailerons was 5 percent of the total Viper compressor output.

## Modifications

Modifications designed to improve slightly the aerodynamic characteristics of the model are as follows: Root fences were installed on the model as shown in figures 1(c) and (f). They extended 5 inches (7.4 percent) above the wing surfaces and were oriented parallel to the model plane of symmetry coincident with the inboard end of the jet augmentor. Augmentor end plates were installed at the outboard edge of the augmentor as shown in figure 1(f). The lower door extensions were 7.5 inches (11 percent  $c_{ref}$ ) as shown on the sketch in figure 2(b). Configuration notation will be F, E, and D for the root fences, end plates, and the door extensions, respectively.

## TESTS

### Static Tests

The static tests were made with the model 12 feet above the decking of the test stand with the model pitched down  $5^\circ$ . The objectives of these tests were to evaluate the static efficiency of the augmentor and to define the static forces exerted by the three blowing systems for use in computing,  $C_{JA}$ ,  $C_{\mu_f}$ , and  $C_{\mu_a}$  during the wind-tunnel tests. Tests were made with and without the upper door flap assembly. With the assembly installed, force and moment data were obtained at various lower door positions,  $d$ , for a given power and flap setting. For all tests, the upper door was set at positions that prevented flow separation inside the inlet of the augmentor.

### Wind-Tunnel Tests

The tests were made primarily with varying angle of attack at constant duct pressure and airspeed. Table II may be used as an index to these tests. A few tests were made with varying flap BLC. For all the tests, the positions of the upper door ( $a$  in fig. 2(b)) or upper door lip were adjusted to maintain zero static pressure difference between the upper and lower side near the lip of the upper door. The position of the lower door ( $d$  in fig. 2(b)) was maintained at the position for which a maximum augmentation ratio was measured during the static tests for a given flap setting. An exception was the  $100^\circ$  flap setting for which  $d$  was limited to about 3.0 inches by model construction factors.

The angle-of-attack range for the tests was  $-12^\circ$  to  $+29^\circ$ . The yaw range was  $0^\circ$  to  $12^\circ$ . The model was tested with flap settings of  $30^\circ$ ,  $45^\circ$ ,  $60^\circ$ ,  $70^\circ$ , and  $100^\circ$ , and aileron settings from  $0^\circ$  to  $70^\circ$ . Most of the tests were made at a dynamic pressure of 8 psf equivalent to a Reynolds number of  $3.0 \times 10^6$  based on the wing root chord. A few tests were made at dynamic pressures of 5, 12, and 20 psf.

## DATA ACQUISITION AND REDUCTION

### Data Acquisition

Three-component force and moment data were obtained during the static tests, and six-component data were obtained during the wind-tunnel tests. For all tests, the moment center was located at the  $c_r/4$  point and  $0.20 c_r$  below the wing chord plane.

Total and static duct pressures and temperatures at specific measuring stations in the duct systems were recorded for the three blowing systems. Calibrations of the duct system and load compressor prior to model assembly were used to evaluate mass rates of flow. The calibrations of the load compressor were also used to evaluate tail-pipe thrust as functions of tail-pipe total pressure and temperature. During the static tests, the tail-pipe exhaust deflection was measured by means of a total head rake 10 feet behind the tail pipes. The center of the wake was found to be within  $1^\circ$  of being parallel to the wing chord plane.

Other data obtained during the tests were as follows: surface pressure measurements of the jet augmentor and control surfaces at the 49 and 84 percent stations ( $\eta = 0.49$  and  $0.84$ ); augmentor exit total and static pressure distributions at one spanwise station; measurements from a total head rake on the upper surface near the trailing edge of the flap; directional pitot static measurements of downwash at the horizontal-tail position; and photographs of wing surface tufts for most test conditions.

### Data Reduction

Blowing parameters.- Thrust values measured during the static tests were used to calculate the blowing parameters for each test condition for corresponding jet augmentor or flap configurations and duct pressures.

Force and moment data.- For all force and moment data presented, the effects of load compressor tail-pipe thrust and inlet ram drag have been subtracted from the measured values. For tests with the model yawed, the forces were resolved with respect to the wind axes and the moments, with respect to the stability axes. Corrections to wind-tunnel force and moment measurements were as follows:

$$C_D = C_{D_u} + (C_T - C_{D_m}) \cos \alpha \cos \psi$$

$$C_L = C_{L_u} - (C_T - C_{D_m}) \sin \alpha$$

$$C_m = C_{m_u} + 0.4 (C_{D_m} - C_T)$$

$$C_y = C_{y_u} - (C_T - C_{D_m}) \cos \alpha \sin \psi$$

$$C_n = C_{n_u}$$

$$C_l = C_{l_u}$$

where  $C_{L_u}$ ,  $C_{D_u}$ ,  $C_{m_u}$ ,  $C_{y_u}$ ,  $C_{n_u}$  and  $C_{l_u}$  were the coefficients based on measured force and moments, and  $\alpha$  and  $\psi$  were geometric angles of attack and yaw.

Wind-tunnel wall corrections.- For power-off test results, corrections for wind-tunnel wall constraint were applied to the data as follows:

$$\alpha = \alpha_u + 0.44 C_{L_u}$$

$$C_D = C_{D_u} + 0.0077 C_{L_u}^2$$

The power-on test results are presented for all the tests without corrections for wind-tunnel wall effects, but some discussion and summary figures presented are based on corrected data. The method used for correcting the data is described in reference 6 and will be referred to as the "CL<sub>AERO</sub>" method. Corrections were obtained using the relations for the power off case and replacing  $C_{L_u}$  with an effective circulation lift coefficient obtained by subtracting from  $C_{L_u}$  the reaction lift resulting from the blowing systems, that is, the summation of the vertical components of  $C_{J_A}$ ,  $C_{\mu_a}$ , and  $C_{\mu_F}$ . The corrections are, therefore:

$$\alpha = \alpha_u + 0.44 C_{L_{AERO}}$$

$$C_D = C_{D_u} + 0.0077 C_{L_{AERO}}^2$$

with the horizontal tail on,

$$C_m = C_{m_u} + 0.40 C_{L_{AERO}}$$

A sampling of the data corrected by this method is presented in figure 4 for comparison with the uncorrected results and the results corrected by the methods of Heyson and Maskell (see refs. 7 and 8). The Heyson method incorporated the modification suggested in reference 9 in which the wake deflection angle given in reference 7 was halved before the wall constraint effects were calculated. The three methods are shown to agree well for angle of attack but the Heyson method gives somewhat higher drag corrections.

## RESULTS

### Static Test Results

Measurements made during the static tests are presented in figure 5 in the form of augmentation ratios, that is, the ratios of the measured reaction

force to the isentropic force  $J_I = m_j V_{j_I}$ , where  $V_{j_I}$  is the jet velocity calculated assuming isentropic flow conditions and  $m_j$  was the measured mass flow rate. These results were assumed to be representative of the jet augmentor performance throughout the wind-tunnel tests and were used to compute  $C_{J_A} = (\text{Static, augmented jet force}/qS)$  for given lower door positions and pressure ratios. For the discussion that follows, the performance of the primary nozzle will be assumed as indicated by the data in figure 5(a). These measurements were made with the flap and upper door removed but with the Coanda surface and lower door in place.

During the wind-tunnel tests, the optimum locations of the lower door were used which produced the highest augmentation ratios shown in figure 5.

Figure 6 shows the variation of jet angle with flap setting. Jet angle,  $\theta$ , is defined as the angle between the wing-reference plane and the jet force vector at zero airspeed. For the present installation, the equivalent jet angle was generally  $10^\circ$  less than the flap setting,  $\delta_f$ . The jet force vector would then be parallel with the lower surface of the flap; see figure 2(d).

#### Wind-Tunnel Results

The basic wind-tunnel data are presented in figures 7 through 24. Table II is an index to the figures. No wind-tunnel wall corrections have been applied to these data. Values of  $C_J$ ,  $C_{\mu_f}$ , and  $C_{\mu_a}$  listed in the figures were the averages obtained during the polars prior to wing stall. The excursions of the actual values from the averages prior to stall were within 3 percent. After stalling was initiated (generally at the wing root), the excursions were sometimes as high as 6 percent of the average values.

Leading-edge slats.- Test results showing the effect of the leading-edge slats are presented in figure 7 for  $\delta_f = 0$ , in figures 18(a) and (b) for  $\delta_f = 60^\circ$  horizontal tail off, and in figure 20(d) for the horizontal tail on. Because of the improvements in aerodynamic characteristics achieved by the slats, all other test results were obtained with full-span slats installed.

Flap deflection.- Test data for the model with the horizontal tail off are presented in figures 8 through 14 for  $\delta_f = 30^\circ$  to  $100^\circ$ . For a jet coefficient of  $C_J = 0.81$  interpolated data are presented in figure 15 for several flap deflections.

Jet coefficient.- The variations of lift with  $C_J$  for constant angle of attack are presented in figure 16 for  $\delta_f = 60^\circ$  and  $70^\circ$ . Data in figure 16 for other test dynamic pressures fair in smoothly with the measurements at  $q = 8$  psf, demonstrating that  $C_J$  as based on measured static thrust serves well as a correlating parameter.

Symmetrical aileron droop.- The effects of symmetrical-aileron droop are presented in figures 10, 12(d), 13(d), and 14(b) for  $\delta_f = 45^\circ$  to  $100^\circ$ . Because the jet augmentor air supply was coupled with the aileron BLC system

supply, the effects of aileron BLC could not be isolated from the effects of augmented-jet thrust in the wind-tunnel tests.

Flap BLC.- Variations of  $C_L$  with  $C_{\mu_f}$  for constant  $C_J$  and  $\alpha$  are presented in figure 17. Tuft observations indicated that for the highest values of  $C_{\mu_f}$  obtained with  $\delta_f = 100^\circ$ , the flow over the flap was separated even though, as shown in figure 17, a lift increment of 0.5 was obtained when BLC was used ( $C_J = 0.8$ ).

Wing modifications.- Data indicating the effects of doors, end plates, and root fences with power on are presented in figure 19. No tests were made with all modifications removed. However, tuft patterns showed that the primary effect of the fences was a small delay in the onset of root stall for model attitudes between  $0^\circ$  and  $4^\circ$ . This delay indicated that for the lower lift range, the fence had little effect on the force characteristics of the model. For the lower lift range, the combined effect of the door extensions and end plates was to increase  $C_L$  by 0.2 and decrease  $C_m$  by 0.1 from that for the model with the root fences installed.

Results with the horizontal tail on.- Data are presented in figure 20 for the model with the horizontal tail. Since tests with the tail on were limited to flap deflections of  $60^\circ$  and  $100^\circ$ , downwash measured with a set of directional probes mounted in place of the horizontal tail are presented in figure 21 for the full range of flap settings considered with tail off. Measurements of the local dynamic pressure indicated that for the conditions represented by figure 21, the local values were within 3 percent of the free-stream dynamic pressure. Calculated pitching-moment contributions of the horizontal tail based on the data of figure 21 indicated that the same degree of static stability would be contributed by the horizontal tail with the  $30^\circ$  and  $70^\circ$  flap settings as was measured with the  $60^\circ$  and  $100^\circ$  settings.

Lateral and directional results.- Six-component data showing the effect of sideslip and ailerons are presented in figures 22 through 24 for the model with the  $60^\circ$  flap setting. The contribution of the vertical tail may be seen by comparing figures 22 and 23.

The effect of differential aileron deflection is summarized in figures 25(a) and (b) for sideslip angles of  $0^\circ$  and  $-8^\circ$ . The aileron provided effective lateral control at low angles of attack, but as angle of attack was increased, control effectiveness decreased consistently and adverse yaw increased. As an evaluation of the measured aileron effectiveness, values, shown in figure 25, were calculated according to antisymmetric loading theory of reference 10 with the addition of the antisymmetric reaction force due to the aileron BLC jets.<sup>1</sup> As shown, the calculations agree with the measured values for  $\alpha = 0^\circ$ , indicating that the ailerons were operating efficiently for the low aircraft attitudes. In comparison to the rolling moments measured for the model in sideslip, the lateral-control effectiveness of the

---

<sup>1</sup>The reaction force coefficient due to aileron BLC was assumed to be,  $\bar{\eta}C_{\mu_a}(\sin \delta_L - \sin \delta_R)$  where  $\bar{\eta}$  was 0.86.

present aileron configuration appears to be adequate for trimming the aircraft at sideslip angles up to about  $8^\circ$  at  $16^\circ$  angle of attack.

The adverse yaw due to the ailerons increased with angle of attack from  $-(\Delta C_n / \Delta C_l)_{\delta_a} = 0.34$  at  $\alpha = -8^\circ$  to  $0.77$  at  $\alpha = 8^\circ$ . These values are considered large compared to desirable lateral control characteristics and should be a subject for future research.

## DISCUSSION

### Jet-Augmentor Performance

Zero airspeed.- With the complete jet augmentor assembly, the static test results (see fig. 5) show that for a given flap setting, augmentation ratios were sensitive to lower door position, with slightly lower values measured for the higher pressure ratios. Results of initial static tests (for which data have not been presented) indicated that upper door position had little or no effect on augmentation ratio unless flow separation occurred on the inside surface of the upper door.

Figure 26 shows that near maximum values of augmentation ratio were obtained for the design flap settings of  $60^\circ$  and  $70^\circ$ . The augmentation ratio dropped rapidly as flap deflection was either increased or decreased from these settings. The augmentation of the isentropic thrust for  $\delta_f = 60^\circ$  and  $70^\circ$  was  $J_A/J_I = 1.25$ , and the augmentation of the measured primary jet (with upper door flap assembly removed) was  $J_A/J_P = 1.42$ . This performance was similar to that obtained with the small bench model Coanda ejectors of reference 11 which were similar in configuration to the present jet augmentor.

For the off-design flap settings, smoke flow studies and oil residue patterns indicated that flow separation occurred for  $\delta_f = 30^\circ$  and  $45^\circ$ . For  $\delta_f = 100^\circ$  local flow separation was extensive on the lower door immediately behind the Coanda surface. Consequently, the off-design performance of the augmentor could probably be improved if the Coanda surface were rotated as flap deflection was changed. Further improvement for  $\delta_f = 100^\circ$  could probably be obtained by minimizing the reduction of augmentor throat area as flap deflection was increased beyond the design settings.

The effect of airspeed.- During the wind-tunnel tests, the performance of the jet augmentor was monitored at one wing station by means of a total and static pressure rake. Typical velocity profiles of the augmentor exhaust measured at a free-stream dynamic pressure of  $7.8$  psf are presented in figure 27. The measurements indicate that the augmentor was functioning as an efficient ejector pump. For  $C_{JA} = 1.26$ , the isentropic velocity of the primary jet was  $1210$  ft/sec, with the velocity distribution at the augmentor

exhaust showing a profile similar to that of well developed channel flow with a maximum velocity of 415 ft/sec.

Integration of the rake measurements gave values of  $C_{JA}$  close to those based on static jet force measurements for corresponding power settings and lower door settings. For example, with the conditions of  $\delta_f = 60^\circ$  and  $C_{JA} = 1.26$ , and uniform augmentor performance assumed along the span, the value of  $C_J$  obtained from the rake measurements was 1.30. This result, as well as the data of figure 16, indicated no reduction in augmented jet thrust with increasing airspeed for the range of airspeeds tested.

#### Effect of the Augmentor on the Longitudinal Characteristics of the Model

Data for zero sideslip showing the effect of augmentor operation on the longitudinal characteristics of the model have been corrected for wind-tunnel-wall effects by means of the  $C_{LAERO}$  method described in reference 6. The results considered in the following discussion are based on these corrected data for the model with full-span leading-edge slats installed unless otherwise noted. The effects of end plates, fences, and door extensions were small compared to the effects of  $C_{JA}$  and  $\delta_f$  (as shown in fig. 19), and the basic test data are used here without adjustment for these effects.

Lift at zero angle of attack.- The variations of lift coefficient for  $\alpha = 0^\circ$  with jet coefficient are presented in figure 28(a) for the flap settings investigated. The measurements show that ratios of lift increase to the equivalent reaction lift change due to the jet,  $C_J \sin \theta$ , varied from about 3.4 to 1.4 for  $\delta_f$  from  $45^\circ$  to  $70^\circ$ .

The variations of lift with flap deflection for  $C_J = 0.81$  as affected by symmetrical aileron deflection and flap BLC are presented in figure 28(b). Deflecting the ailerons symmetrically to  $45^\circ$  increased lift coefficient 0.5 which was twice that predicted by linear theory. Additional lift was obtained by increasing the aileron droop to  $70^\circ$  for the higher flap deflections. These results show that there was a favorable influence of the ailerons on the augmented jet flap lift.

Figure 28(b) also indicates that lift increments due to BLC were significant, but these increments did not increase for flap deflections above  $60^\circ$ . In addition, with or without BLC, maximum values of lift at  $\alpha = 0^\circ$  were measured at about  $\delta_f = 70^\circ$ . For  $\delta_f = 100^\circ$ , tuft patterns indicated that flow separation appeared on most of the flap surface behind the flap knee for all test conditions, and the use of the existing BLC system improved the flow only in the vicinity of the flap knee. The above results illustrate the need for a more effective BLC system in order to increase the flap lift effectiveness at the high flap settings.

Stall characteristics.- The full-span slats were effective in increasing the angle of attack for wing stall or maximum lift from  $10^\circ$  to  $18^\circ$  (see fig. 18 for  $\delta_f = 60^\circ$ ). With or without slats, flow separation initiated at

the wing root near  $0^\circ$  angle of attack in the form of a wedge of separated flow with its apex at the intersection of the leading edge and fuselage. As angle of attack was increased to  $\alpha = 4^\circ$ , this area of separated flow progressed back to the jet-augmentor intake and increased in width. As angle of attack increased to that near  $C_{L_{max}}$ , the area of separated flow progressed outboard rapidly when the slats were retracted. With the slats installed, this outboard progression of the flow was delayed; consequently  $C_{L_{max}}$  increased even though the upper surface of the slat was stalled. With the slats on, the flow on the outboard wing panels ahead of the ailerons did not separate. These results indicate that higher slat deflections, particularly on the inboard wing sections, would bring further delays in wing stall and increases in  $C_{L_{max}}$ .

Maximum lift.- The variation of  $C_{L_{max}}$  with jet coefficient for the model with leading-edge slats installed is presented in figure 29. For values of  $C_J$  between 0.8 and 2.0, the ratio of the increase in  $C_{L_{max}}$  to the corresponding increase in  $C_J$  was about 2 for flap settings of  $60^\circ$  and higher. Figure 29 demonstrates that for the given wing leading-edge configuration (full-span slats),  $C_{L_{max}}$  for the higher flap deflections was largely dependent on jet coefficient and to a lesser degree on flap setting.

#### Lift-Drag Characteristics of the Model

Drag polars for several flap configurations and power settings are presented in figure 30. Lines representing conditions for constant descent angle are superimposed on the data. The data on the left side of the figure show that at maximum lift, the descent angle would be about  $8^\circ$  for all jet coefficients with  $\delta_f = 60^\circ$ ; the data on the right show the effect of flap setting. For  $C_J = 0.81$  a maximum descent angle capability of  $15^\circ$  was obtained with  $\delta_f = 100^\circ$ ,  $\delta_a = 45^\circ$ , and  $C_{\mu_f} = 0$ . With  $\delta_f = 70^\circ$  and  $C_J = 1.30$ , a maximum lift coefficient of over 6 was obtained while a  $10^\circ$  descent angle capability was maintained.

#### Longitudinal Stability and Control

Pitching-moment data for the model with the horizontal tail are presented in figure 31. The data which have been corrected for wall constraint effects on the downwash show increases in stability and stabilizing moments through stall.

The data of figure 31 were used to derive the characteristics of the model trimmed for level flight. These results are presented in figure 32 for a static margin of 5 percent. In addition to the trim data obtained directly from the test data (tail volume coefficient = 1.35), trim characteristics were estimated for the trimmed model with a smaller volume coefficient of 1.0. (It was assumed here that the contribution of the tail to the pitching moment was proportional to tail volume only.) The required moment centers (for a 5 percent static margin and  $C_J = 1.15$ ) were 0.30 and 0.37  $c_r$  for tail volumes of 1.00 and 1.35, respectively. The results of

these trim calculations show that the model could be trimmed with moderate elevator settings with the smaller tail volume of 1.0 (which is typical of the values incorporated in some current STOL aircraft). The data of figure 15 indicated that the maximum moments required for trim were obtained with flap deflections between  $60^\circ$  and  $70^\circ$  for  $C_J = 0.81$ . Since in any specific aircraft application, tail incidence and center of gravity could be variables, it appears that pitch control would not be limiting for the present flap configuration.

#### Comparison With Jet Flap Characteristics

Since both the augmented-jet flap and jet flap concepts could be applied to the same type of aircraft (i.e., gas turbine powered STOL aircraft), it is of interest to compare the relative merits of each concept. The fundamental similarity between the two concepts is that in both cases a jet sheet is expelled at the trailing edge of the wing. In the case of a jet flap, the high velocity jet issues out at the knee of the flap and is blown along the upper surface of the flap. Two- and three-dimensional theories developed by Spence and Maskell for this flap are presented in references 12 and 13. Numerous experimental results exist, some of which are presented in references 1 through 4. In the case of the augmented jet flap, the high velocity jet combines with the secondary air and exhausts at an angle approaching the deflection of the trailing-edge flap between boundaries consisting of the trailing-edge flap and the lower door. Because a theory that fully accounts for this configuration is lacking, the following comparisons are based primarily on test results.

Jet thrust.- As indicated in figure 26 for the augmented jet flap at an optimum flap setting of  $60^\circ$  or  $70^\circ$ , the augmentor increased the available isentropic thrust,  $J_I$ , by the ratio of 1.25. A similarly defined ratio of static thrust to isentropic thrust for high velocity jets issuing from jet flaps would fall between 0.75 and 0.85 for the configurations discussed in references 1 to 4. If a value of 0.8 is assumed, the static thrust from the augmentor would then be  $1.25/0.8$  or about 1.5 times that of a jet flap for the same isentropic thrust. If the external aerodynamics of an aircraft with a jet augmented flap are assumed to be equivalent to those of an aircraft equipped with a basic jet flap for the same jet reaction, a propulsive system would be required for the augmentor wing which produces only two-thirds of the isentropic thrust of that required for a jet flapped aircraft.

Lift.- Flap lift increments as functions of jet coefficient ( $\alpha = 0^\circ$ ) are presented in figure 33(a) for the augmented-jet flap model and in figure 33(b) for basic jet flap models. The data for the augmented jet flap were adjusted to zero symmetric aileron deflection by means of the symmetrical aileron lift increments measured with  $\delta_F = 45^\circ$ . For the jet flap models, the measured lift increments were adjusted for flap span and wing planform changes to that

of the present model configuration by means of the linear theory of reference 14.<sup>2</sup> The assumption was made that lift is proportional to  $(1 + t/c)$  (see ref. 13). Where static jet thrust data were not available, the static thrust was assumed to be 85 percent of the isentropic value. The corresponding values of jet coefficients were derived by assuming them proportional to  $S_F/S$ .

Values of lift increment presented in figures 33(a) and (b) corresponding to  $C_J = 1.15$  are shown in figure 34 as functions of jet angle. The theoretical values were derived by combining linear span loading theory and the two-dimensional lift effectiveness for jet flaps presented in reference 12. For jet angles of  $60^\circ$  and less, the augmented jet flap produced slightly higher lift increments than the basic jet flaps. The curvature or the reduction in slope of the augmented jet flap data is probably caused by the reduction of flap BLC effectiveness with increasing flap deflection. If the theory adequately predicts the effect of flap chord, the differences in lift increments between the two flap systems could be accounted for by differences in flap chord. If it is assumed that for identical jet reaction forces the external aerodynamics of the two types of flap are equivalent, for the same isentropic jet thrust, the lift of the augmented jet flap would be 22 percent higher (assuming  $\Delta C_L \sim C_J$ )<sup>1/2</sup> than that of the jet flap since the ratio of measured jet reaction forces of the two systems was 1.5.

#### Center-of-Pressure Location

Figure 35 shows center-of-pressure variations with flap lift increment for the augmentor wing and jet flap models for a jet angle of  $60^\circ$ . All curves represent conditions with the models at zero angle of attack with the jet coefficient varying. For comparison, the jet flap center-of-pressure locations were adjusted forward by an amount calculated to represent the induced effects of the flapped sections on the outboard wing panel of the augmented jet flap model. Since all models (except that of ref. 1) had fuselages, none of the data were adjusted for fuselage induced effects. The results in figure 35 indicate that the center-of-pressure locations on the augmented jet flap model were about 10-percent chord forward of the locations measured on the jet flap models (with flap chord ratios of about 0.1). The effect of flap chord predicted by the two-dimensional theory of reference 12 indicates that the larger effective flap chord could account, in part, for the more forward center-of-pressure locations of the augmented jet flap.

---

<sup>2</sup>The linear theory of reference 14 gives the flap lift effectiveness parameters as a function of flap span. Where  $\Delta C_{LJ}$  is the measured lift increment for the corresponding jet flap model, the adjusted lift increment based on the augmented jet flap model geometry is

$$\Delta C_L = \Delta C_{LJ} \frac{C_{L\delta_A} (1 + t/c)_A}{C_{L\delta_J} (1 + t/c)_J}$$

## CONCLUDING REMARKS

Results of the static tests showed that the thrust of the augmented jet flap was about 1.42 times the measured thrust and 1.25 times the isentropic thrust of the primary jet for flap deflections of  $60^\circ$  and  $70^\circ$ . No significant reduction in augmentation ratio was measured at forward speed.

Results of the wind-tunnel tests showed the following: (1) For a flap setting of  $60^\circ$ , maximum lift coefficients of about 6 were obtained for a jet coefficient of 1.30 for the model with a full-span leading-edge slat; (2) for angles of attack prior to wing stall, symmetrical aileron deflection and flap BLC each increased lift coefficient about 0.5; (3) for the complete model with a high positioned horizontal tail with a tail volume of 1.0, the model could be trimmed for all flap settings, and the pitching-moment changes measured through wing stall were stabilizing.

Comparisons with conventional jet flaps showed that, for jet angles of  $60^\circ$  and for the same jet reaction forces, the augmented jet flap produced slightly higher lift and more forward center-of-pressure locations than those produced by 10-percent chord jet flaps. For the same isentropic thrust, the augmented jet flap produced 50 percent more jet force and 22 percent more lift than that of the jet flap.

Ames Research Center  
National Aeronautics and Space Administration  
Moffett Field, Calif., 94035, Mar. 12, 1968  
721-01-00-14-00-21

## REFERENCES

1. Gainer, Thomas G.: Low-Speed Wind-Tunnel Investigation to Determine the Aerodynamic Characteristics of a Rectangular Wing Equipped with a Full-Span and an Inboard Half-Span Jet-Augmented Flap Deflected  $55^{\circ}$ . NASA MEMO 1-27-59L, 1959.
2. Butler, S. F. J.; Guyett, M. B.; and Moy, B. A.: Six-Component Low-Speed Tunnel Tests of Jet-Flap Complete Models With Variations of Aspect Ratio, Dihedral, and Sweepback, Including the Influence of Ground Proximity. R. A. E. Rep. Aero 2652, June 1961.
3. Alexander, A. J.; and Williams, J.: Wind-Tunnel Experiments on a Rectangular-Wing Jet-Flap Model of Aspect-Ratio 6. R & M No. 3329, British A. R. C., 1964.
4. Weiberg, James A.; and Holzhauser, Curt A.: Large-Scale Wind-Tunnel Tests of an Airplane Model With an Unswept, Tilt Wing of Aspect Ratio 5.5, and With Four Propellers and Blowing Flaps. NASA TN D-1034, 1961.
5. Whittle, D. C.: The Augmentor-Wing - a New Means of Engine Airframe Integration for STOL Aircraft. ICAS Paper 64-574, 1964.
6. Pope, Alan; and Harper, John J.: Low-Speed Wind Tunnel Testing. John Wiley and Sons, Inc., 1966.
7. Heyson, Harry H.: Linearized Theory of Wind-Tunnel Jet-Boundary Corrections and Ground Effect for VTOL-STOL Aircraft. NASA TR R-124, 1962.
8. Maskell, E. C.: The Interference on a Three-Dimensional Jet-Flap Wing in a Closed Wind Tunnel. R & M No. 3219, British A. R. C., Aug. 1959.
9. Heyson, Harry H.; and Grunwald, Kalman J.: Wind-Tunnel Boundary Interference for V/STOL Testing. NASA SP-116, 1966, pp. 409-434.
10. DeYoung, John: Theoretical Antisymmetric Span Loading for Wings of Arbitrary Plan Form at Subsonic Speeds. NACA TR 1056, 1951.
11. Scott, W. J.: Experimental Thrust Augmentation of a Variable Geometry, Two-Dimensional Coanda Wall Jet Ejector. NRC of Canada LR-394, January, 1964.
12. Spence, D. A.: The Lift on a Thin Aerofoil with a Blown Flap. Aero Quarterly Aug. 1958, R. A. E. TN Aero 2450, May 1956 (Plus Addendum).
13. Maskell, E. C.; and Spence, D. A.: A Theory of the Jet Flap in Three Dimensions. Proc. Roy. Aero. Soc. 1958, vol. 251, R. A. E. Rep. Aero 2612, Sept. 1958.
14. DeYoung, John: Theoretical Symmetric Span Loading Due to Flap Deflection for Wings of Arbitrary Plan Form at Subsonic Speeds. NACA TR 1071, 1952.

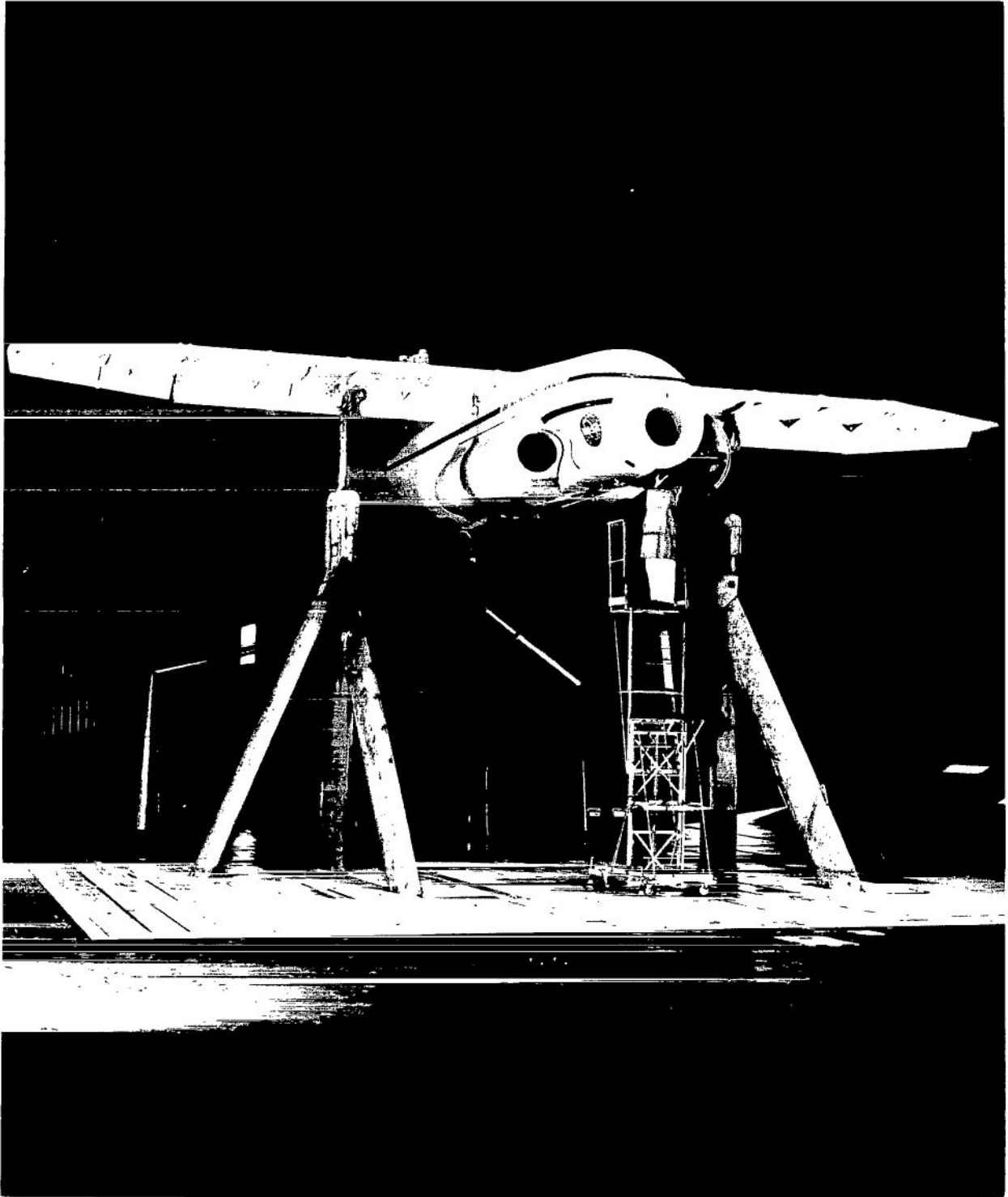
TABLE I.- GEOMETRIC DATA

Wing	
Area, sq ft . . . . .	222
Span (tip radius fairings off) ft . . . . .	42.16
Aspect ratio . . . . .	8.0
Root chord, $c_r$ , ft . . . . .	5.67
Tip chord, ft . . . . .	2.83
Mean aerodynamic chord, ft . . . . .	5.39
Airfoil section 16 percent NACA 747A forward of 40 percent $c$ NACA 0016-34, aft of 40 percent camber 2.23 percent $C_{Ldesign} = 0.3$	
Fuselage	
Width, ft . . . . .	5.29
Height, ft . . . . .	5.29
Length, ft . . . . .	35.33
Horizontal tail	
Area, sq ft . . . . .	75.0
Span, ft . . . . .	17.28
Aspect ratio . . . . .	3.98
Taper ratio . . . . .	0.67
Root chord, ft . . . . .	5.20
Location of tail $\bar{c}/4$ ,	
$z/c_r$ . . . . .	1.26
$l/c_r$ . . . . .	3.99
Elevator area, sq ft . . . . .	37.5
Vertical tail	
Area, sq ft . . . . .	33.3
Aspect ratio . . . . .	1.04
Span (above top of fuselage), ft . . . . .	5.88
Chord (constant) . . . . .	5.67
Sweep, deg . . . . .	34.9
Section, NACA 63-015 mod	
Location of tail $\bar{c}/4$ ,	
$z/c_r$ . . . . .	0.74
$l/c_r$ . . . . .	3.48

TABLE II.- FIGURE INDEX FOR THE WIND TUNNEL RESULTS

Figure	$\beta$ , deg	$\delta_f$ , deg	$\delta_a$ , deg	Slats	Tail		BLC	Wing modification	Variable; effect	
					Horizontal	Vertical			$\alpha$ ;	slat,F
7	0	0	0	Off,On	Off	On	Off	---	$\alpha$ ;	slat,F
8		30	↓	On	↓	↓	↓	F	$C_J$	
9		45	45	↓	↓	↓	↓	↓	$\delta_a$	
10		45	0,45	↓	↓	↓	↓	↓	$\delta_a, \delta_f$	
11		30,45	0,45	↓	↓	↓	Off,On	↓	$C_J$	
12(a)		60	45	↓	↓	↓	Off	D,E	$C_J, q$	
(b)		↓	↓	↓	↓	↓	↓	↓	BLC	
(c)		↓	↓	↓	↓	↓	---	↓	$\delta_a$	
(d)		↓	---	↓	↓	↓	Off	↓	$C_J$	
13(a)		70	45	↓	↓	↓	On	D	$C_J, q$	
(b)		↓	↓	↓	↓	↓	↓	↓	$\delta_a$	
(c)		↓	↓	↓	↓	↓	↓	↓	$C_J$	
(d)		↓	---	↓	↓	↓	↓	↓	$\delta_a, BLC$	
14(a)		100	45	↓	↓	↓	Off	F	$\delta_f$	
(b)		↓	---	↓	↓	↓	---	↓	$C_J, q$	
15		---	45	↓	↓	↓	Off	↓	BLC; $\delta_f, C_J$	
16(a)		60	↓	↓	↓	↓	On	↓	$\alpha$ ;	
(b)		70	↓	↓	↓	↓	---	↓	slats	
17		---	↓	↓	↓	↓	---	↓	wing mod.	
18(a)		60	↓	↓	---	↓	Off	↓	tail	
(b)		↓	↓	↓	---	↓	On	↓	$C_J, BLC$	
19	On	↓	↓	On	On	---	---	$\delta_e$		
20(a)	60	45	↓	On	On	Off	F	slats		
(b)	↓	↓	↓	On	On	---	↓	$C_J$		
(c)	↓	↓	↓	↓	↓	Off	↓	$\epsilon; \delta_f$		
(d)	↓	↓	↓	---	↓	↓	---	$\psi$		
(e)	100	↓	↓	On	↓	↓	F	$\delta_a^*$		
21	---	↓	↓	↓	Off	↓	↓			
22(a)	---	60	↓	↓	↓	Off	↓			
(b)	---	↓	↓	↓	↓	↓	↓			
23(a)	---	↓	↓	↓	↓	On	↓			
(b)	---	↓	↓	↓	↓	↓	↓			
24(a)	0	---	---	↓	↓	Off	↓			
(b)	↓	---	---	↓	↓	↓	↓			
(c)	-8	---	---	↓	↓	↓	↓			
(d)	↓	---	---	↓	↓	↓	↓			

\*Lateral control



(a) Front view of model in the wind tunnel.

A-35827

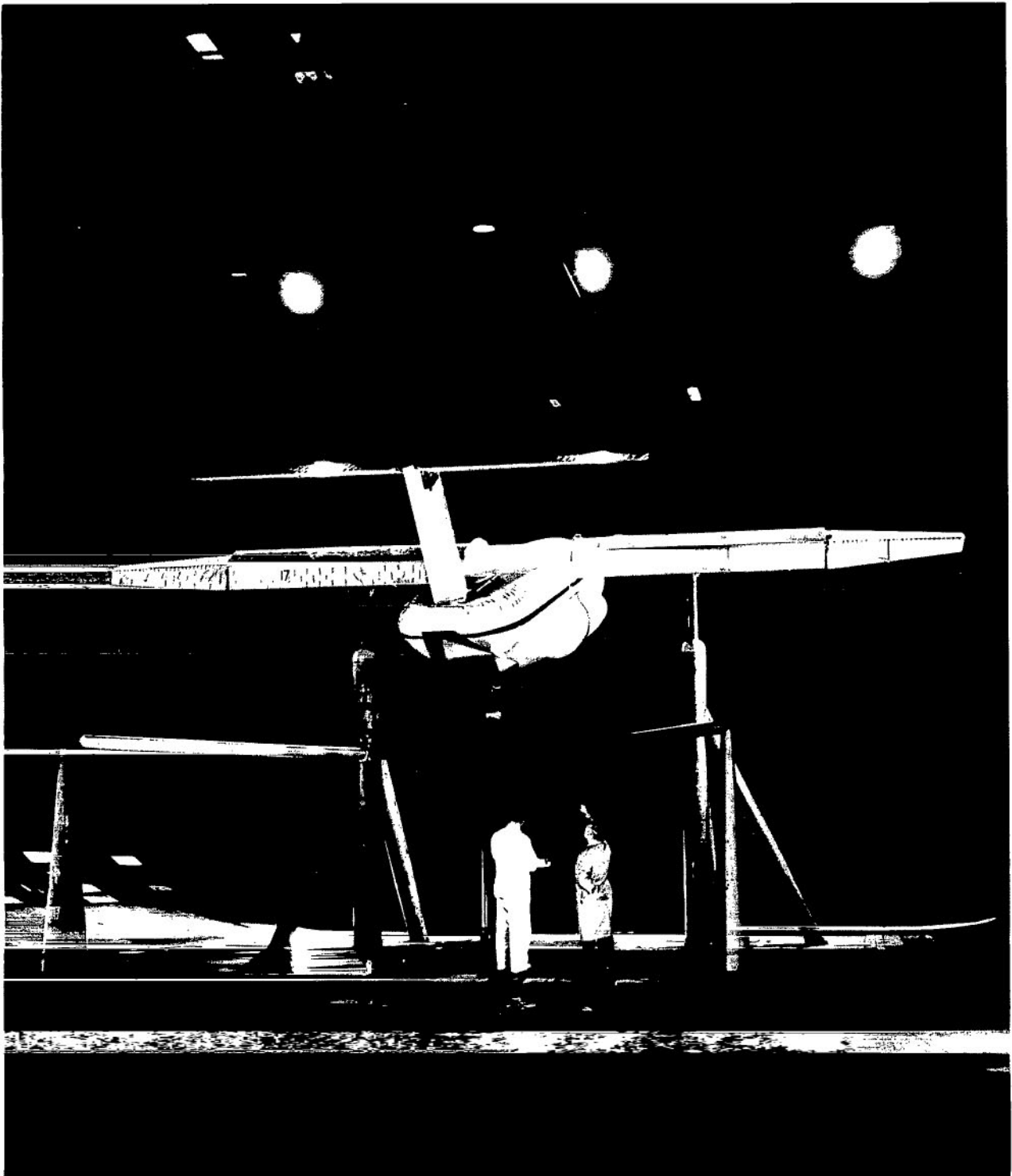
Figure 1.- Views of model installations and assemblies.



(b) Rear view of model in the wind tunnel with tail off;  $\alpha = 0^\circ$ .

A-35828

Figure 1.- Continued.



(c) Rear view of model in the wind tunnel with tail on;  $\alpha = 10^\circ$ .

A-35826

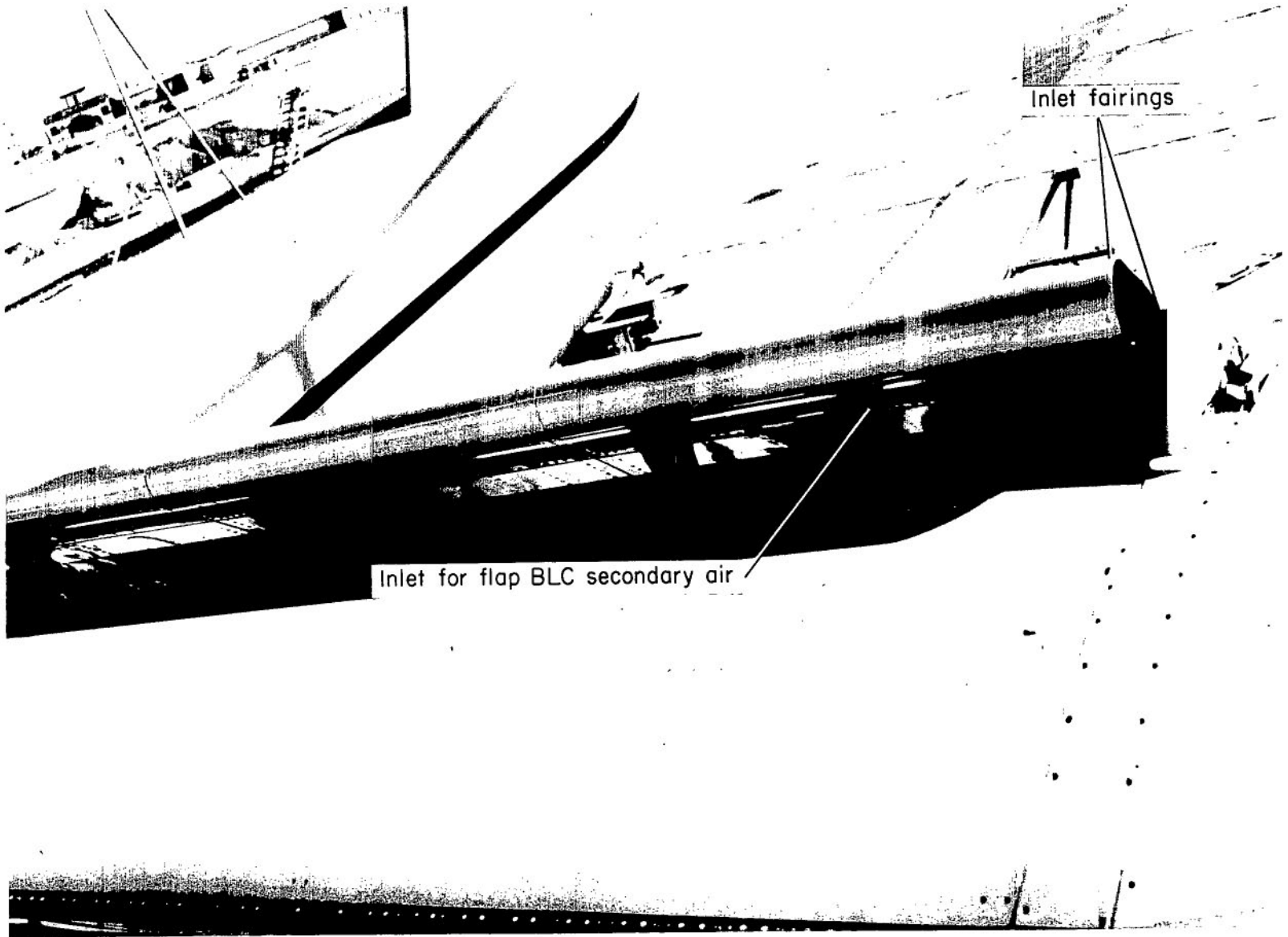
Figure 1.- Continued.



(d) View of model installed on the static test stand.

A-35726-2

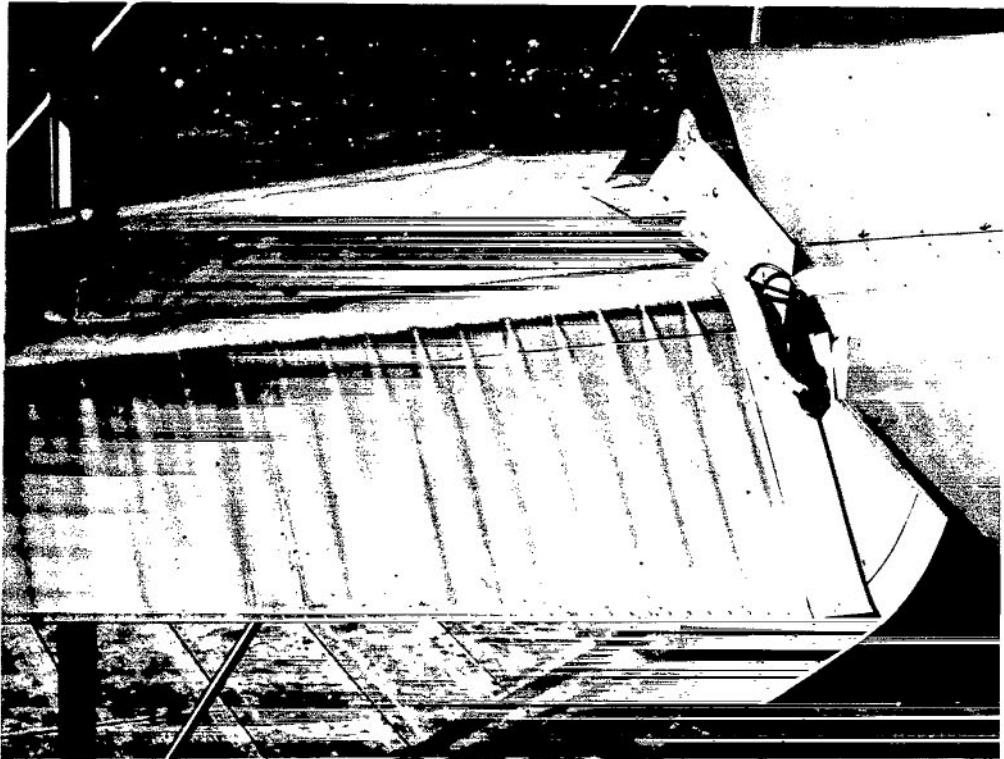
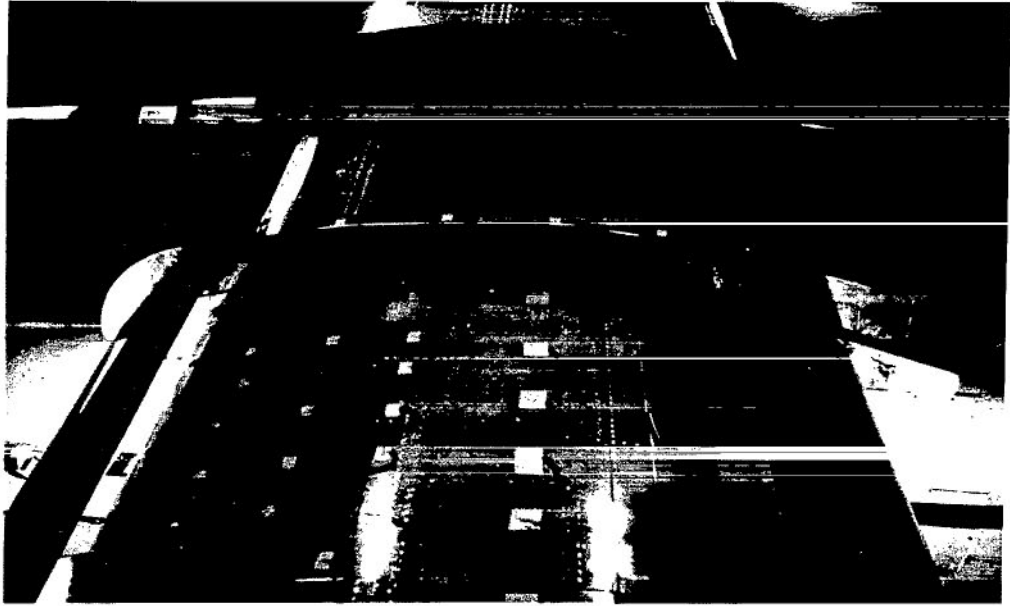
Figure 1.- Continued.



(e) Front view of augmentor with inlet fairings used in the static tests.

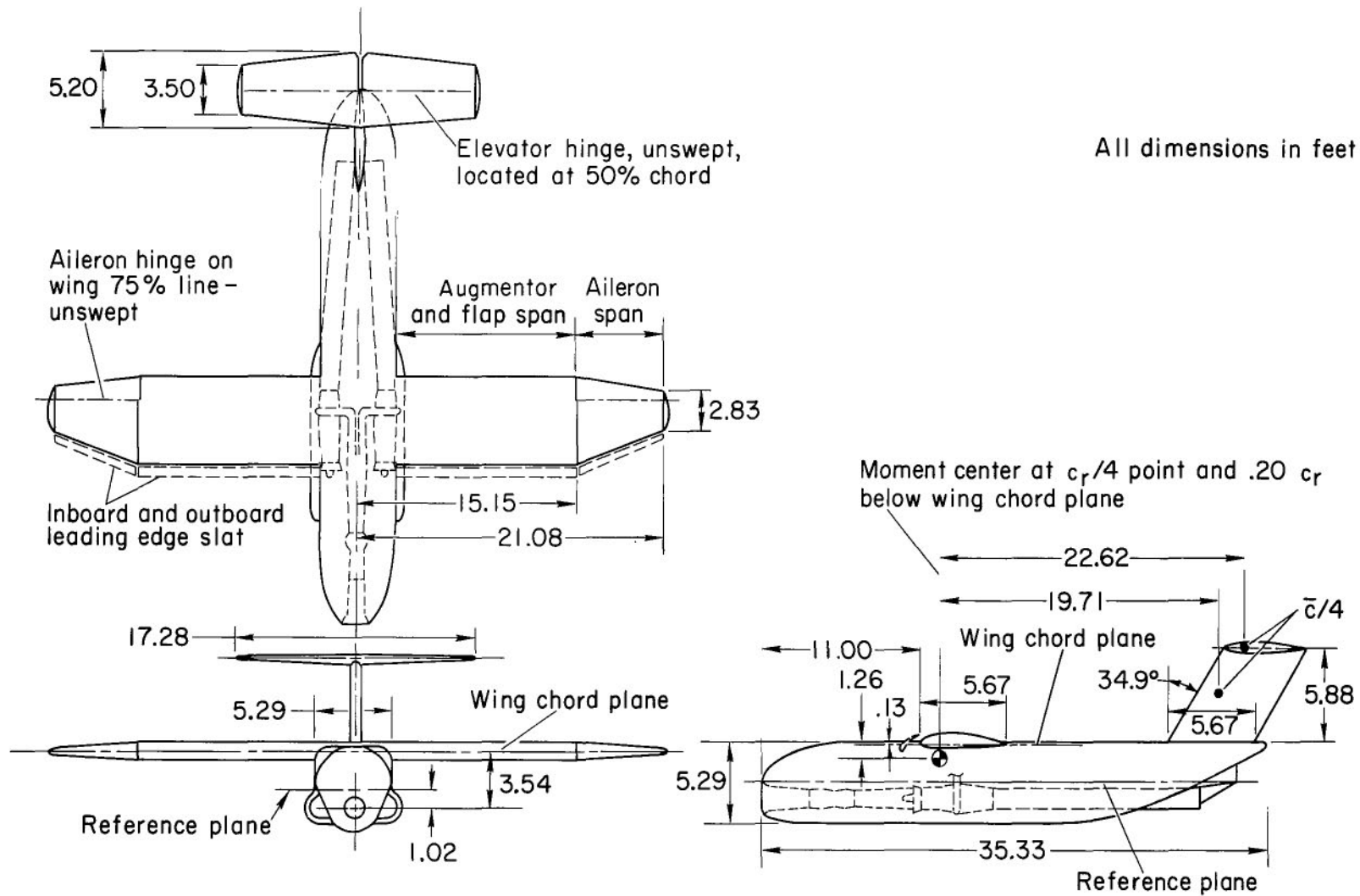
A-35726-13.1

Figure 1.- Continued.



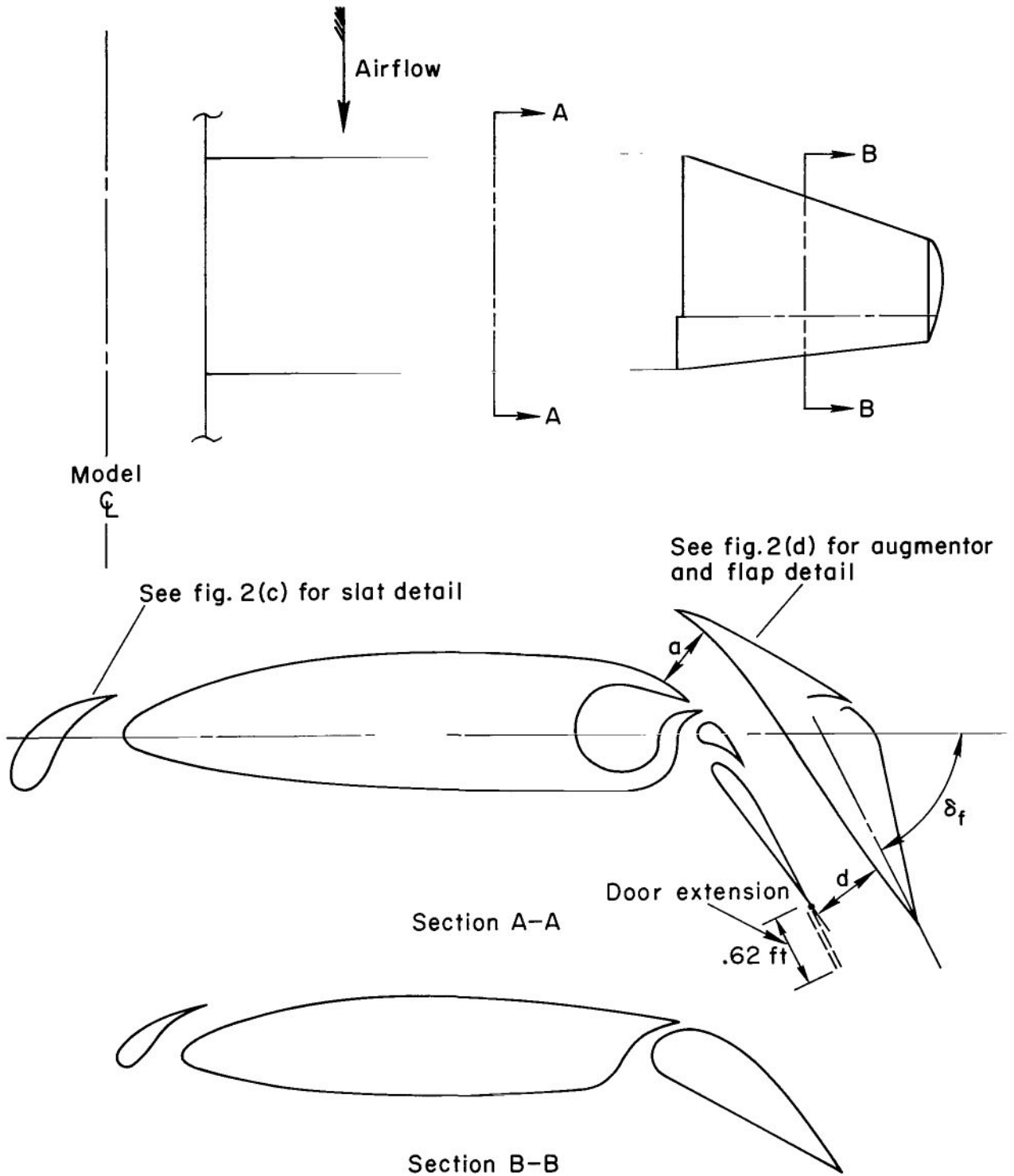
(f) Root fence (top), and end-plate installations. A-35726-14

Figure 1.- Concluded.



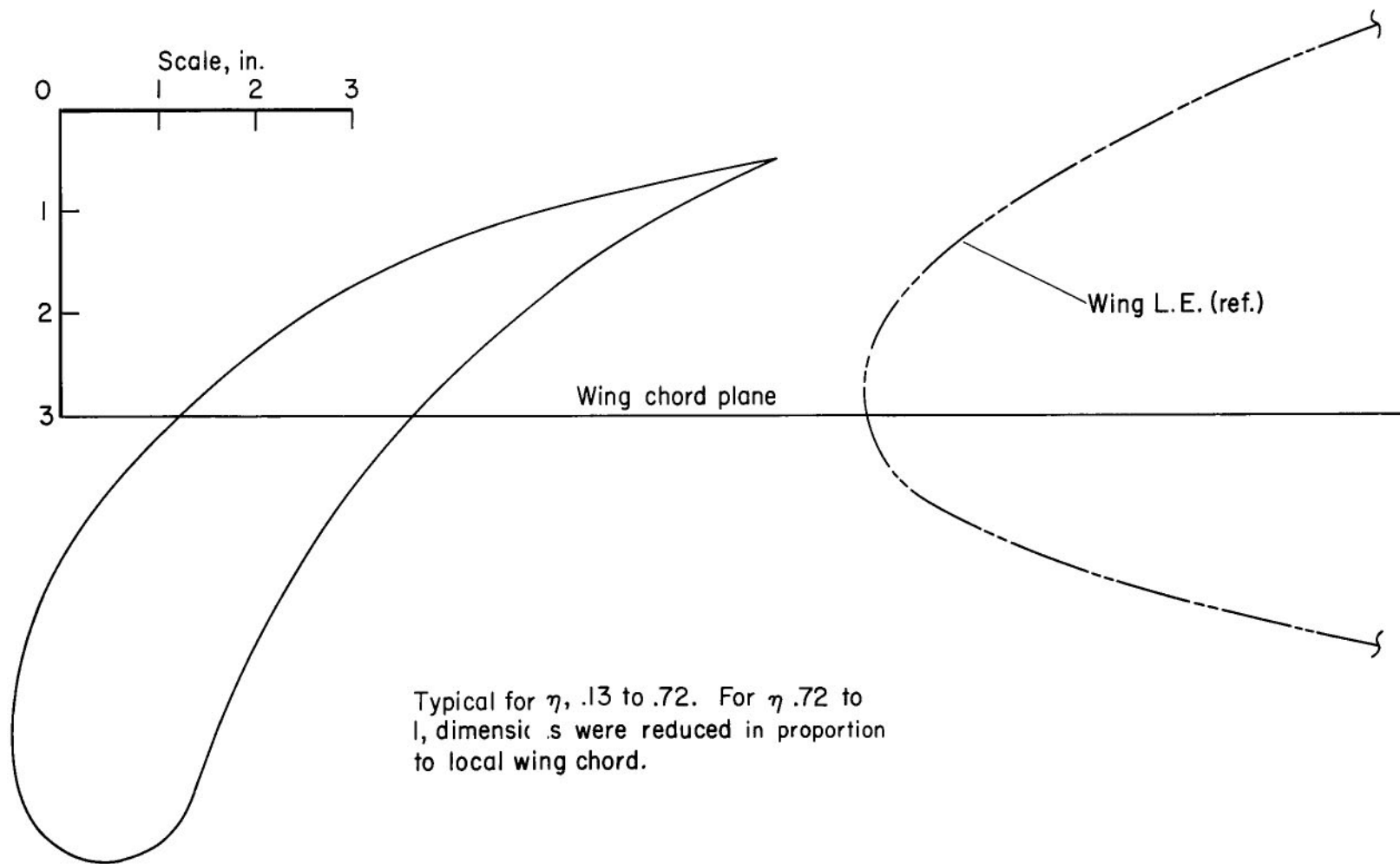
(a) Three-view drawing of the model.

Figure 2.- Geometric details of the model.



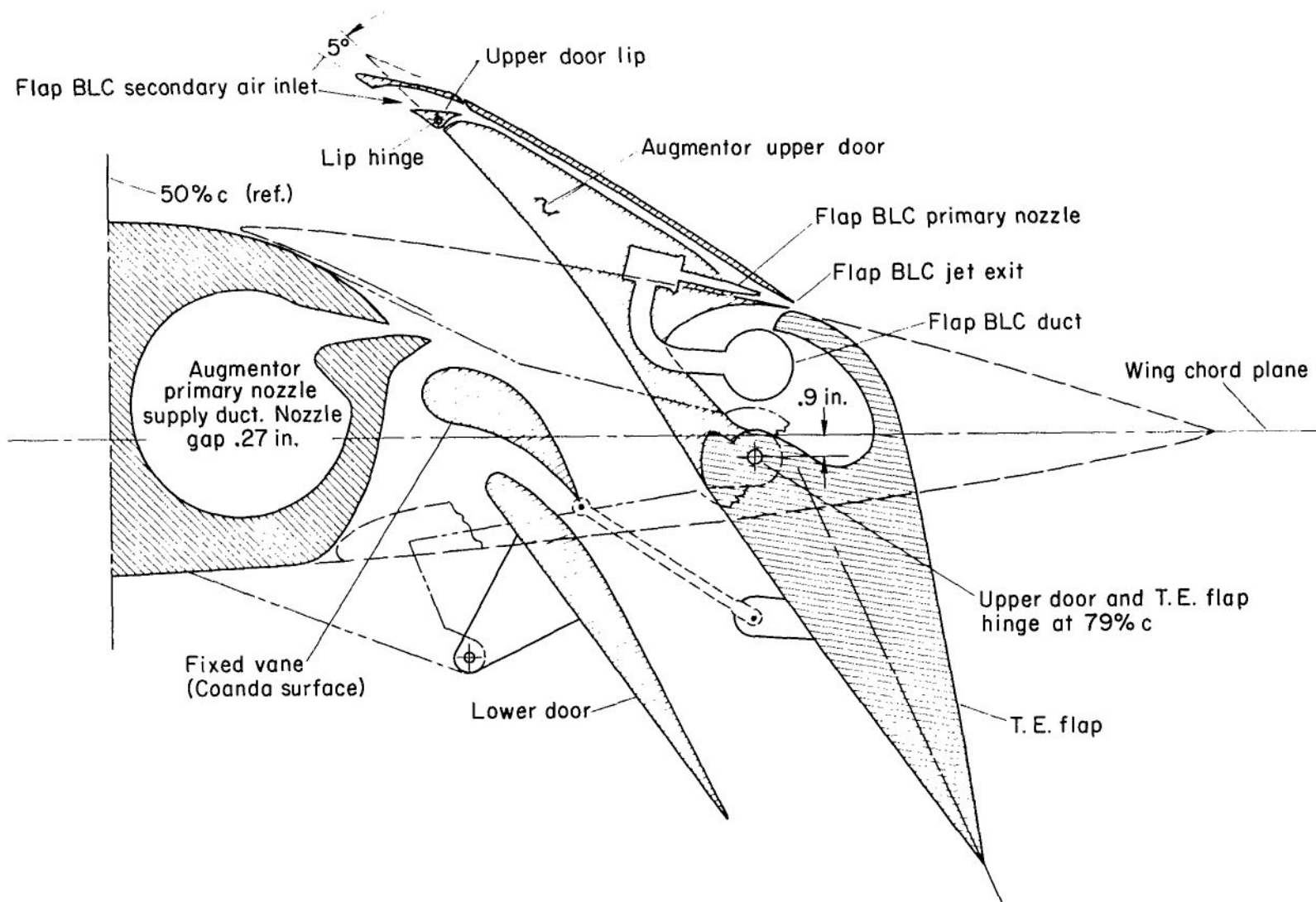
(b) Wing assembly views.

Figure 2.- Continued.



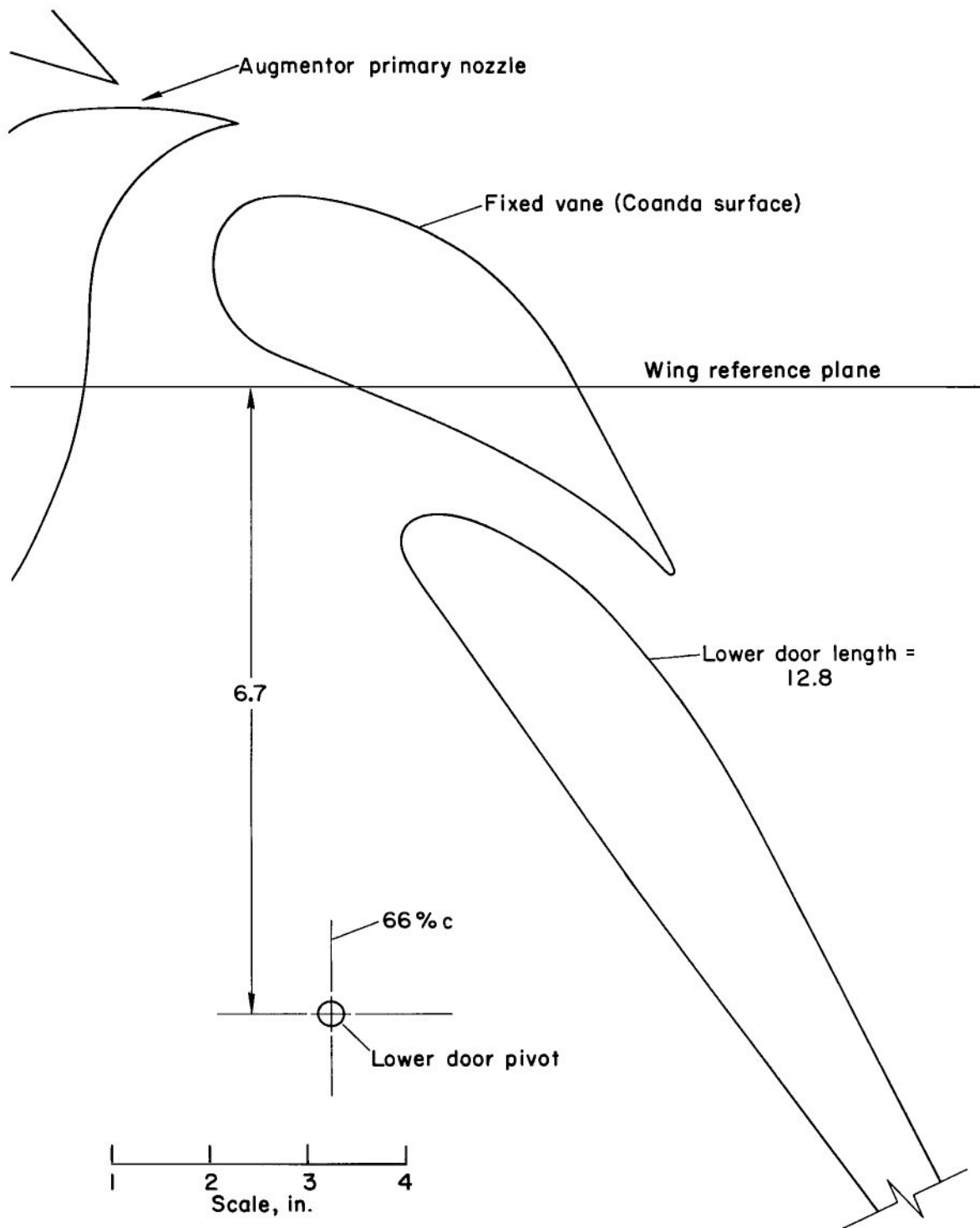
(c) Detail of leading-edge slat.

Figure 2.- Continued.



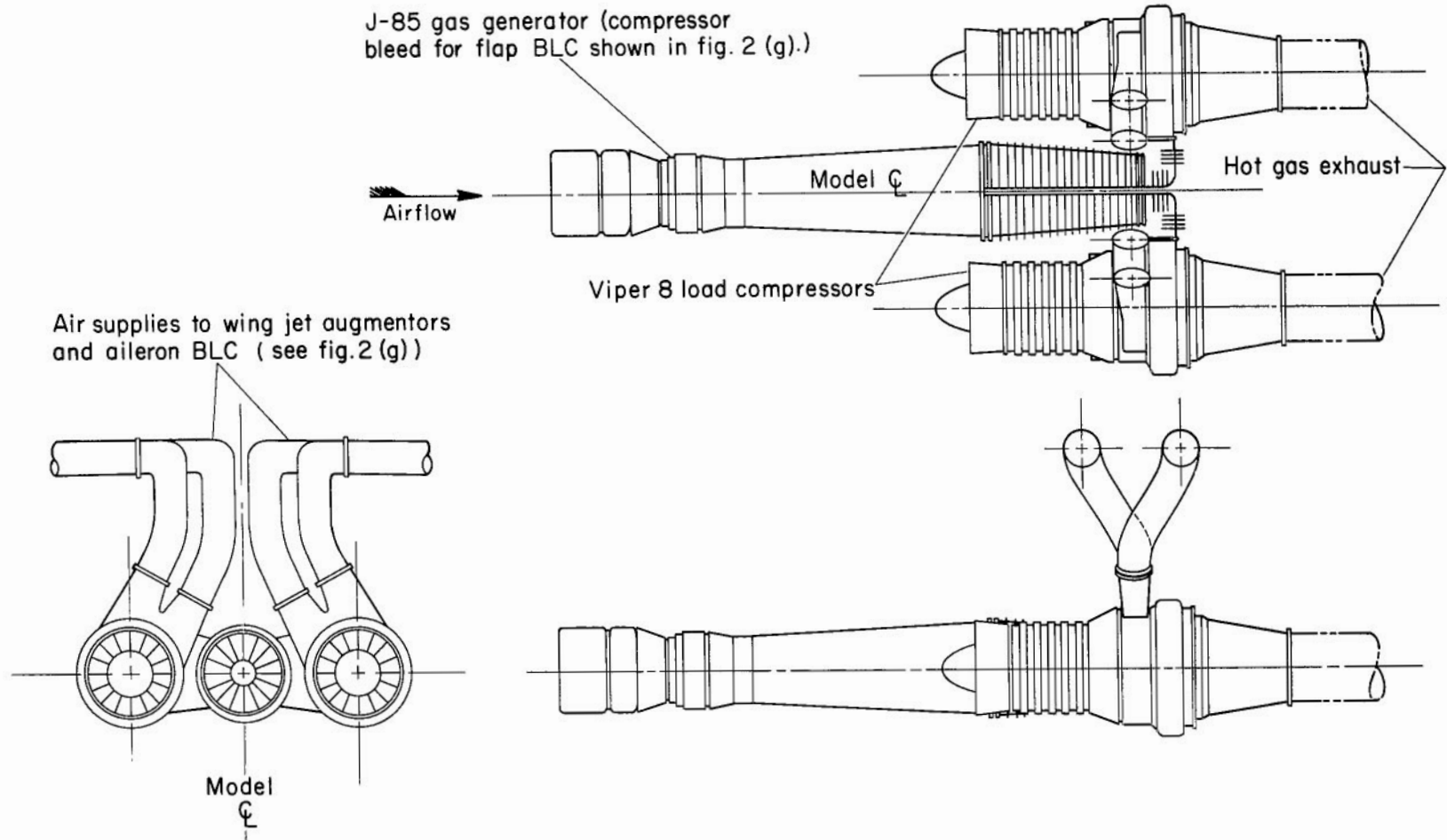
(d) Details of the augmentor.

Figure 2.- Continued.



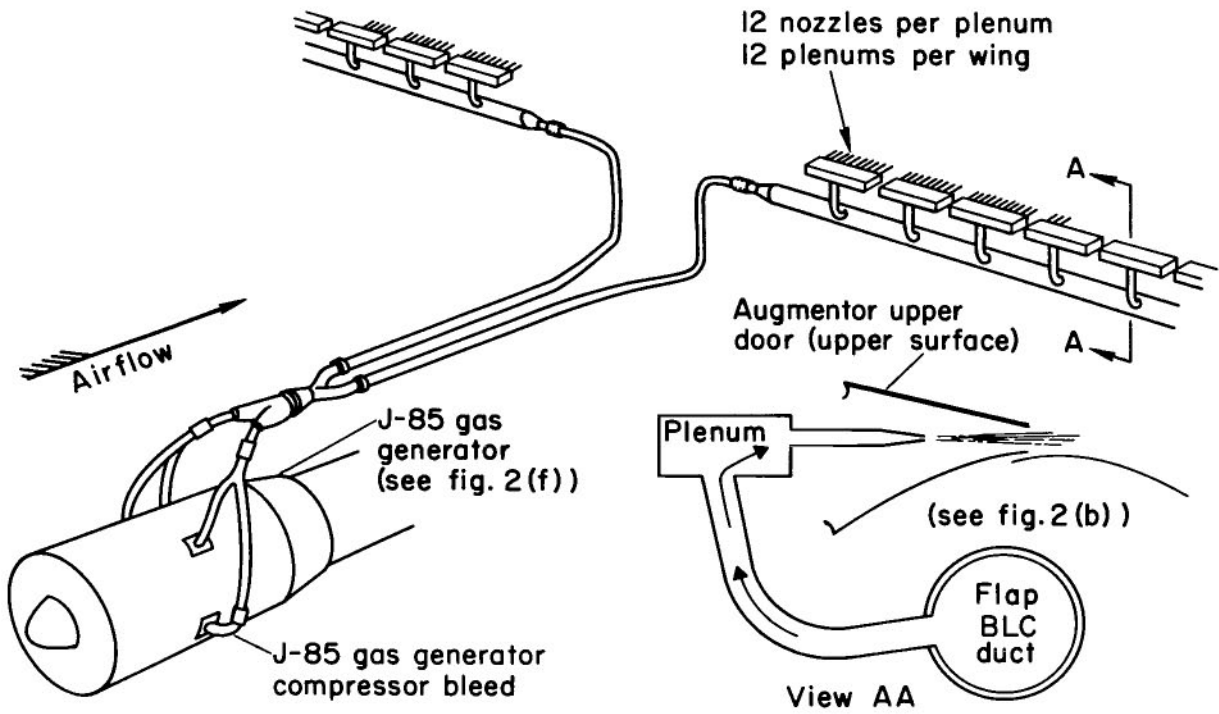
(e) Cross section of the fixed vane and lower door.

Figure 2.- Continued.

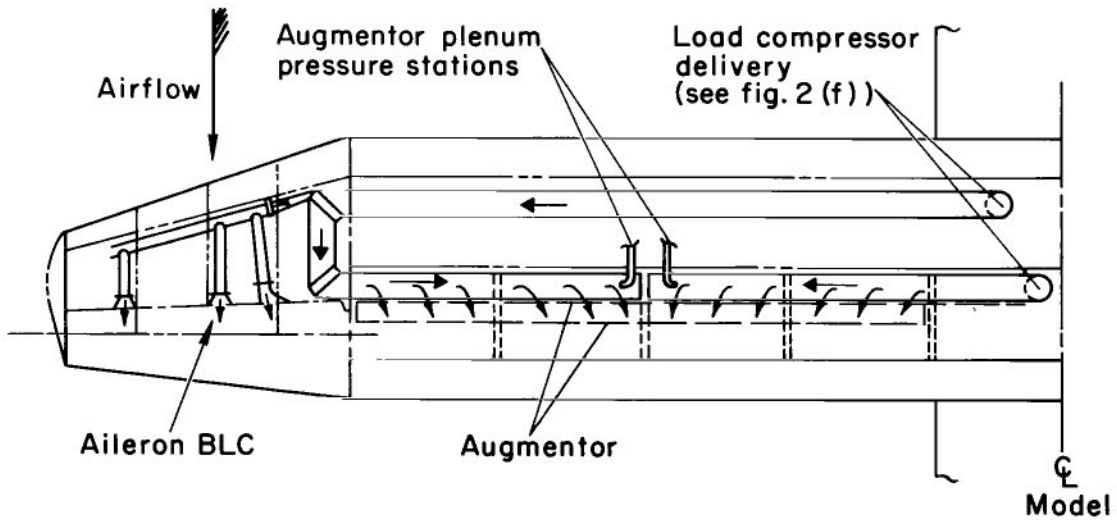


(f) Compressor assembly.

Figure 2.- Continued.



Flap BLC system



Jet augmentor and aileron BLC systems

(g) Duct system.

Figure 2.- Concluded.

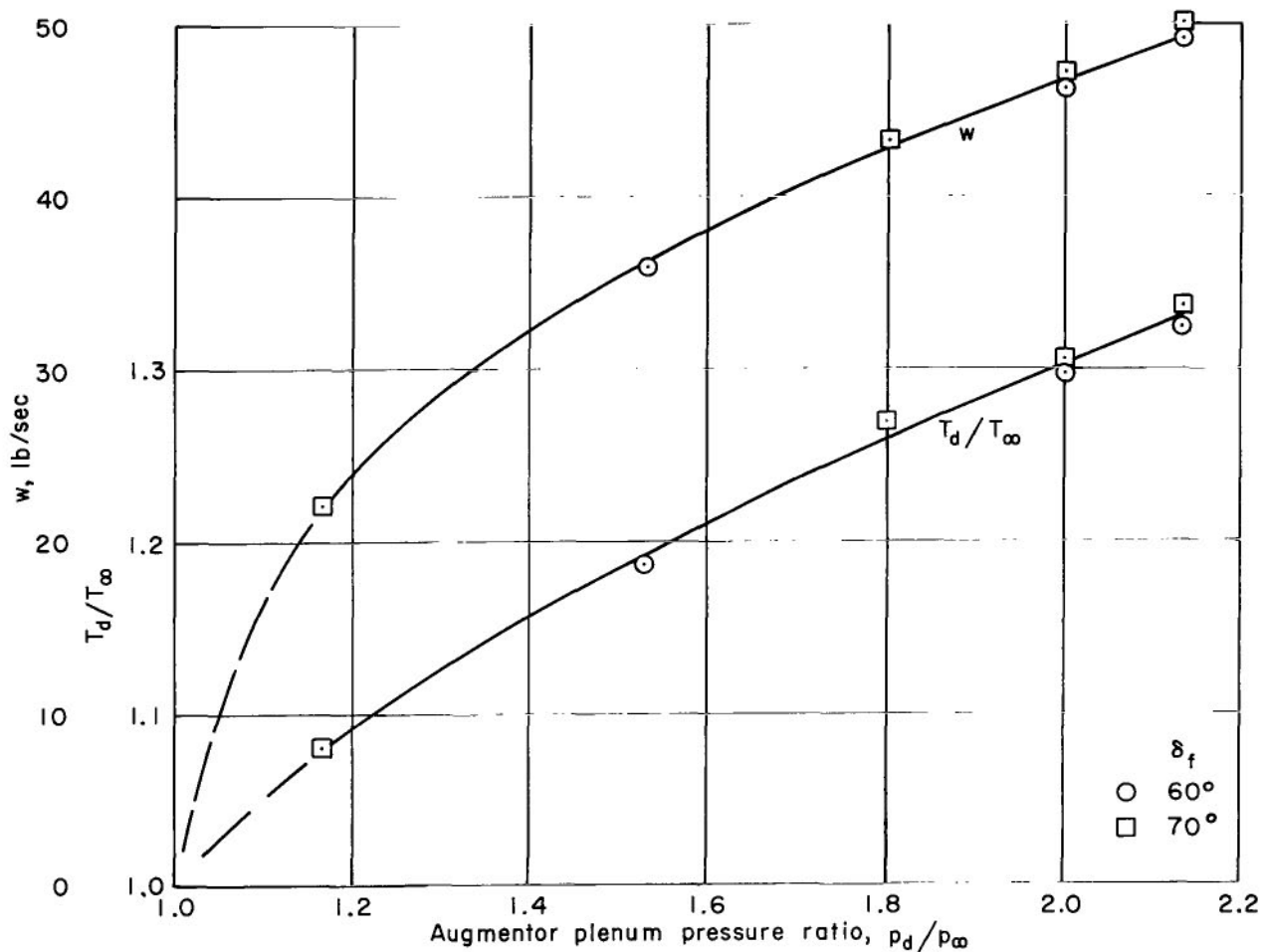


Figure 3.- Typical variations of total weight rate of flow and temperature ratio with duct pressure ratio for the air supplying the augmentor-aileron duct system;  $\delta_a = 45^\circ$ .

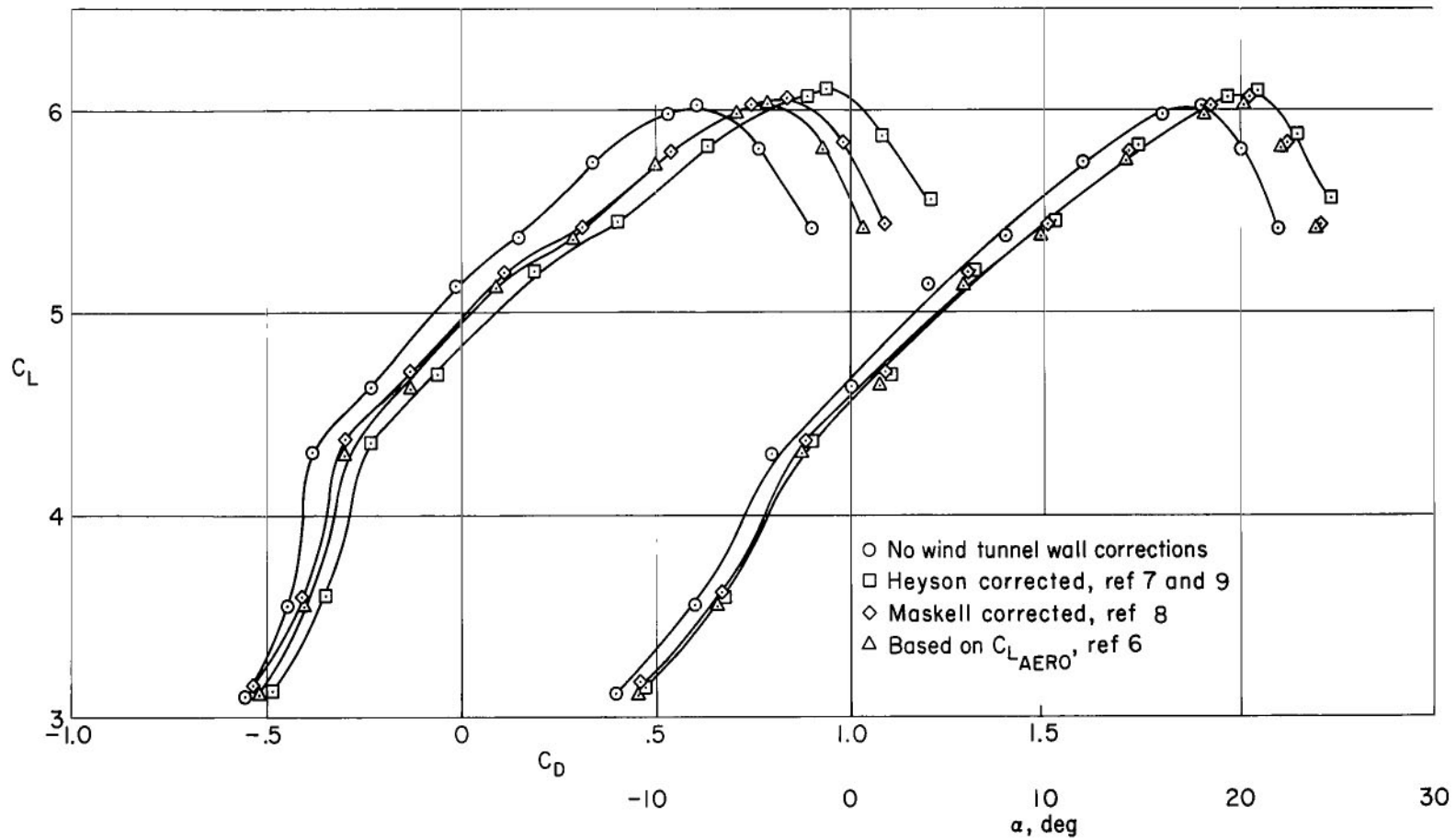
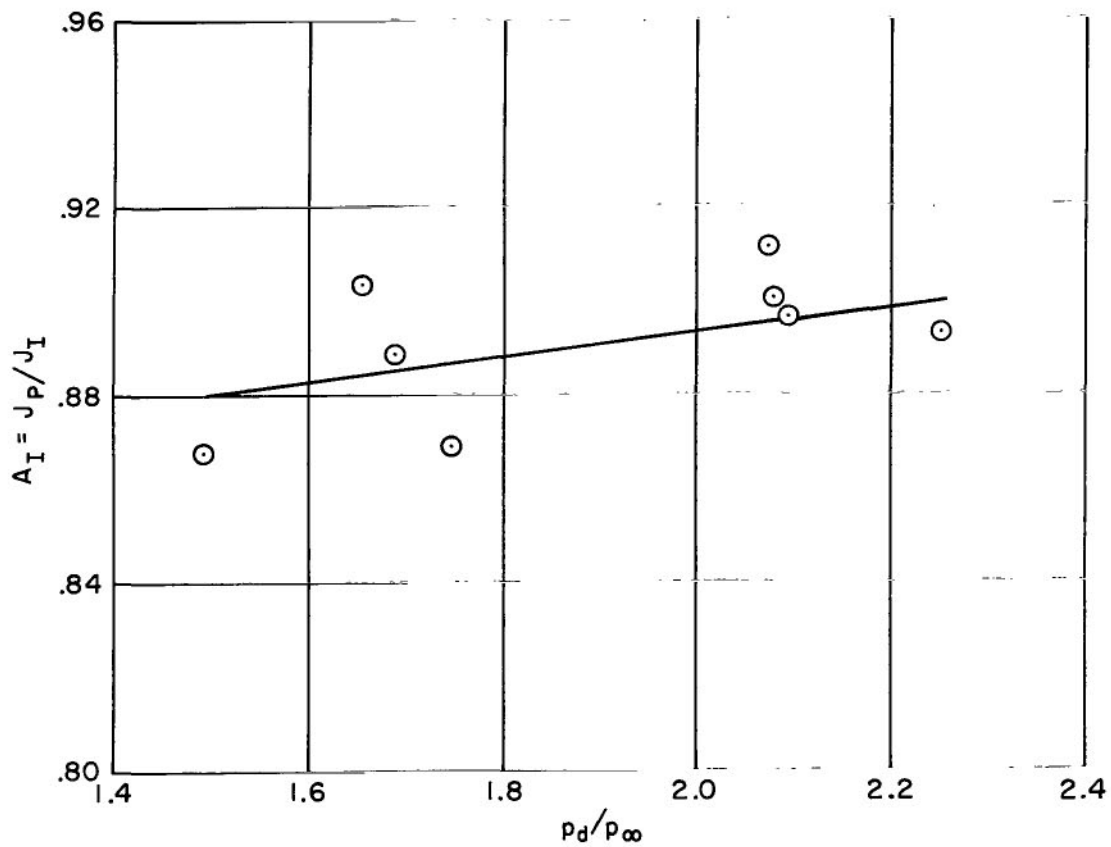
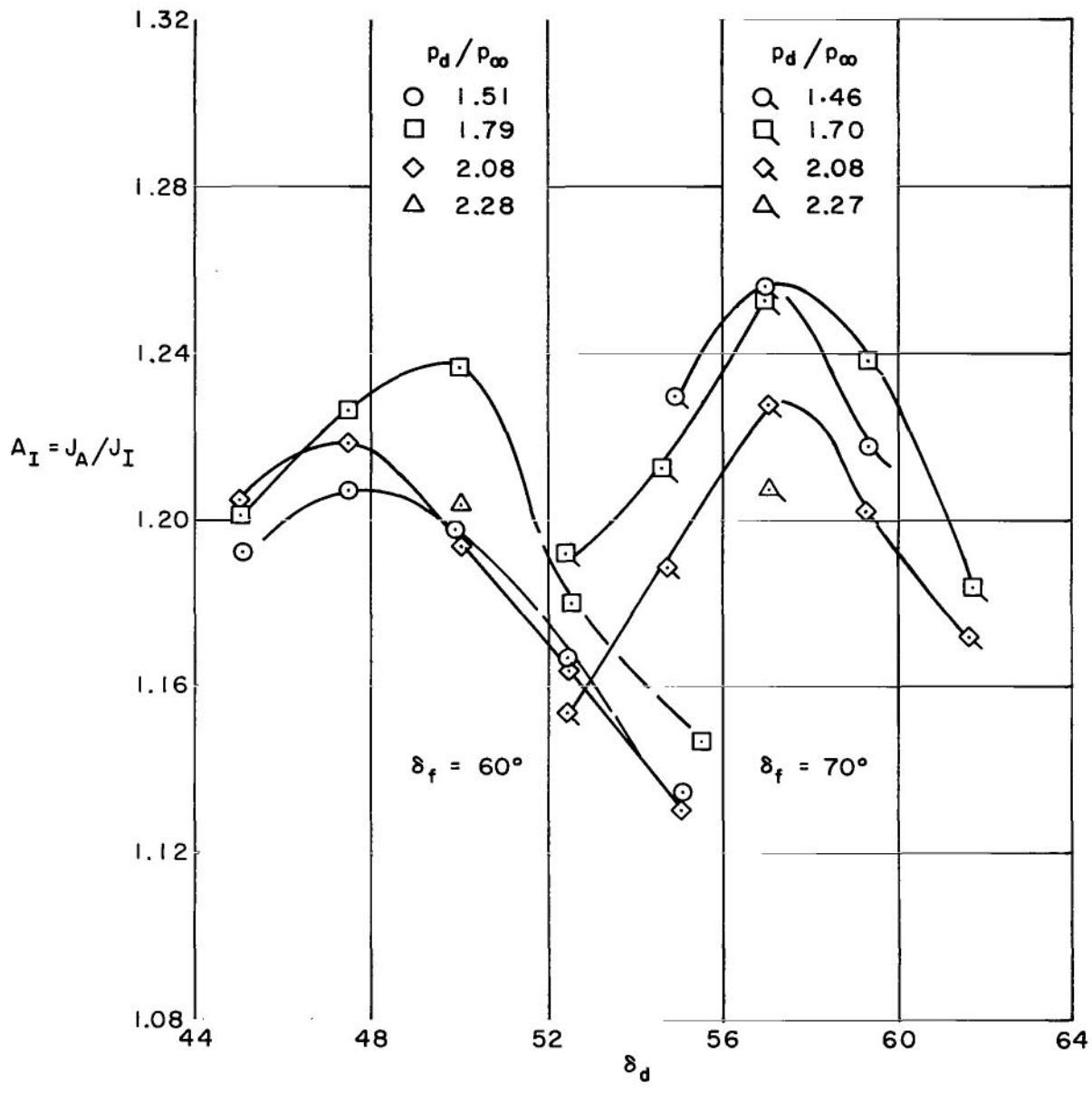


Figure 4.- Comparison of data corrected for wind-tunnel wall effects;  $\delta_F = 60^\circ$ ,  $\delta_a = 45^\circ$ ,  $C_J = 1.30$ ,  $C_{\mu_a} = 0.040$ ,  $C_{\mu_F} = 0$ , tail off.



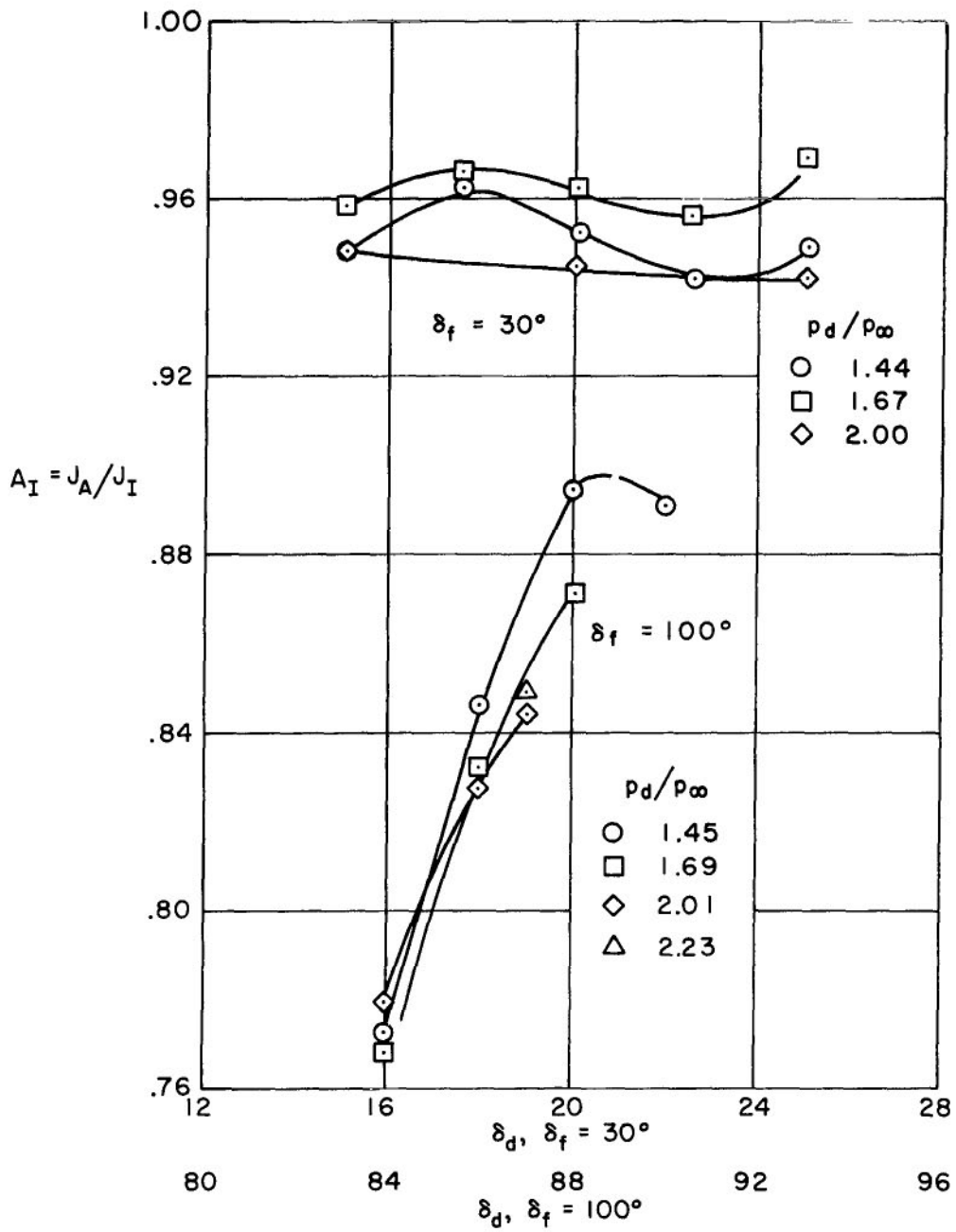
(a) Upper door and flap assembly removed;  $\delta_f = 60^\circ$ ,  $\delta_a = 0^\circ$ .

Figure 5.- Augmentation ratio as affected by pressure ratio and lower door position, measured on the static test stand.



(b) Complete augmentor;  $\delta_f = 60^\circ$  and  $70^\circ$ .

Figure 5.- Continued.



(c) Complete augmentor;  $\delta_f = 30^\circ$  and  $100^\circ$ .

Figure 5.- Concluded.

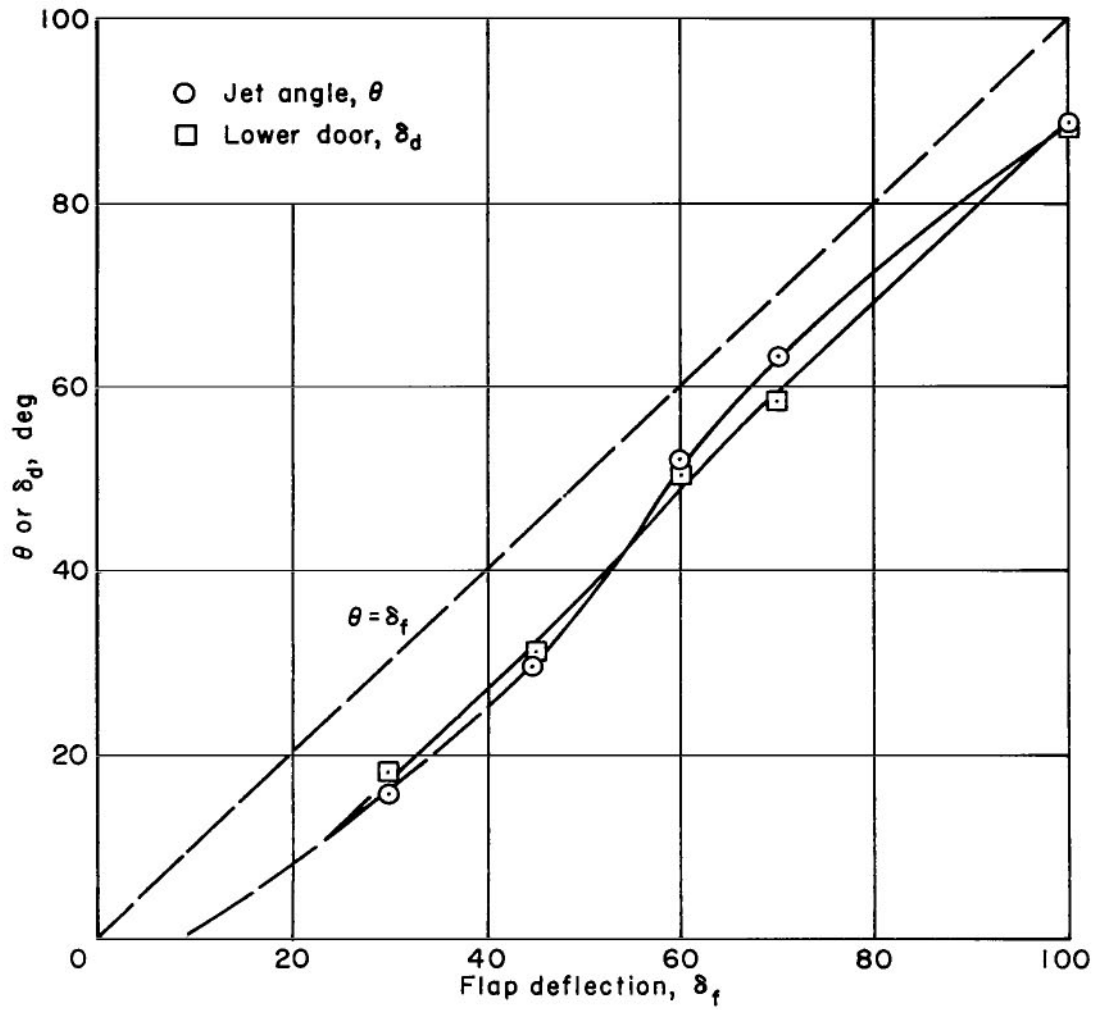


Figure 6.- Jet angle and lower door positions measured on the static test stand.

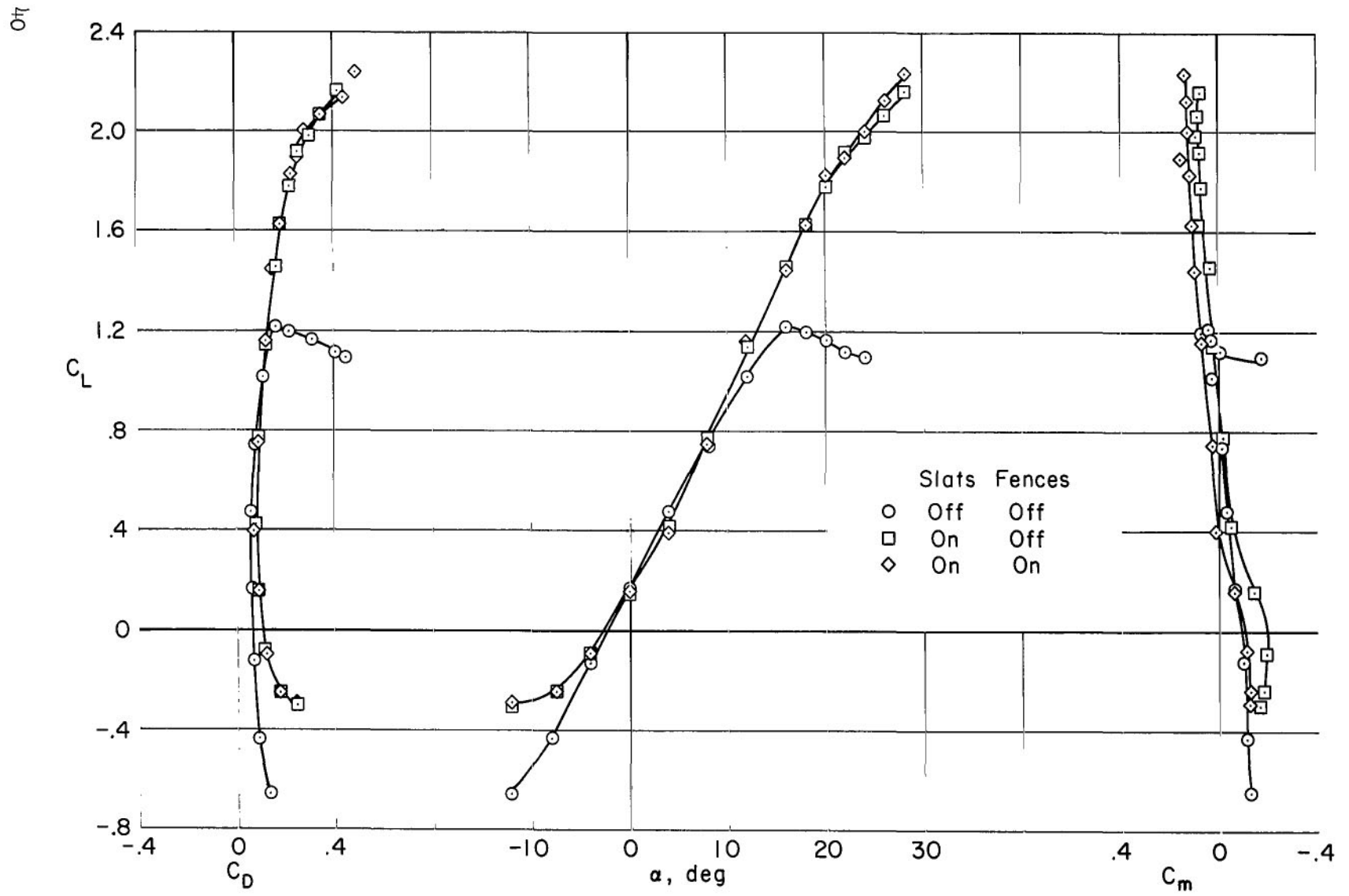


Figure 7.- Characteristics of the model with flaps retracted; tail off.

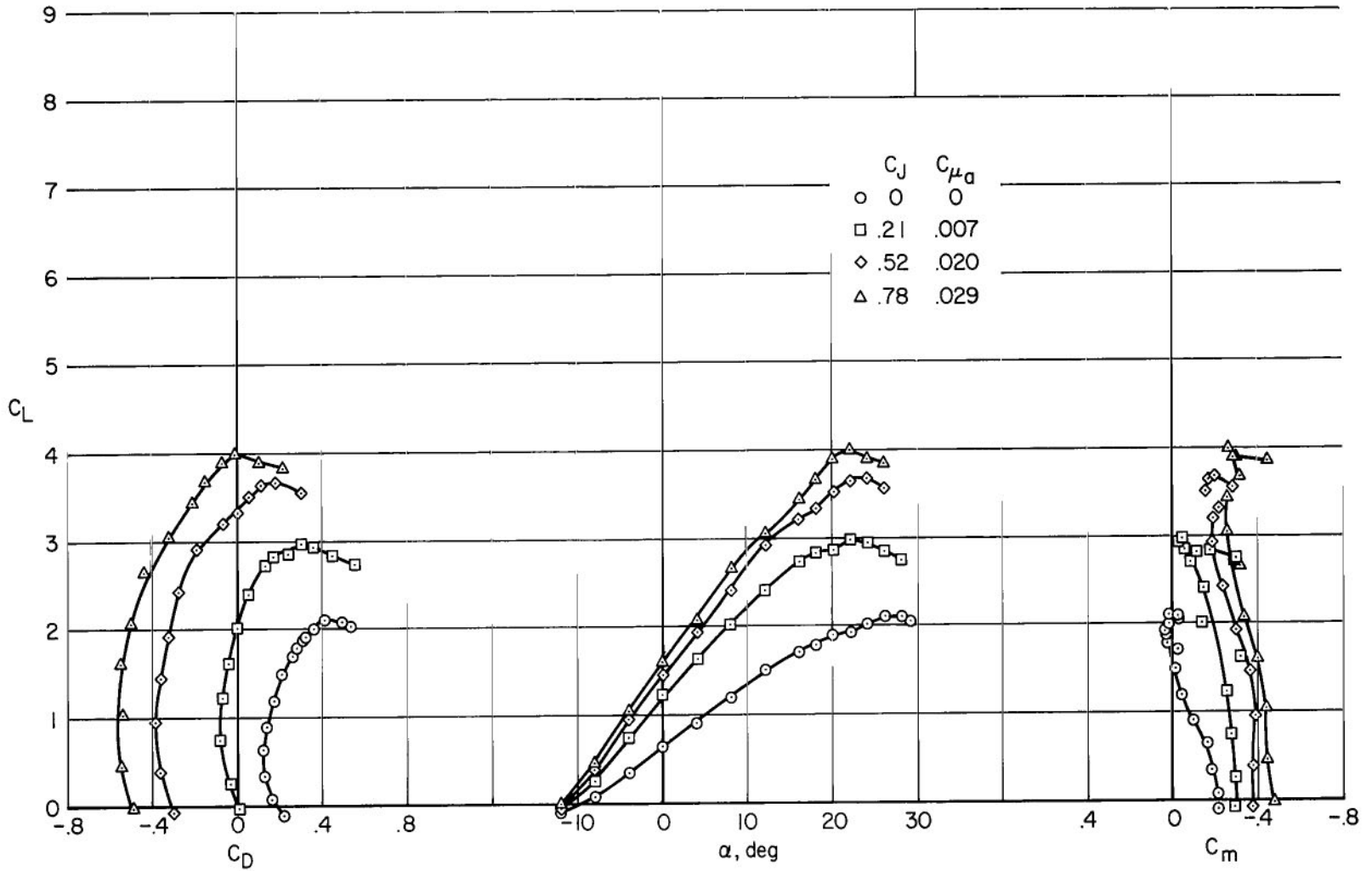


Figure 8.- The effect of  $C_J$  on the longitudinal characteristics with  $\delta_F = 30^\circ$ ;  $\delta_a = 0^\circ$ ,  $C_{\mu_F} = 0$ ,  $F$ , tail off.

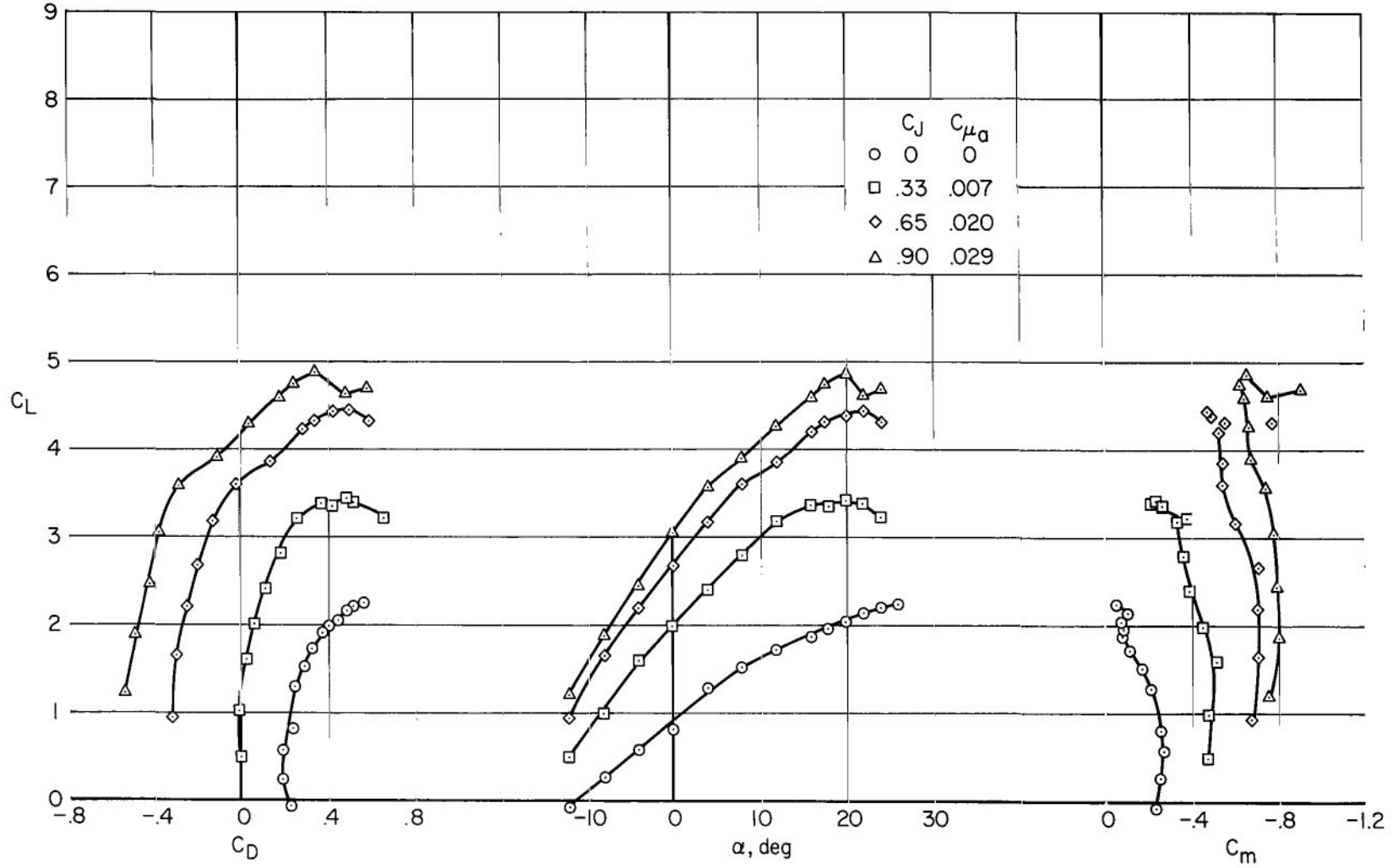


Figure 9.- The effect of  $C_J$  on the longitudinal characteristics with  $\delta_F = 45^\circ$ ;  $\delta_a = 45^\circ$ ,  $C_{\mu F} = 0$ ,  $F$ , tail off.

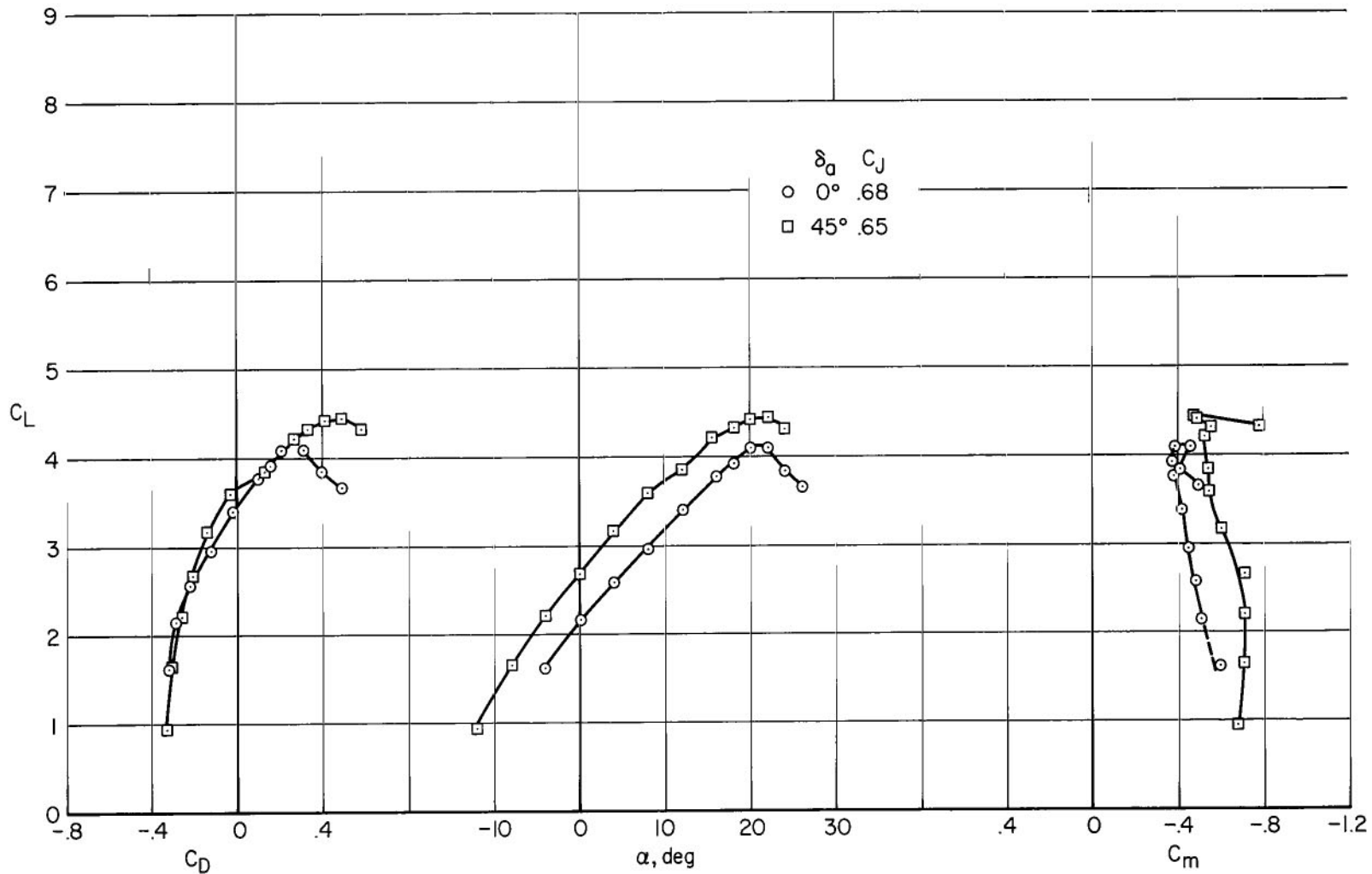


Figure 10.- The effect of symmetrical aileron deflection on the longitudinal characteristics with  $\delta_f = 45^\circ$ ;  $C_{\mu_a} = 0.20$ ,  $C_{\mu_f} = 0$ , F, tail off.

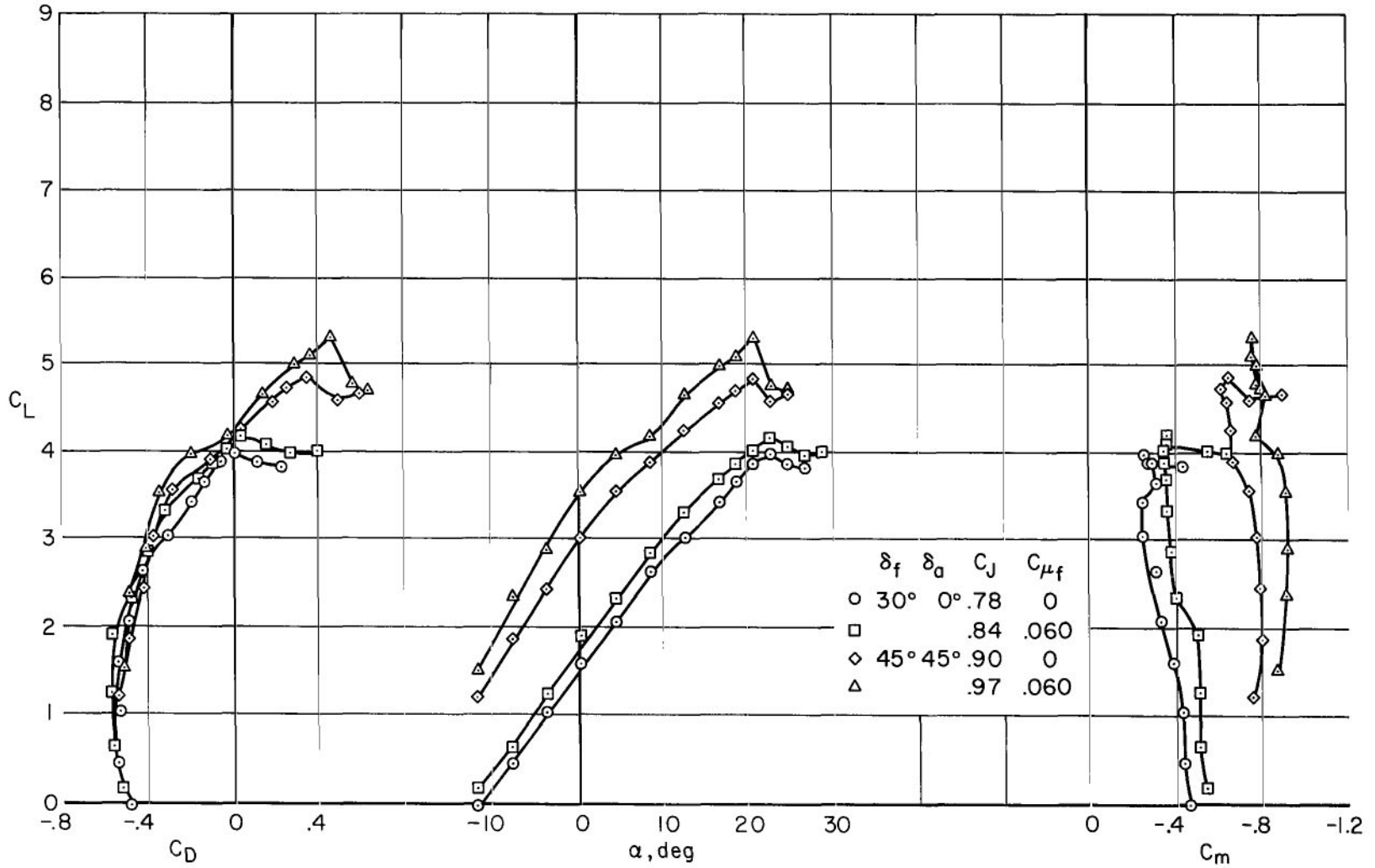
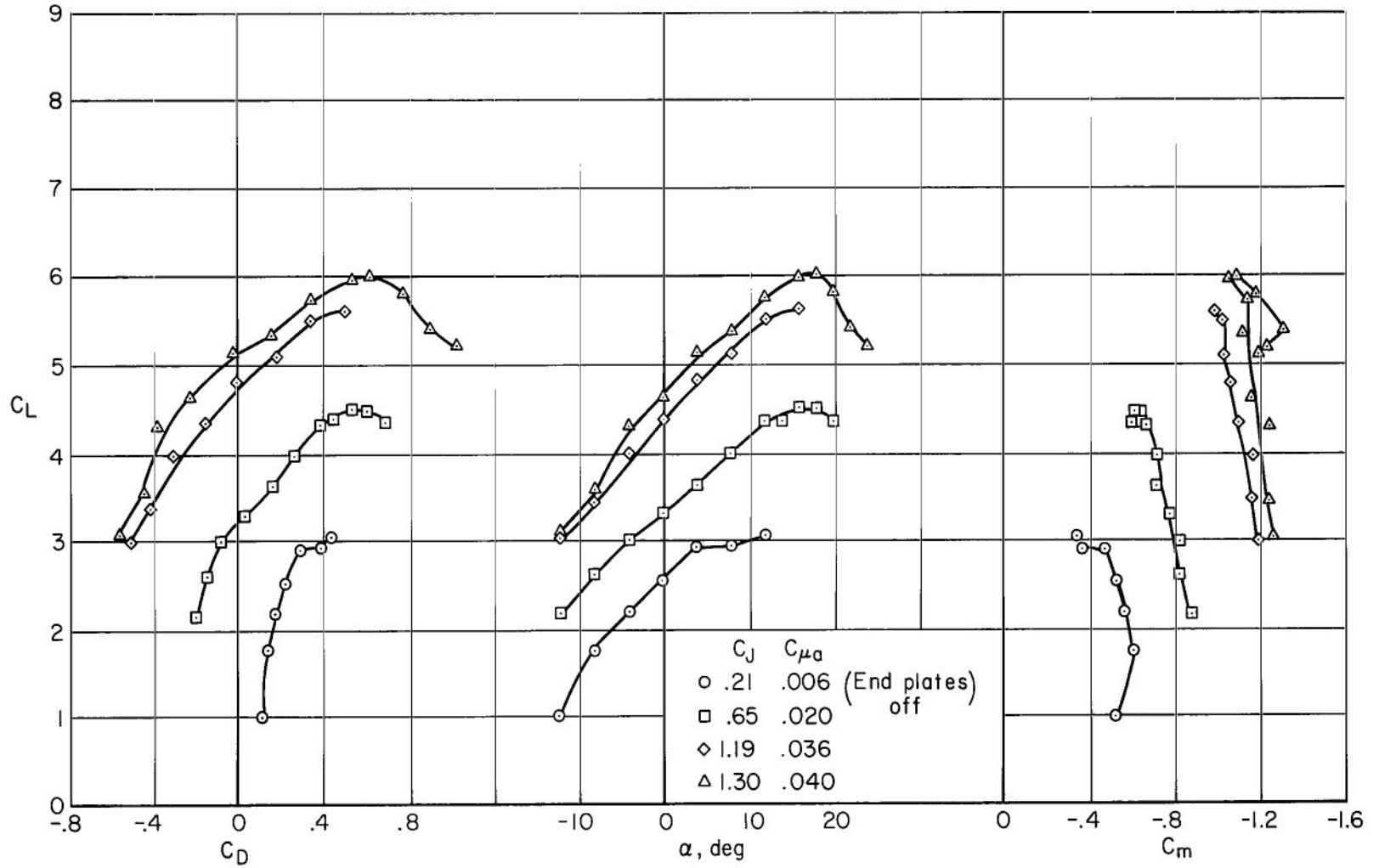
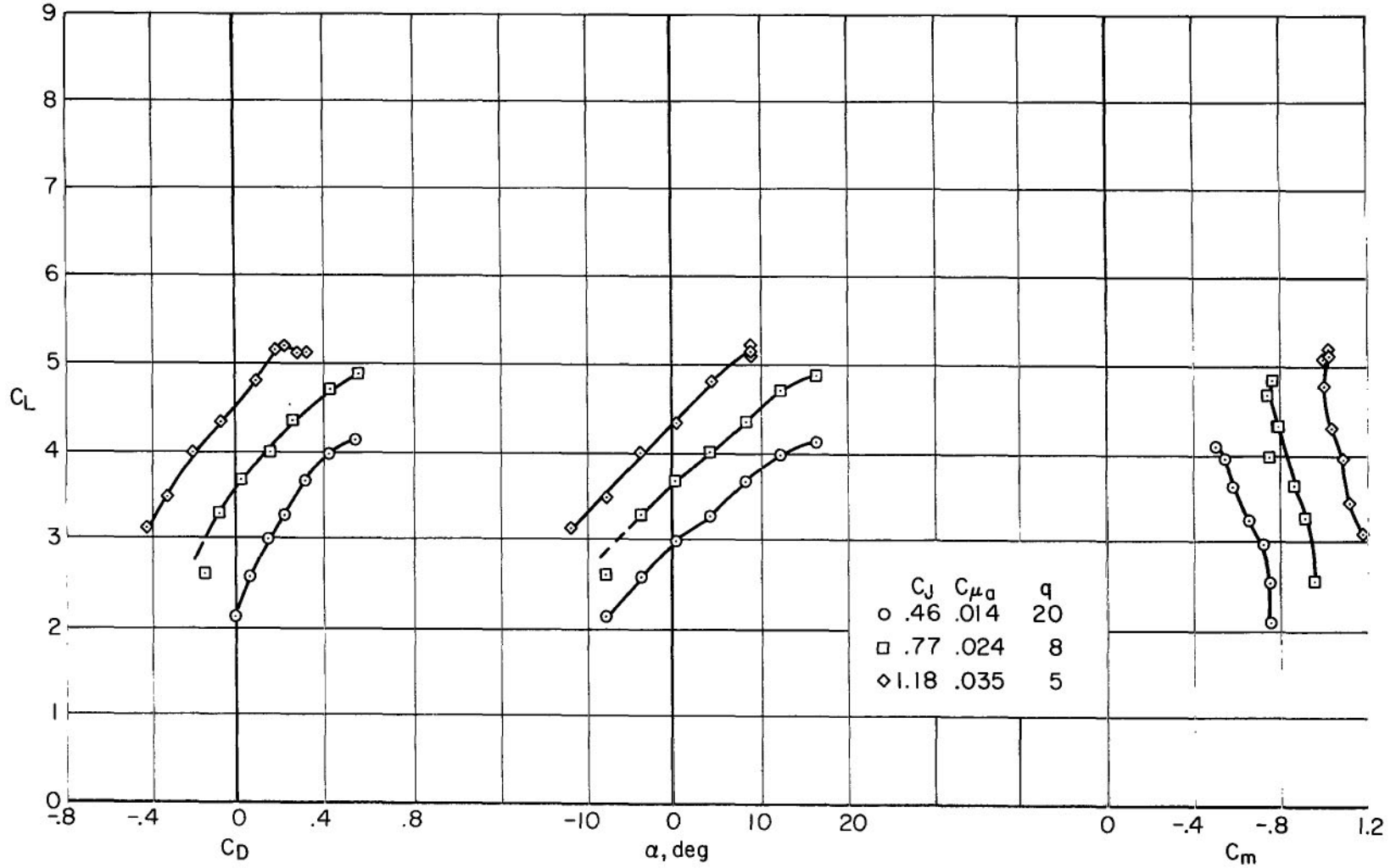


Figure 11.- Longitudinal characteristics with and without flap BLC for  $\delta_f = 30^\circ$  and  $45^\circ$ ;  $C_{\mu_a} = 0.029$ ,  $F$ , tail off.



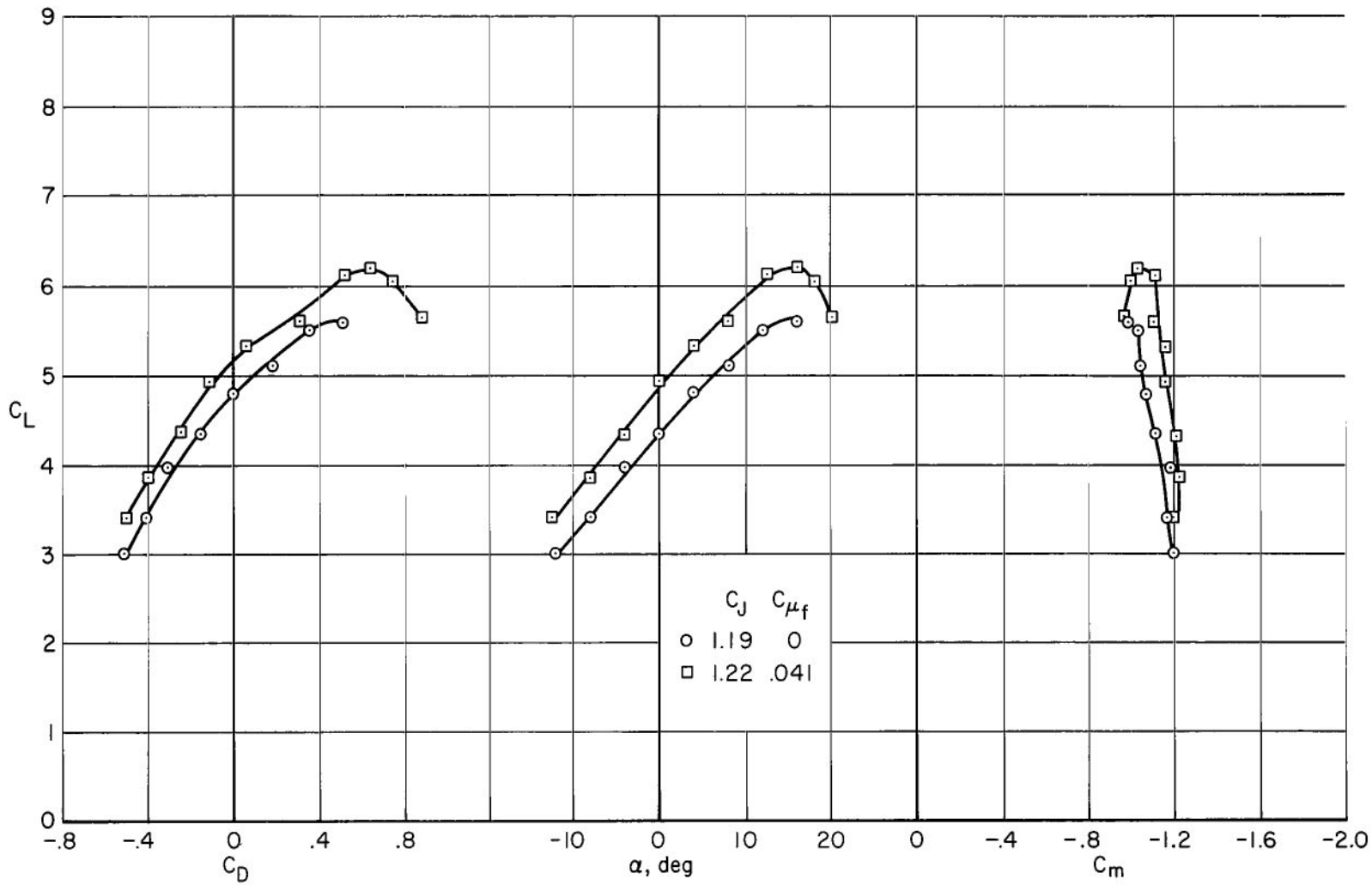
(a) Effect of  $C_J$ ;  $\delta_a = 45^\circ$ ,  $C_{\mu F} = 0$ ,  $q = 8$ .

Figure 12.- Longitudinal characteristics of the model with  $\delta_F = 60^\circ$ ; D, E, tail off.



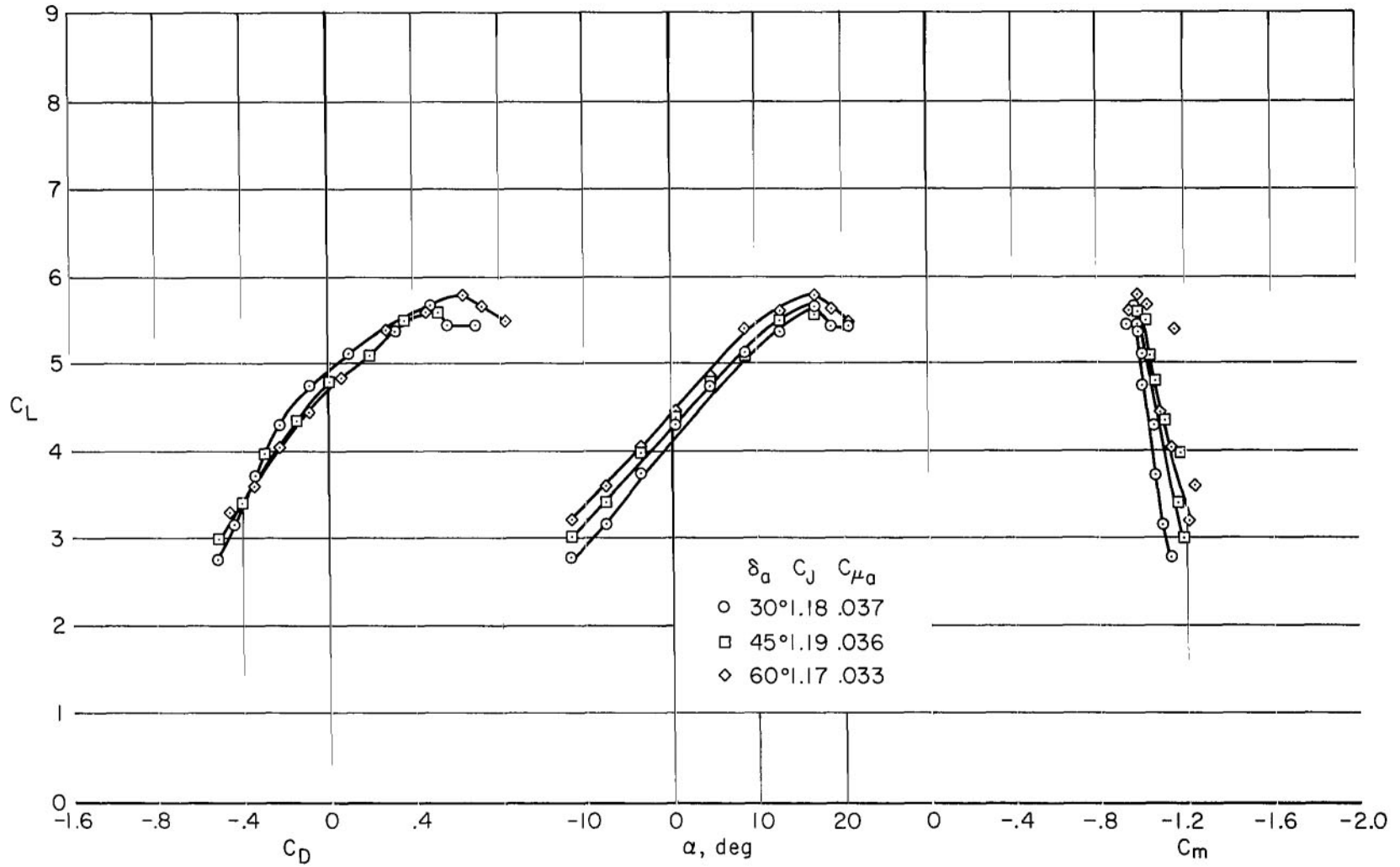
(b) Effect of  $C_J$  changed by varying dynamic pressure;  $\delta_a = 45^\circ$ ,  $C_{\mu F} = 0$ .

Figure 12.- Continued.



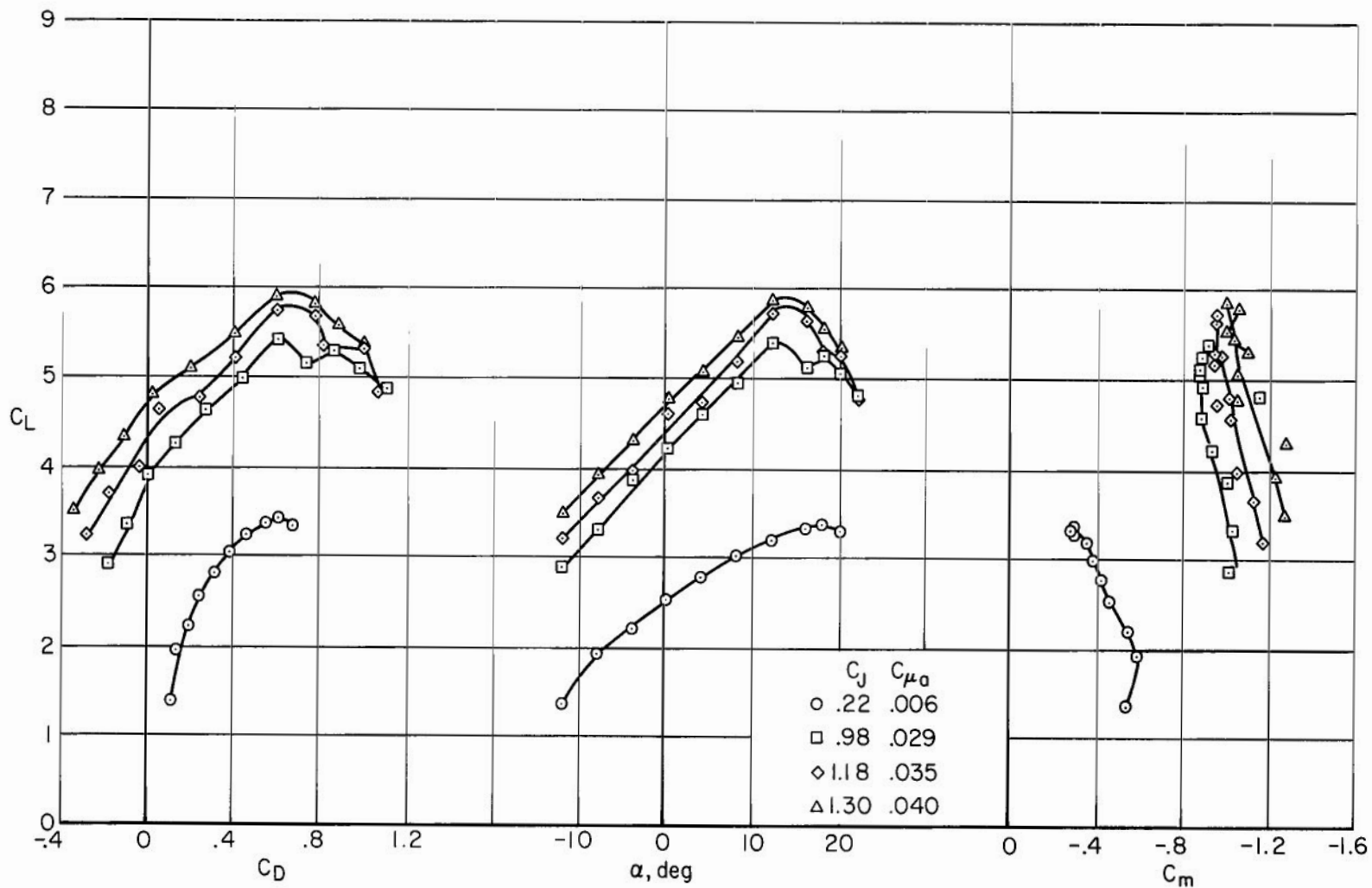
(c) Effect of flap BLC;  $\delta_a = 45^\circ$ ,  $C_{\mu_a} = 0.036$

Figure 12.- Continued.



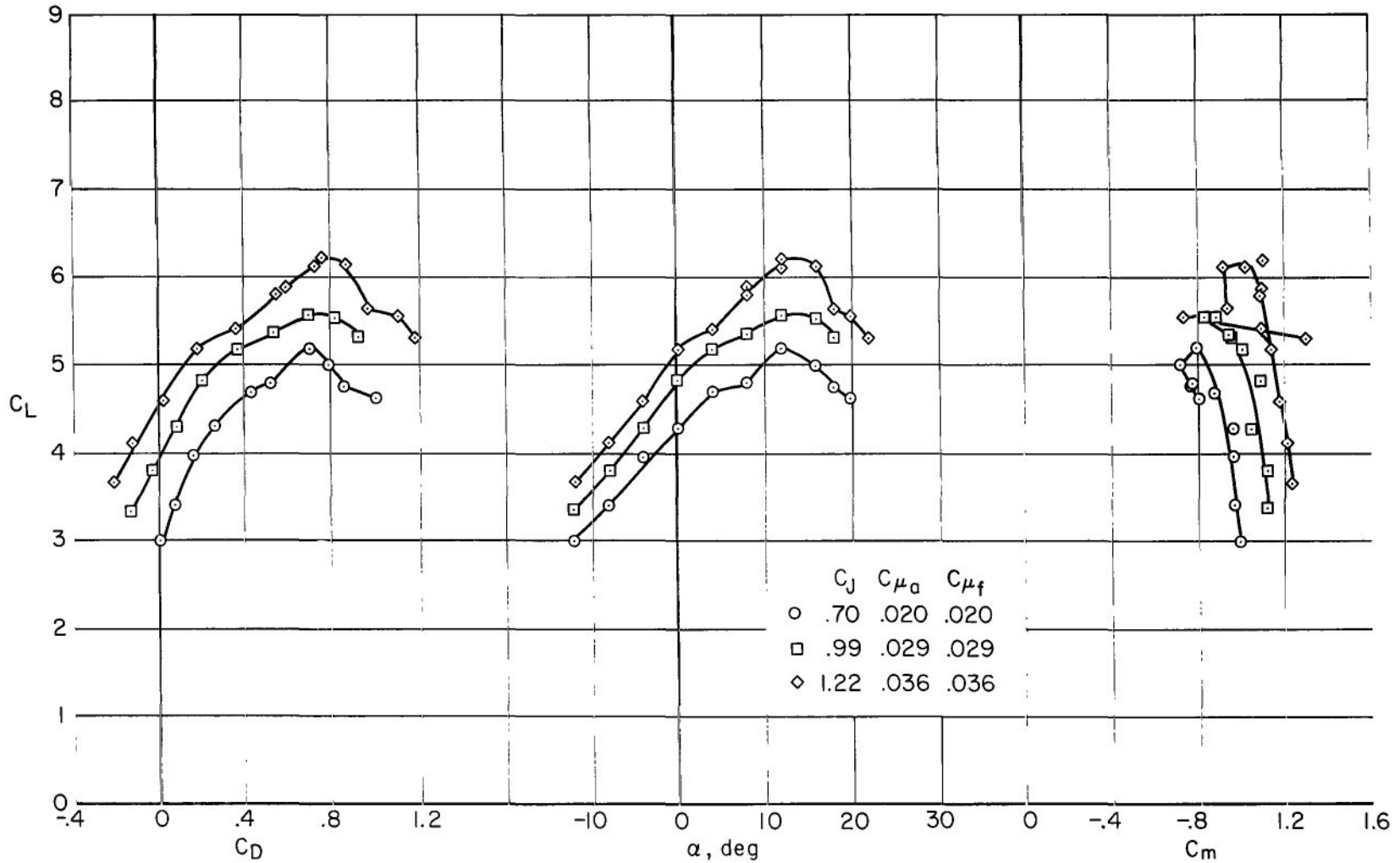
(d) Effect of aileron deflection;  $C_{\mu f} = 0$ .

Figure 12.- Concluded.



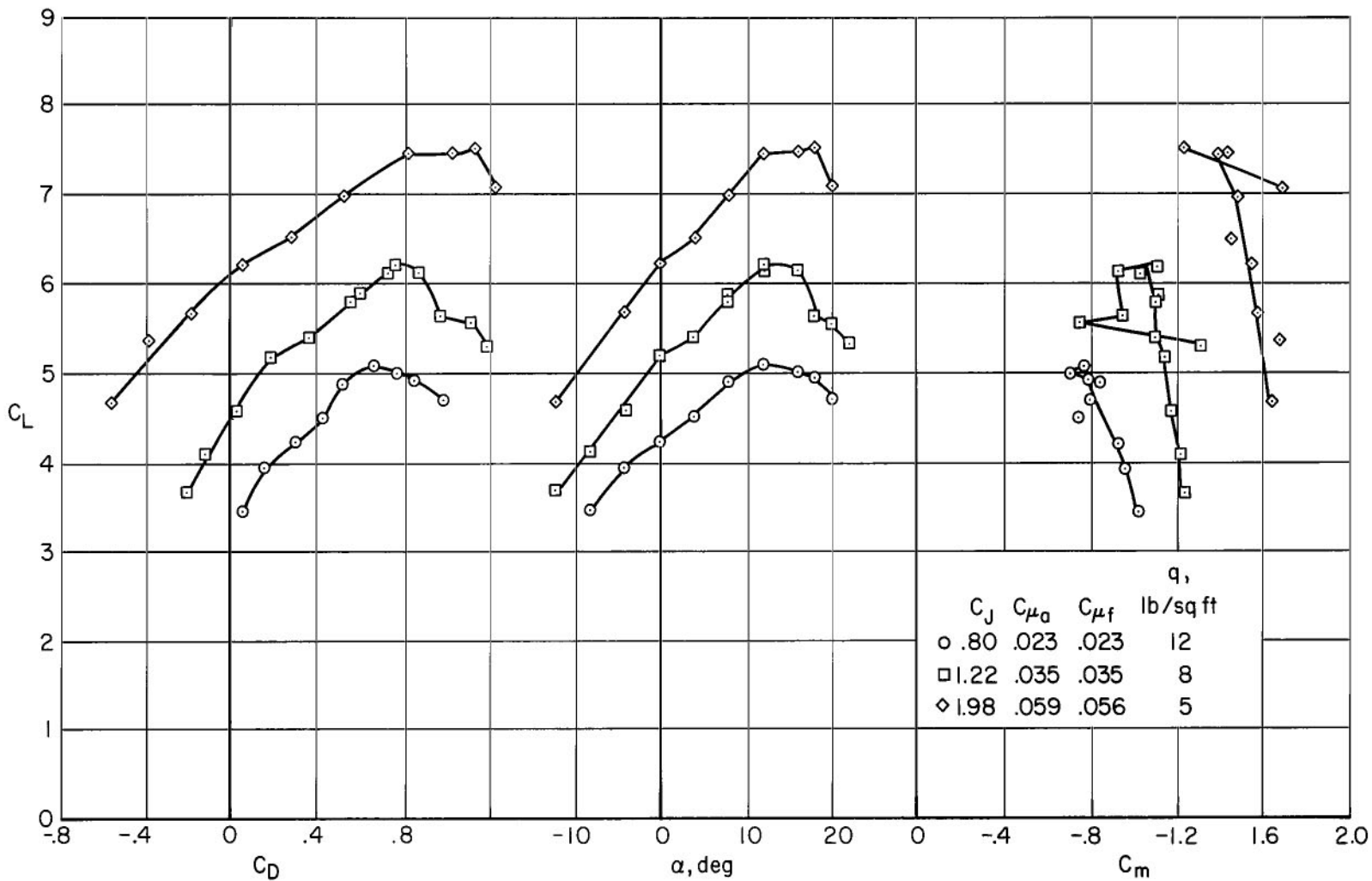
(a) Effect of  $C_J$ ;  $C_{\mu f} = 0$ ,  $\delta_a = 45^\circ$ ,  $q = 8$ .

Figure 13.- Longitudinal characteristics of the model with  $\delta_f = 70^\circ$  and tail off; D.



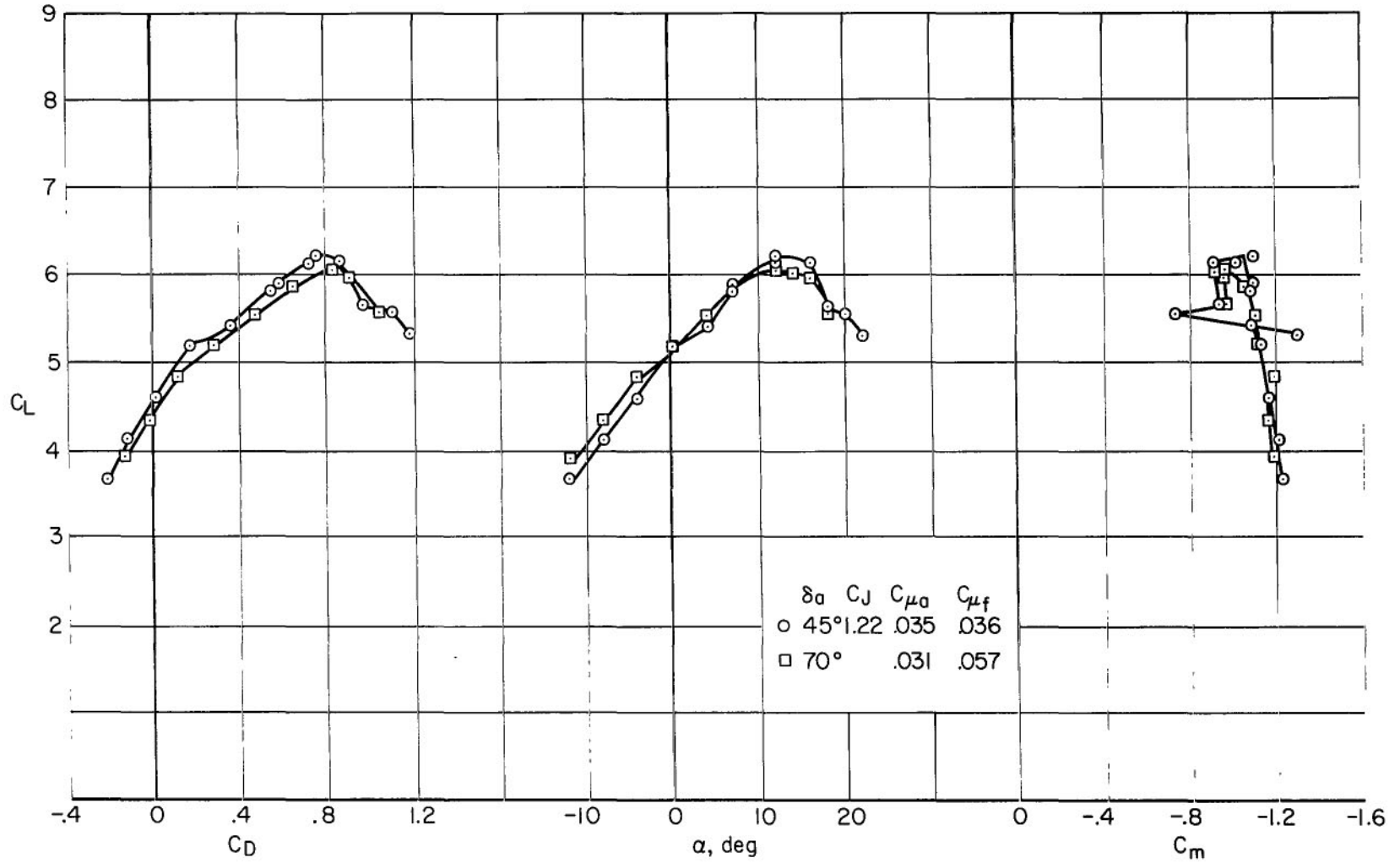
(b) Effect of  $C_J$  with flap BLC on;  $\delta_a = 45^\circ$ .

Figure 13.- Continued.



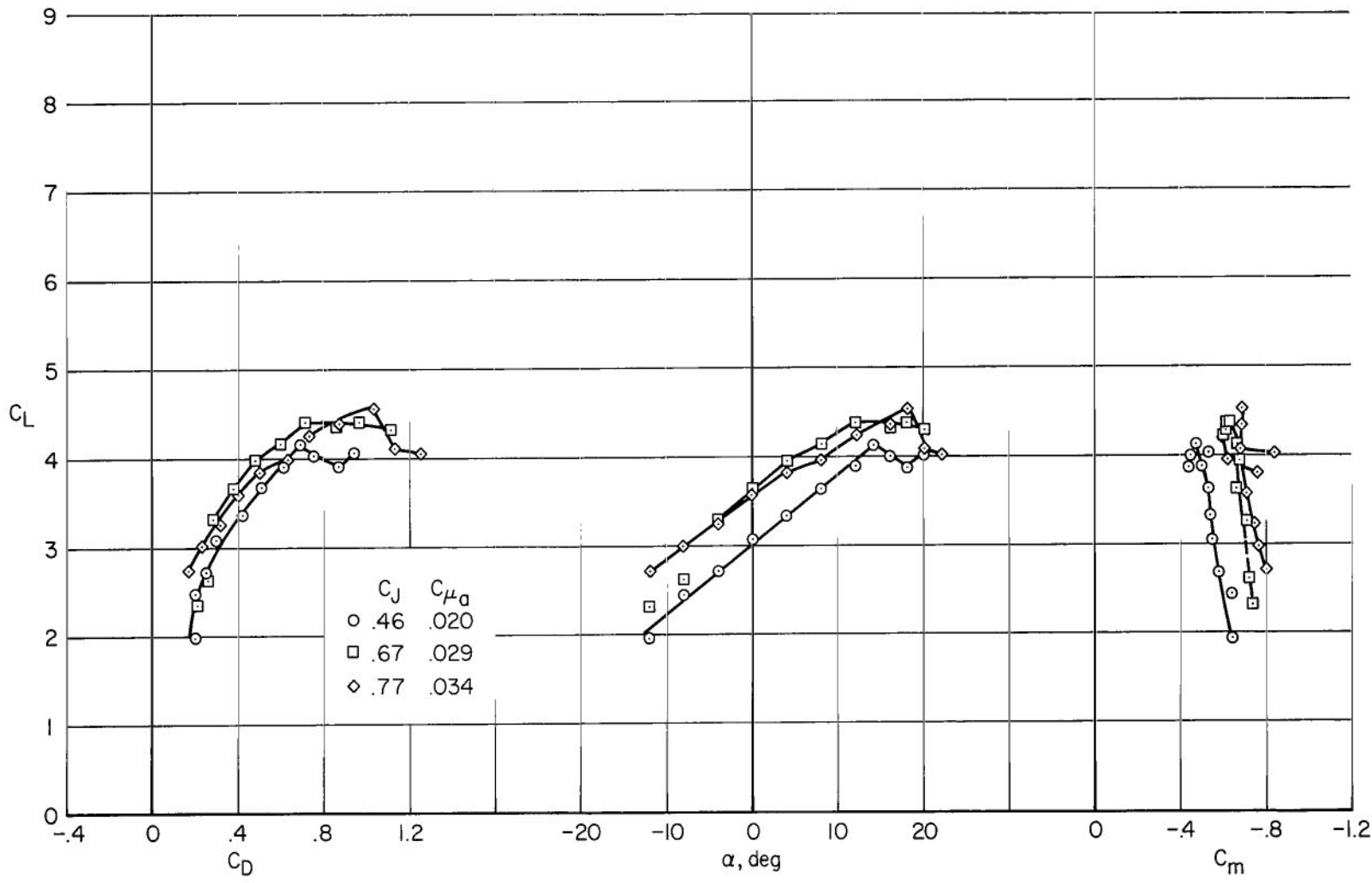
(c) Effect of  $C_J$  changed by varying dynamic pressure;  $\delta_a = 45^\circ$ .

Figure 13.- Continued.



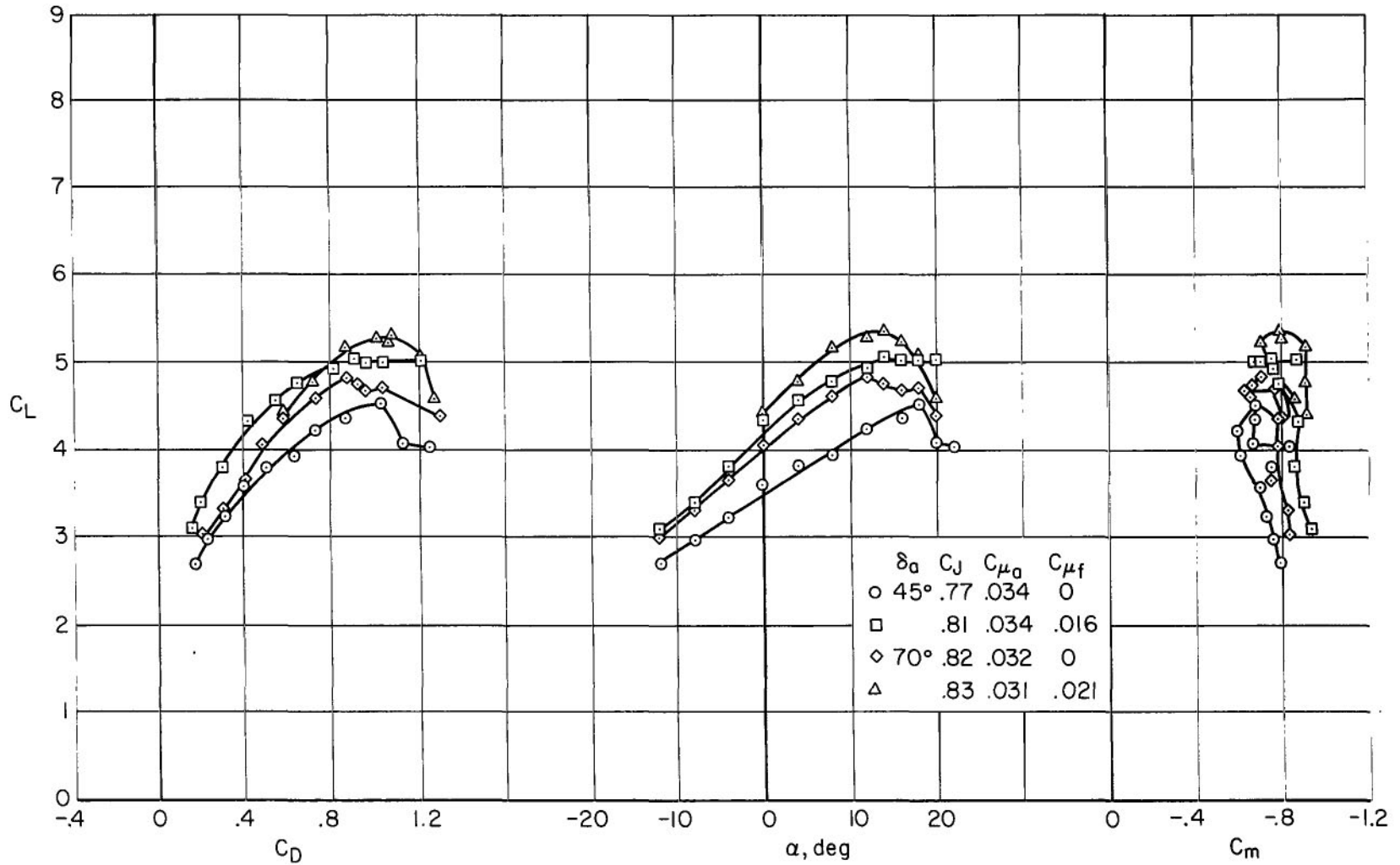
(d) Effect of symmetrical aileron deflection; BLC on.

Figure 13.- Concluded.



(a) Effect of  $C_J$ ;  $\delta_a = 45^\circ$ ,  $C_{\mu_F} = 0$ .

Figure 14.- Longitudinal characteristics of the model with  $\delta_f = 100^\circ$  and tail off; F.



(b) Effect of ailerons and flap BLC.

Figure 14.- Concluded.

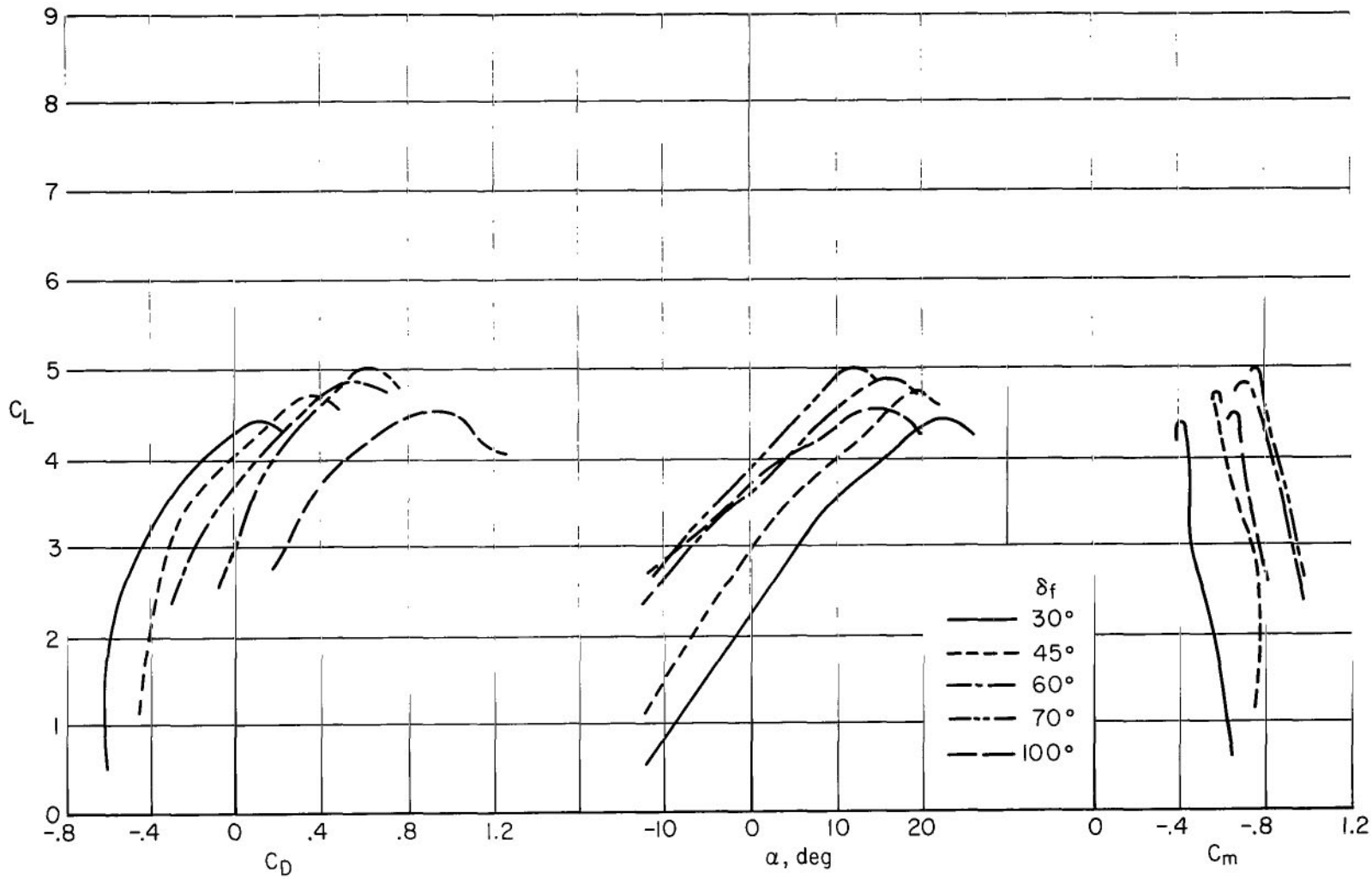
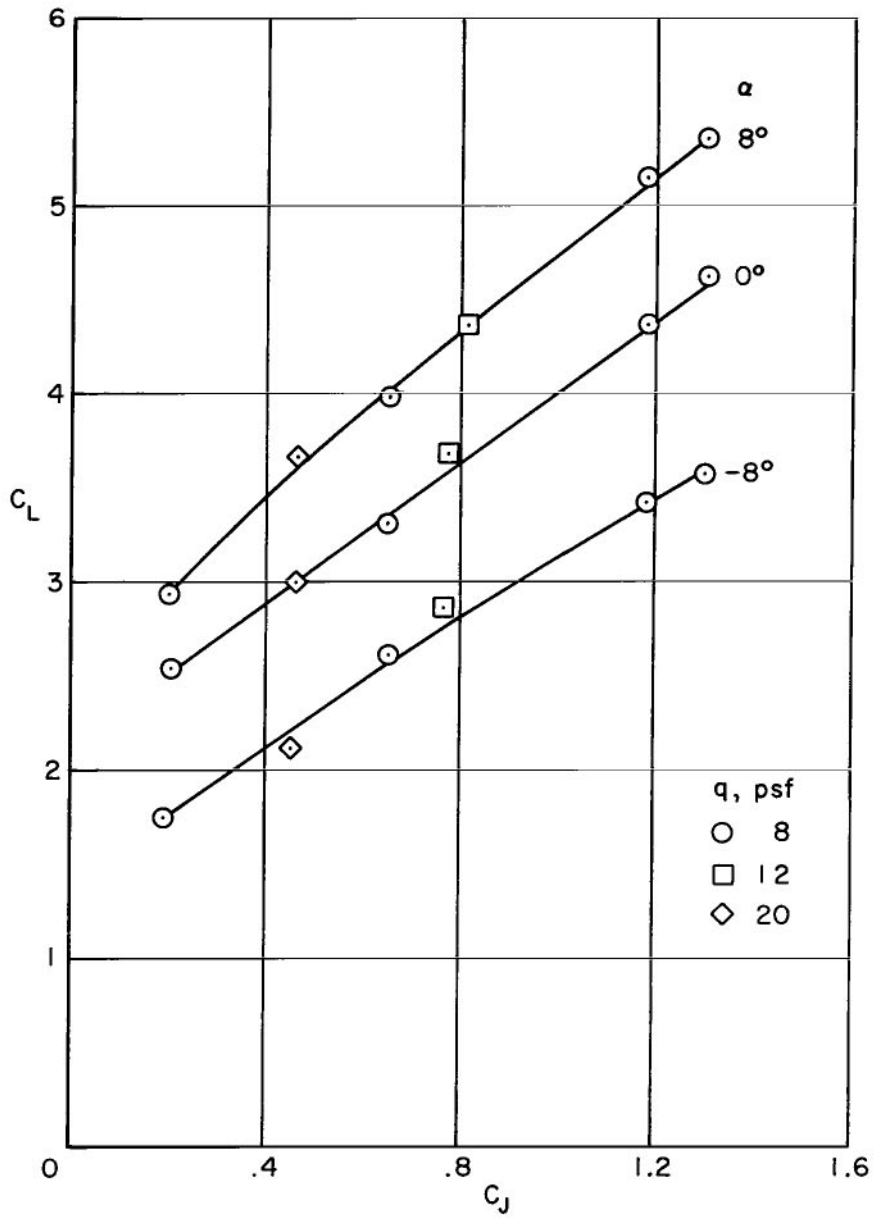
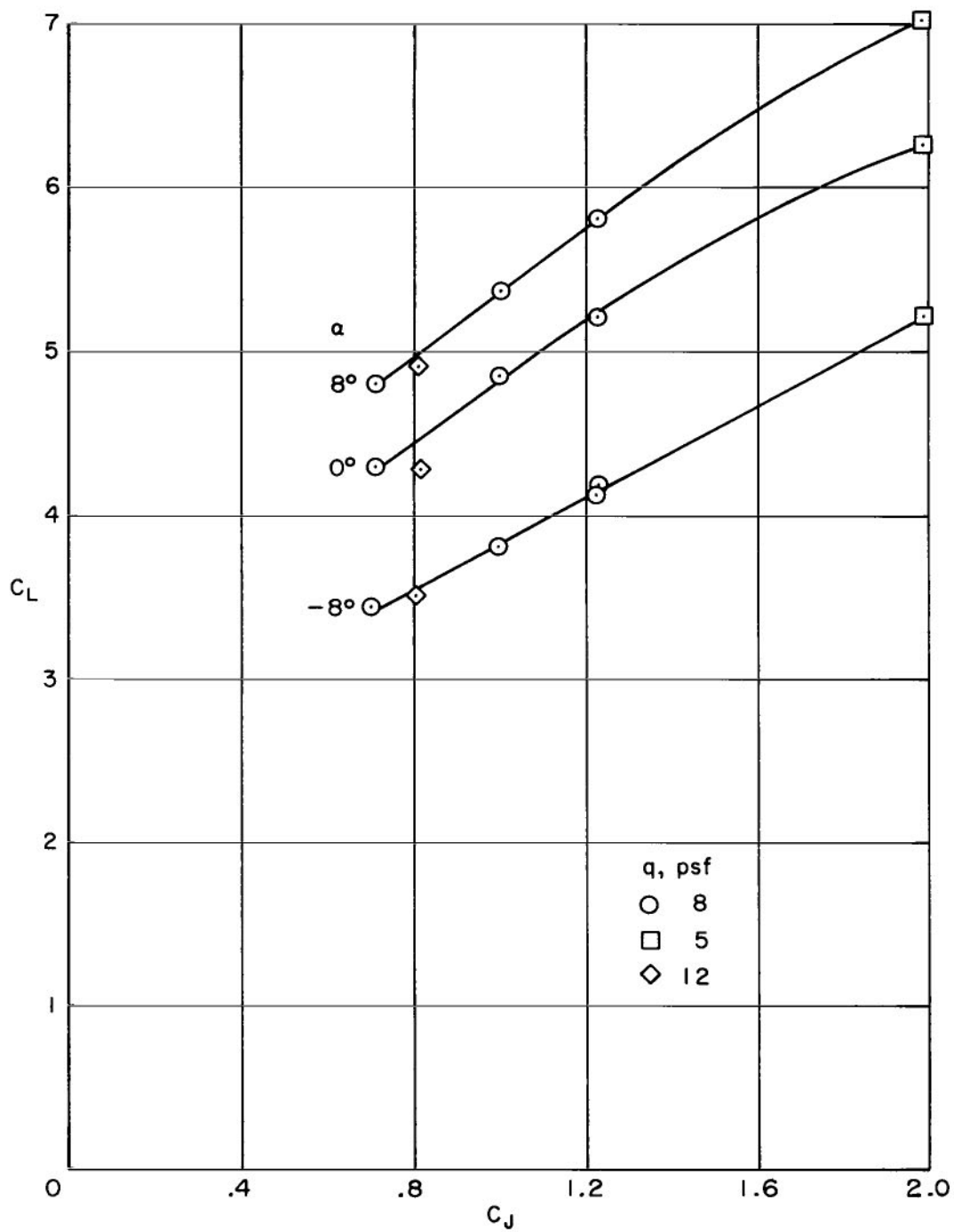


Figure 15.- The effect of augmentor flap deflection on the characteristics of the model with  $C_J = 0.81$ ;  $\delta_a = 45^\circ$ ,  $C_{\mu_a} = 0.03$ ,  $C_{\mu_f} = 0$ , tail off.



(a)  $\delta_F = 60^\circ$ ; BLC off.

Figure 16.- The variation of lift with jet coefficient for several airspeeds.



(b)  $\delta_F = 70^\circ$ ; BLC on.

Figure 16.- Concluded.

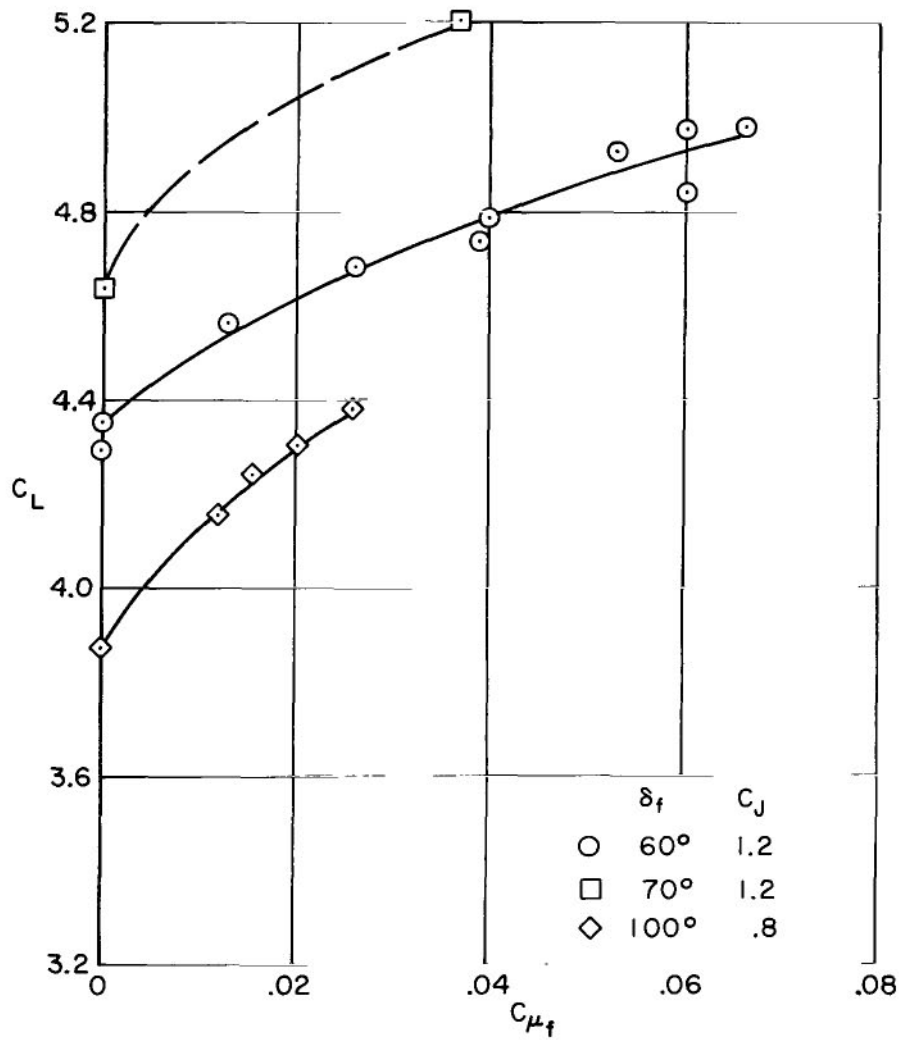
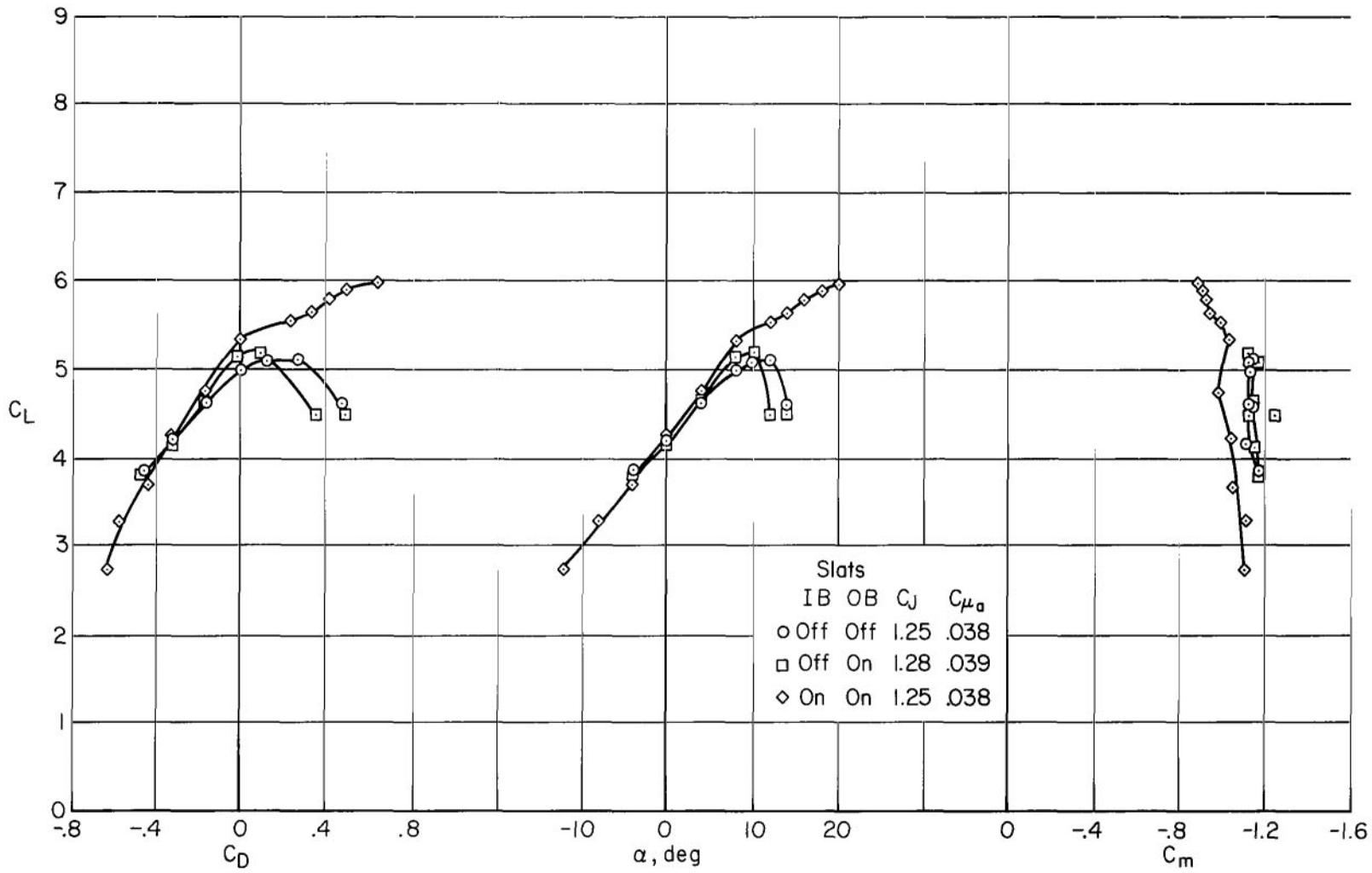
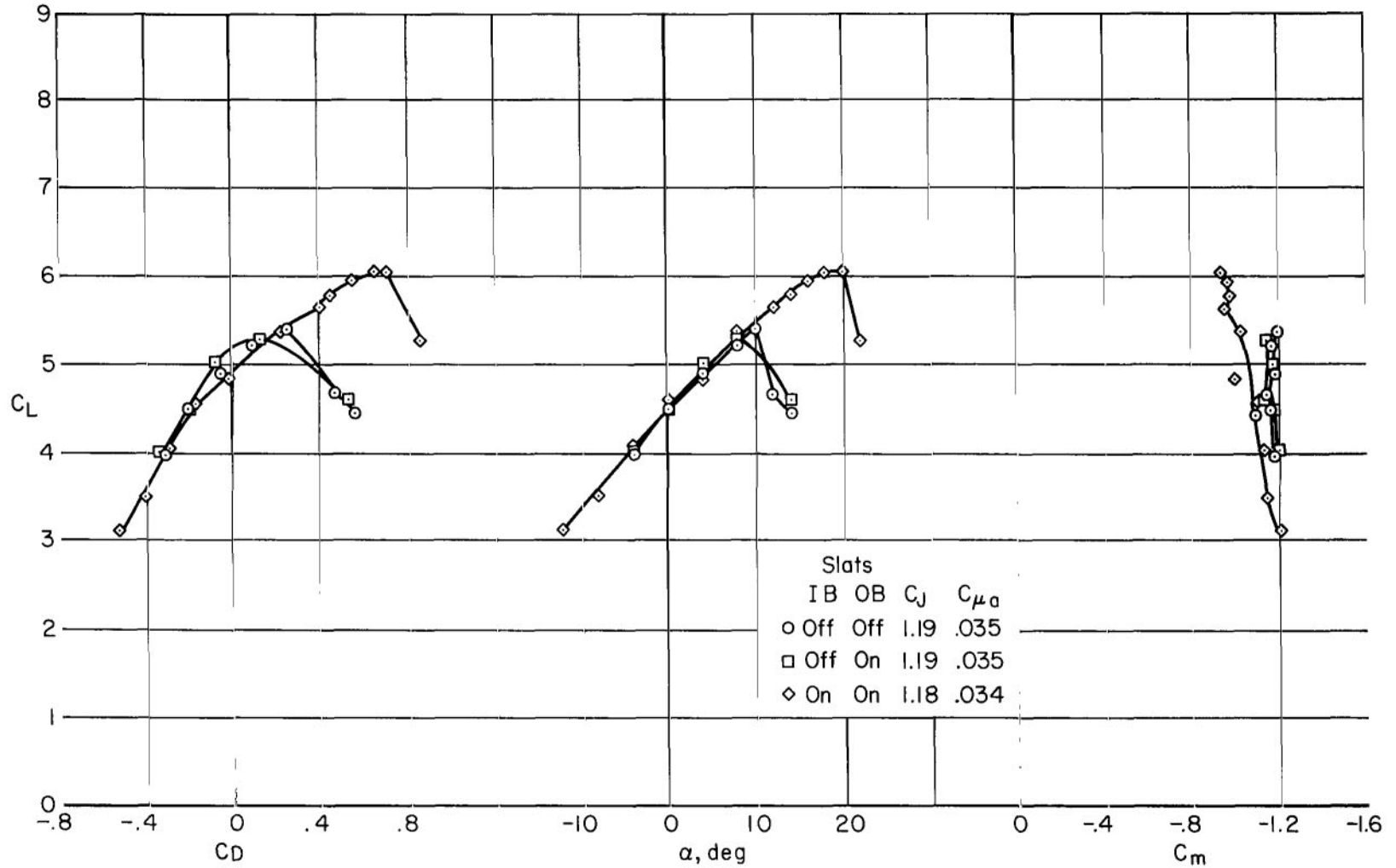


Figure 17.- The variation of lift coefficient with flap BLC coefficient,  $C_{\mu_f}$ , for zero angle of attack.



(a)  $C_{\mu_f} = 0$

Figure 18.- The effect of leading-edge slats on the characteristics of the model with tail off;  $\delta_f = 60^\circ$ ,  $\delta_a = 45^\circ$ , F.



(b)  $C_{\mu f} = 0.038$

Figure 18.- Concluded.

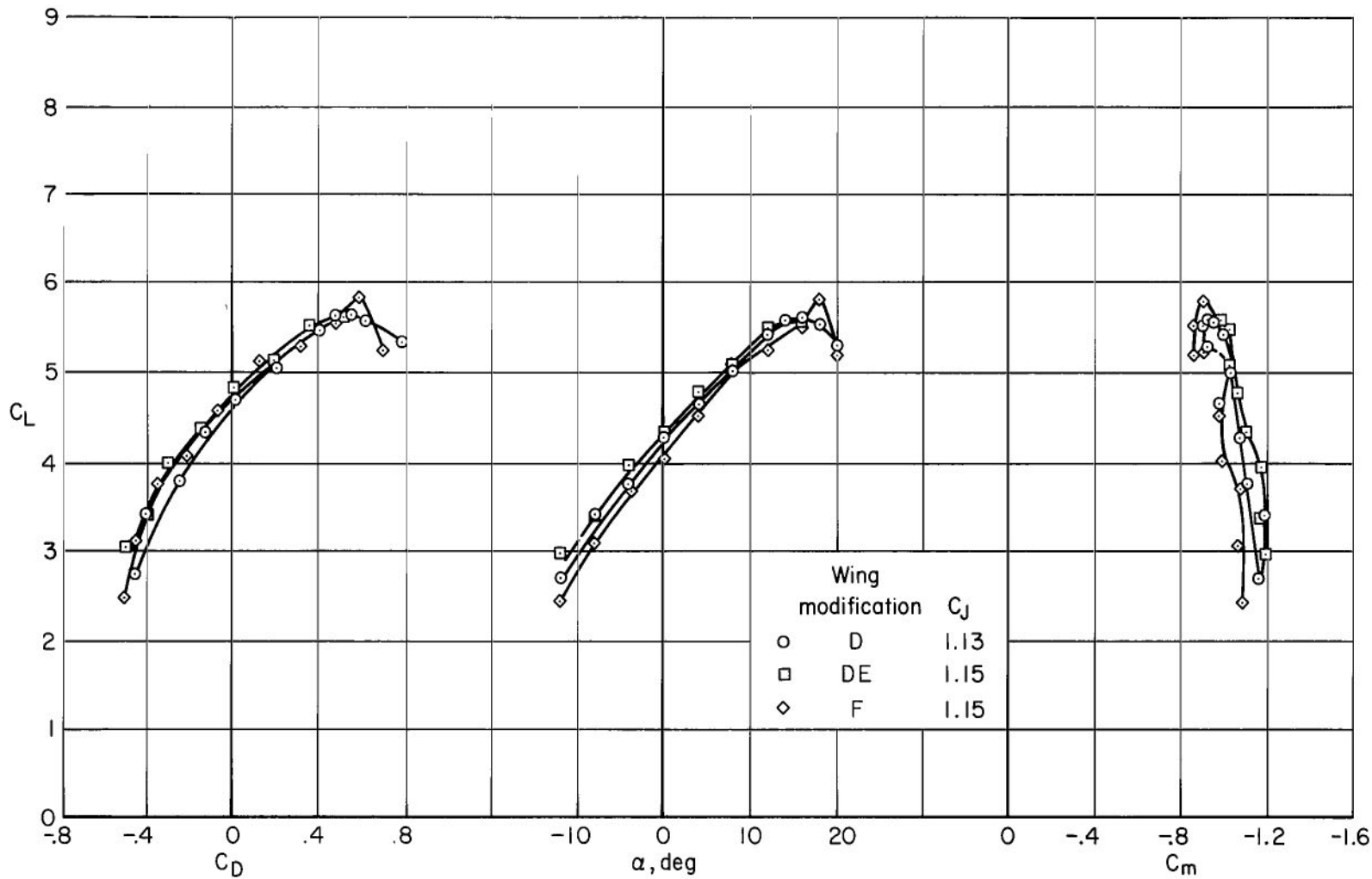
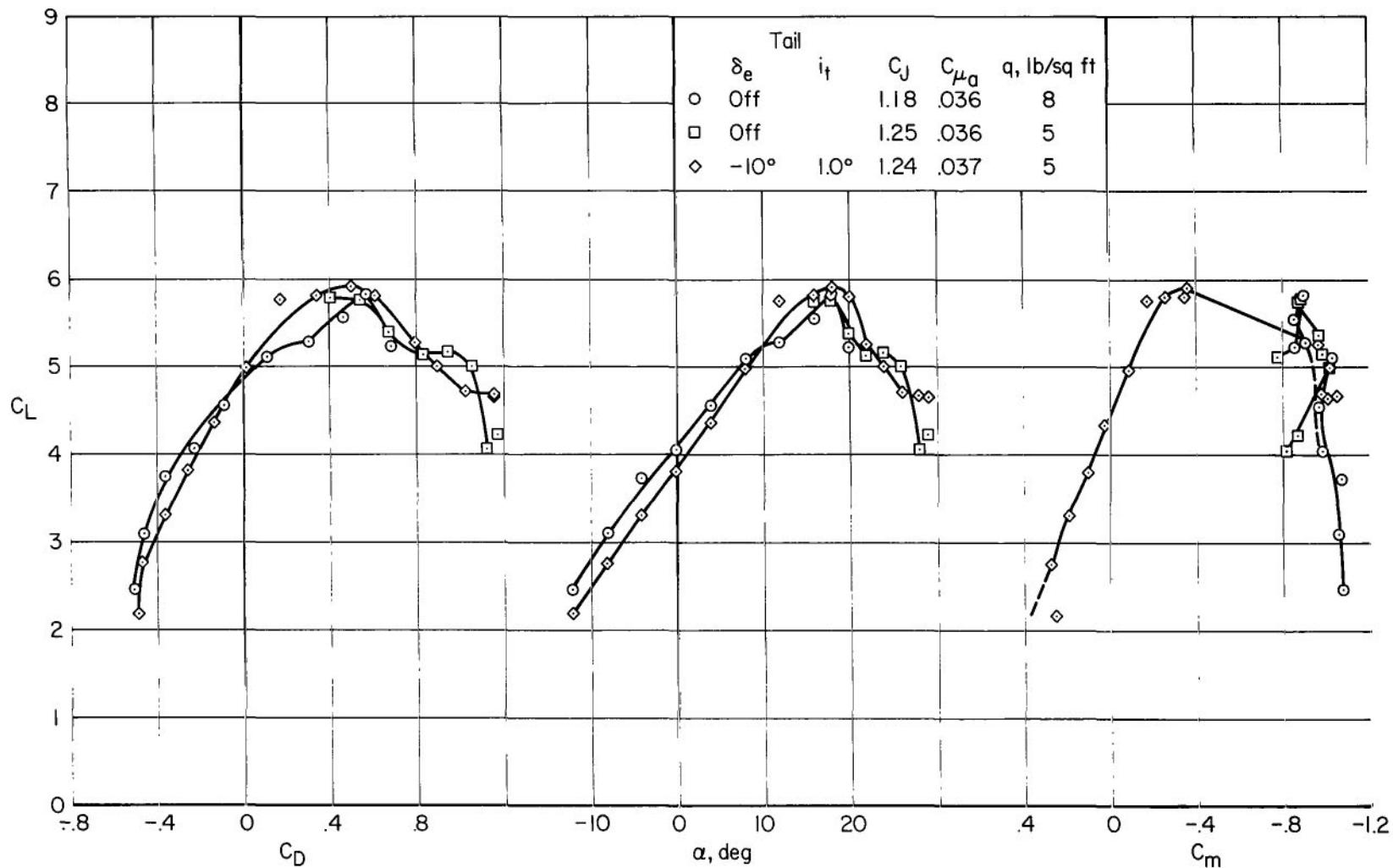
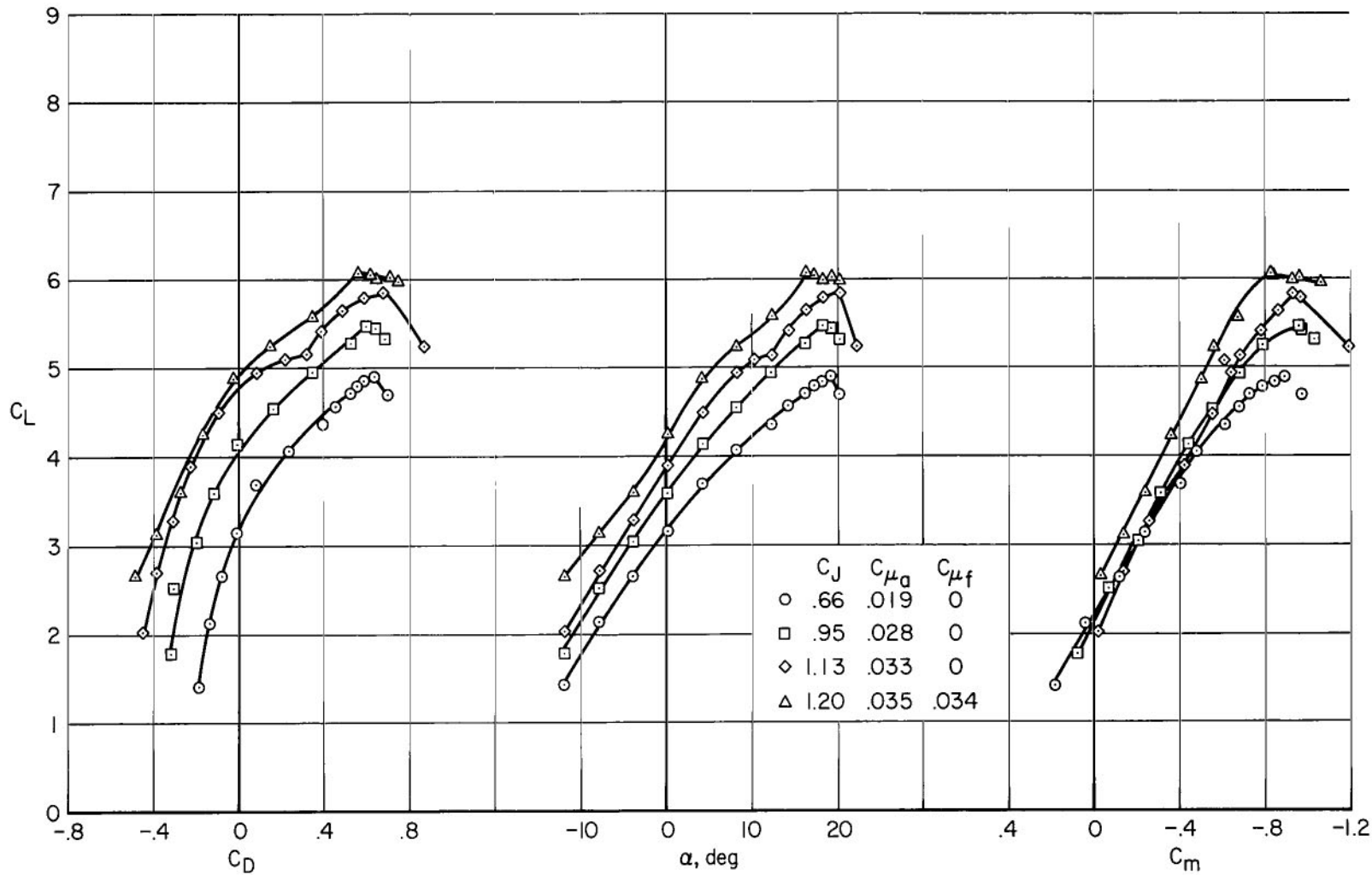


Figure 19.- The effect of wing modifications on the longitudinal characteristics of the model;  
 $\delta_f = 60^\circ$ ,  $\delta_a = 45^\circ$ , tail off.



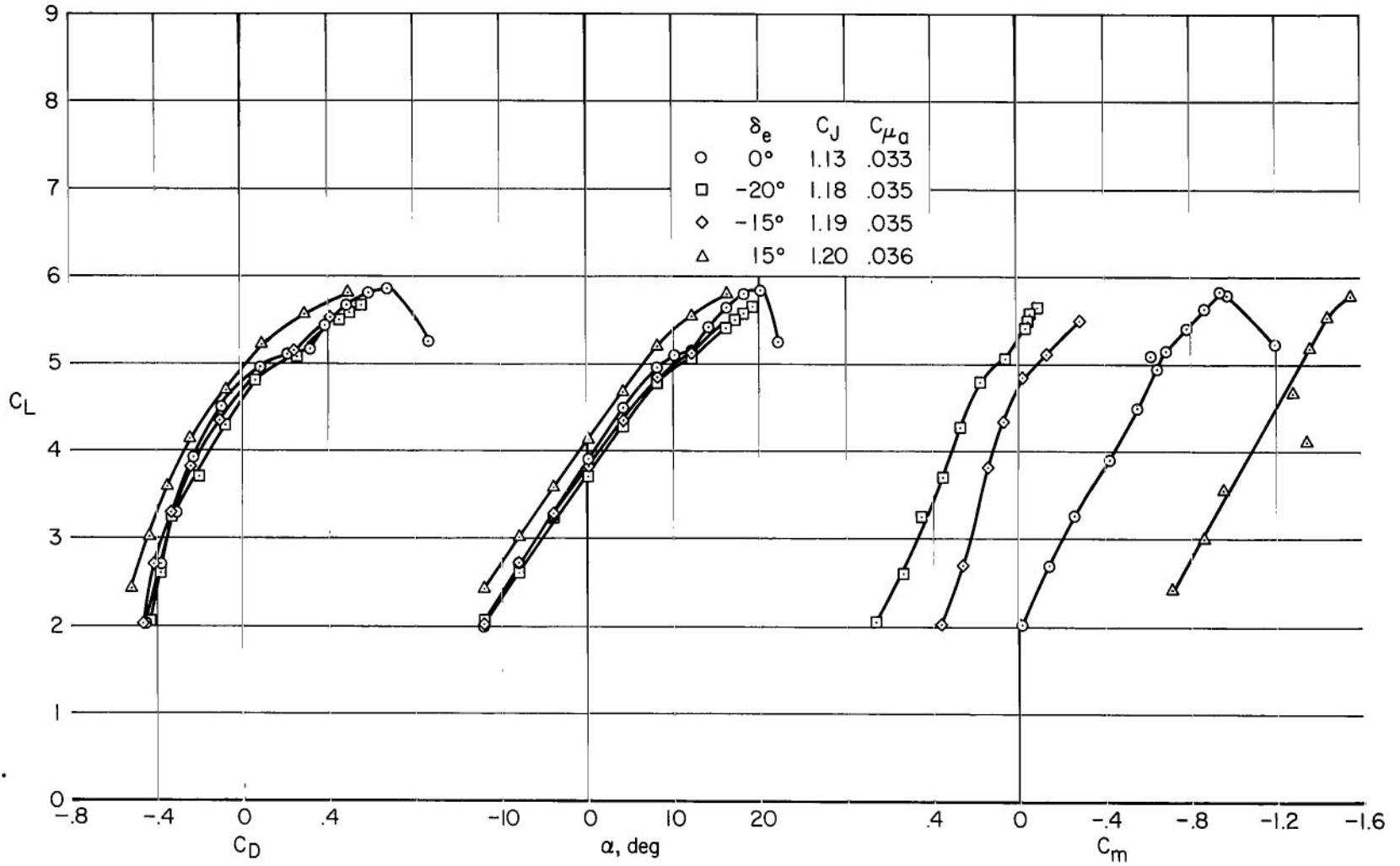
(a) Comparison of tail on and tail off;  $\delta_f = 60^\circ$ ,  $C_{\mu_f} = 0$ .

Figure 20.- Longitudinal characteristics of the model with the horizontal tail on for  $\delta_f = 60^\circ$  and  $100^\circ$ ;  $\delta_a = 45^\circ$ , F.



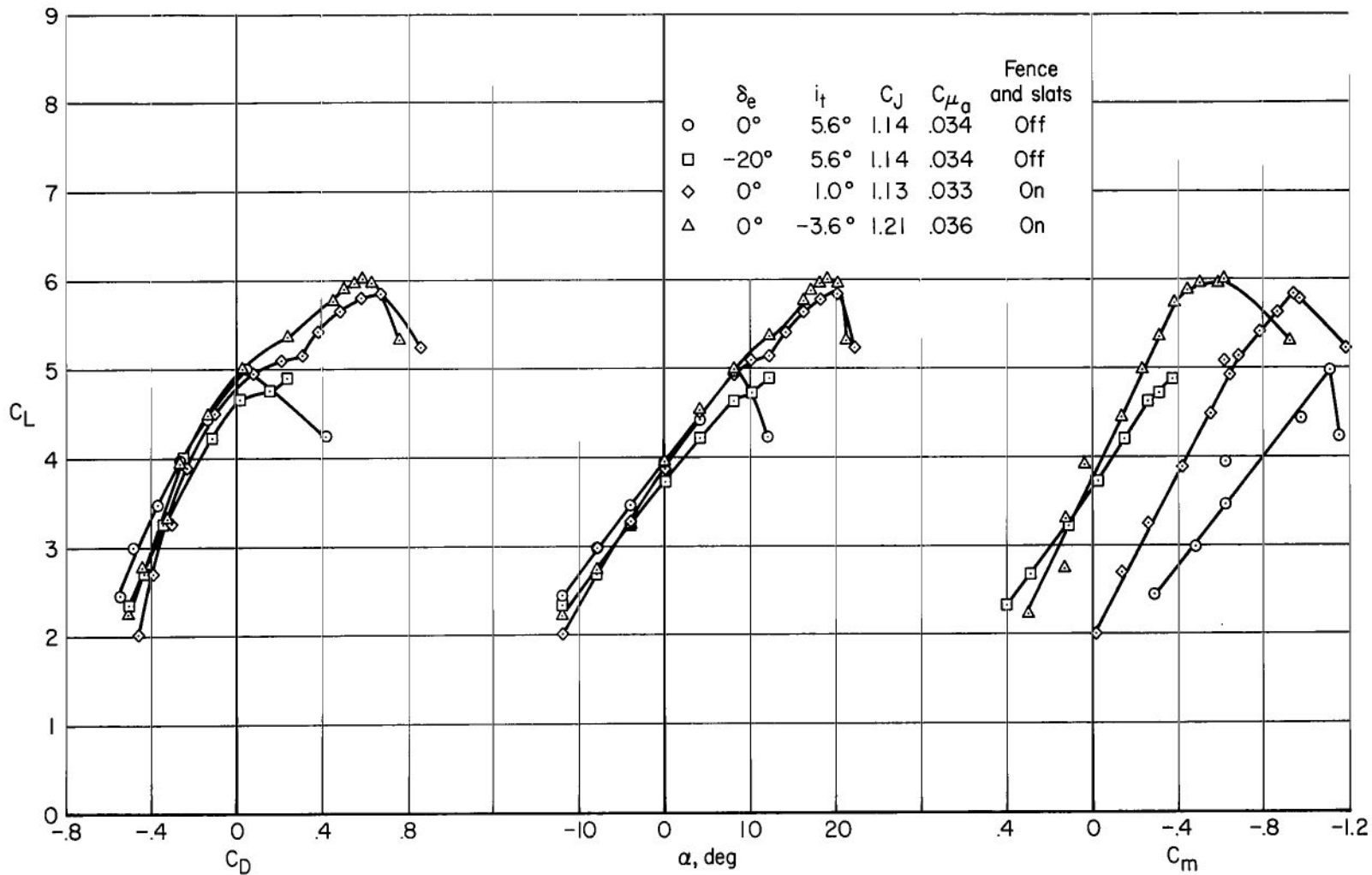
(b) Effect of  $C_J$  and flap BLC;  $\delta_f = 60^\circ$ ,  $i_t = 1.0^\circ$ ,  $\delta_e = 0^\circ$ .

Figure 20.- Continued.



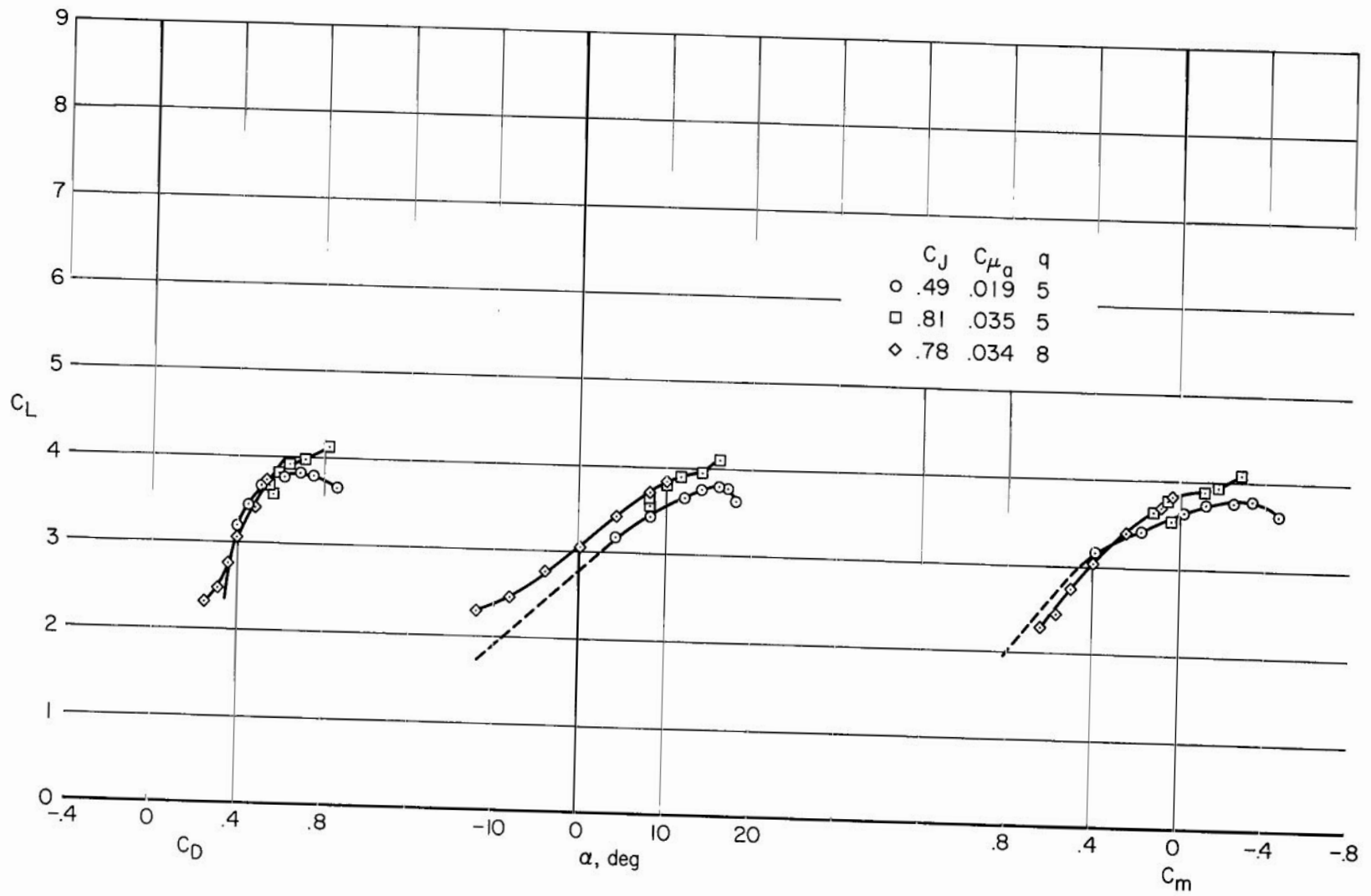
(c) Effect of the elevator;  $\delta_F = 60^\circ$ ,  $C_{\mu_F} = 0$ .

Figure 20.- Continued.



(d) Effect of the leading-edge slats combined with root fences;  $\delta_a = 60^\circ$ ,  $C_{\mu f} = 0$ .

Figure 20.- Continued.



(e) Effect of  $C_J$ ;  $\delta_f = 100^\circ$ ,  $C_{\mu_f} = 0$ ,  $i_t = 1^\circ$ ,  $\delta_e = -10^\circ$ .

Figure 20.- Concluded.

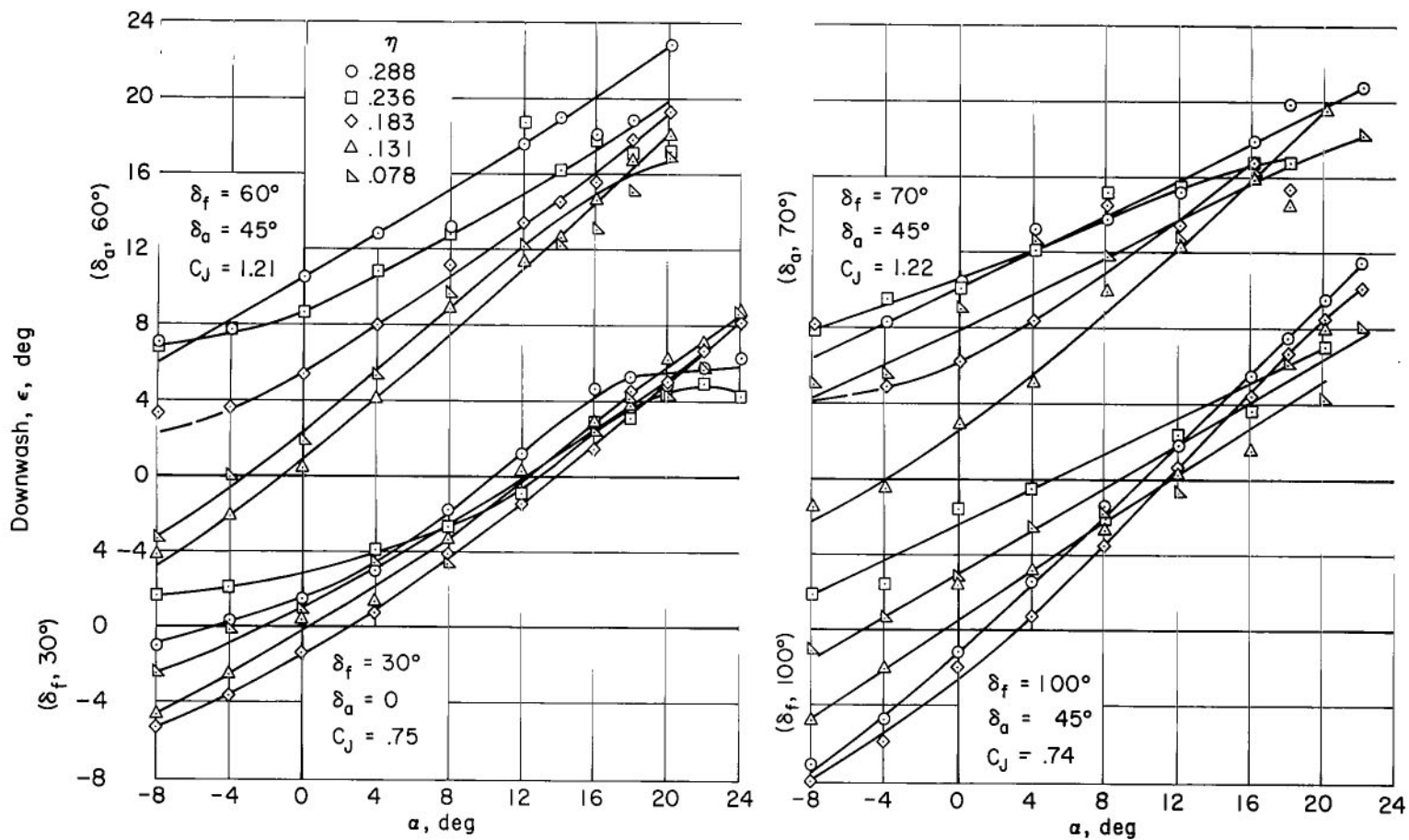


Figure 21.- Downwash measurements of the horizontal tail location.

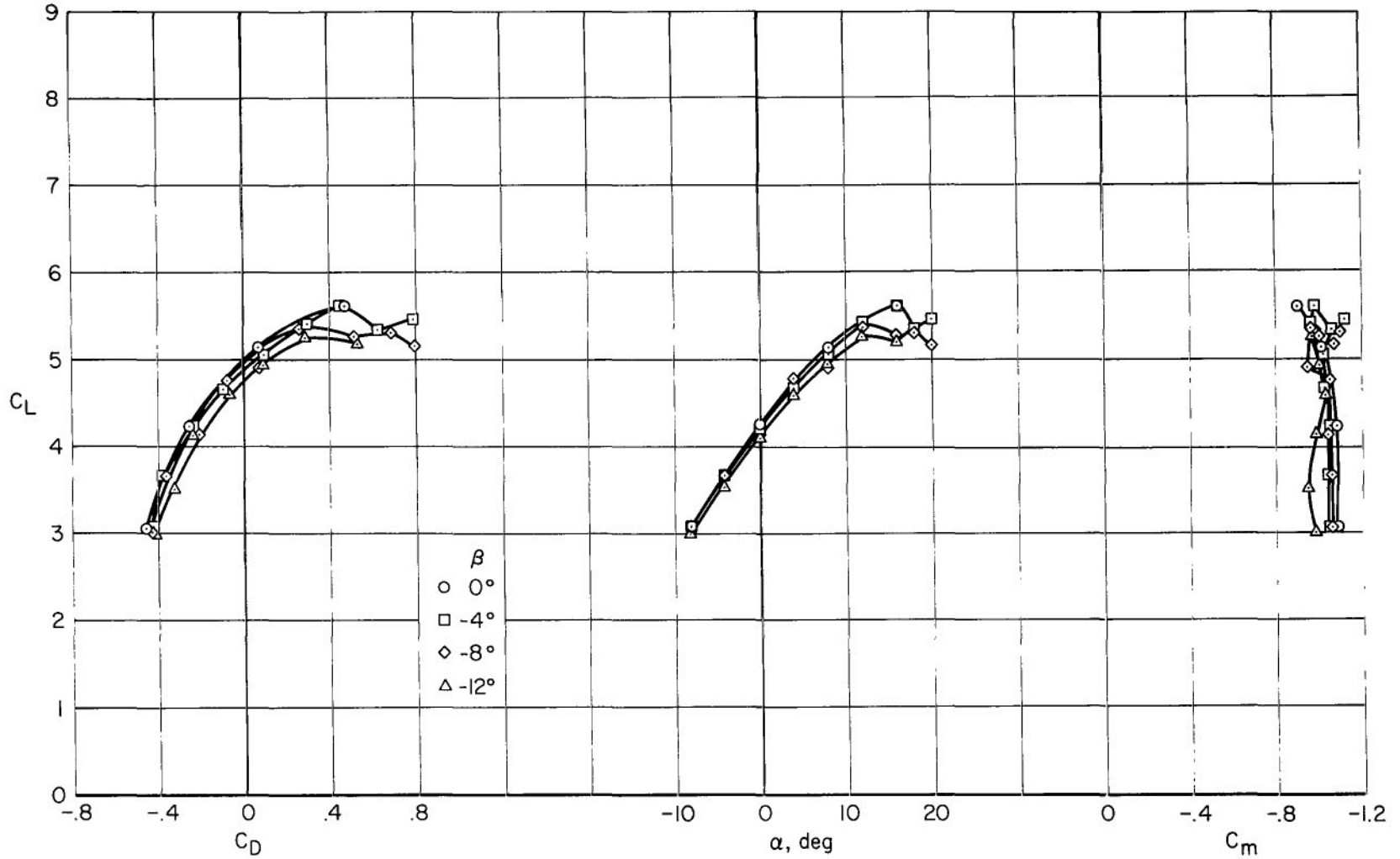
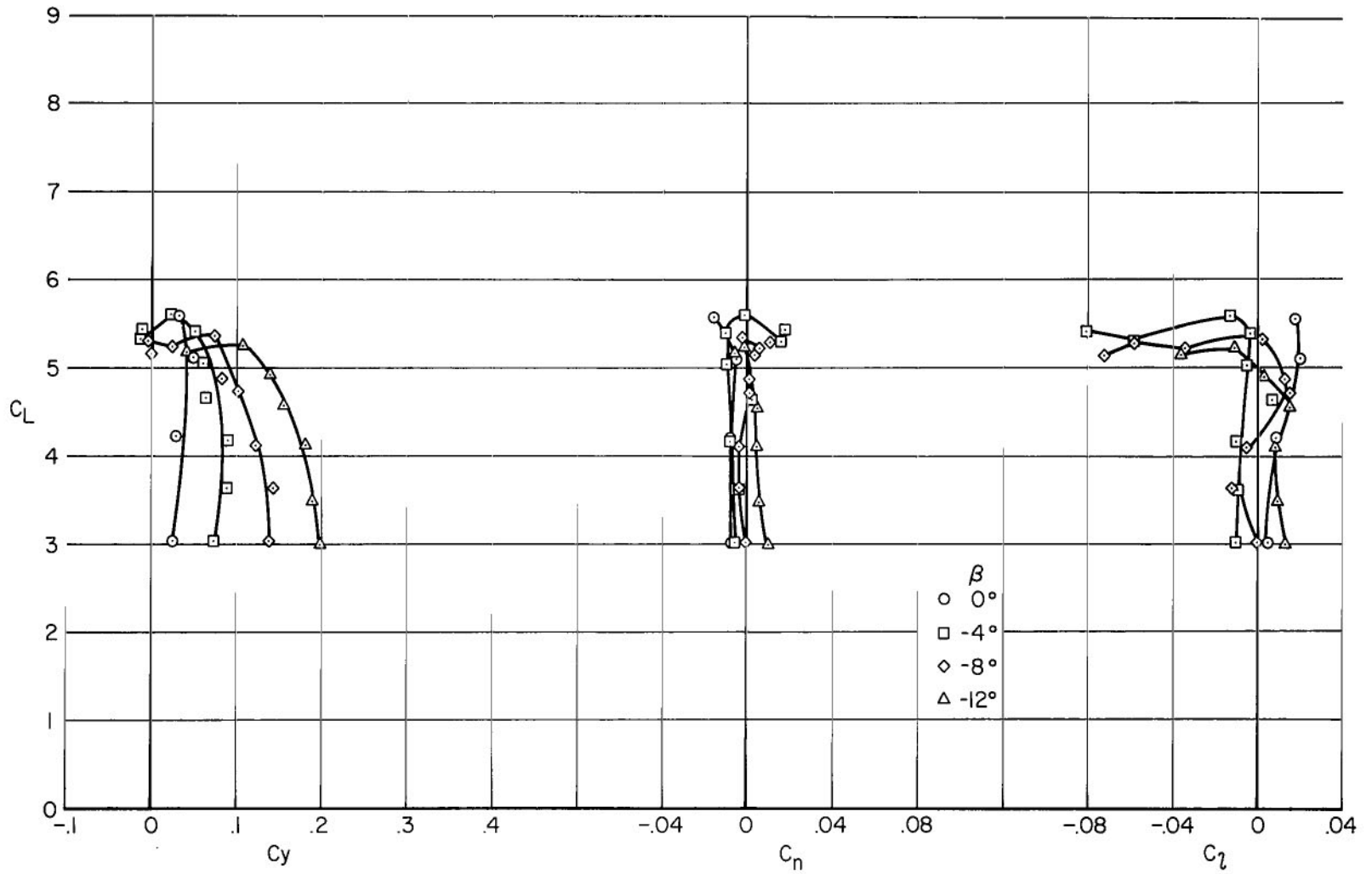
(a)  $C_L$  vs.  $C_D$ ,  $\alpha$ , and  $C_m$ 

Figure 22.- Characteristics of the model with vertical tail off as affected by yaw;  $\delta_f = 60^\circ$ ,  $\delta_a = 45^\circ$ ,  $C_J = 1.21$ ,  $C_{\mu_a} = 0.036$ ,  $C_{\mu_f} = 0$ , F, tail off.



(b)  $C_L$  vs.  $C_y$ ,  $C_n$ , and  $C_l$

Figure 22.- Concluded.

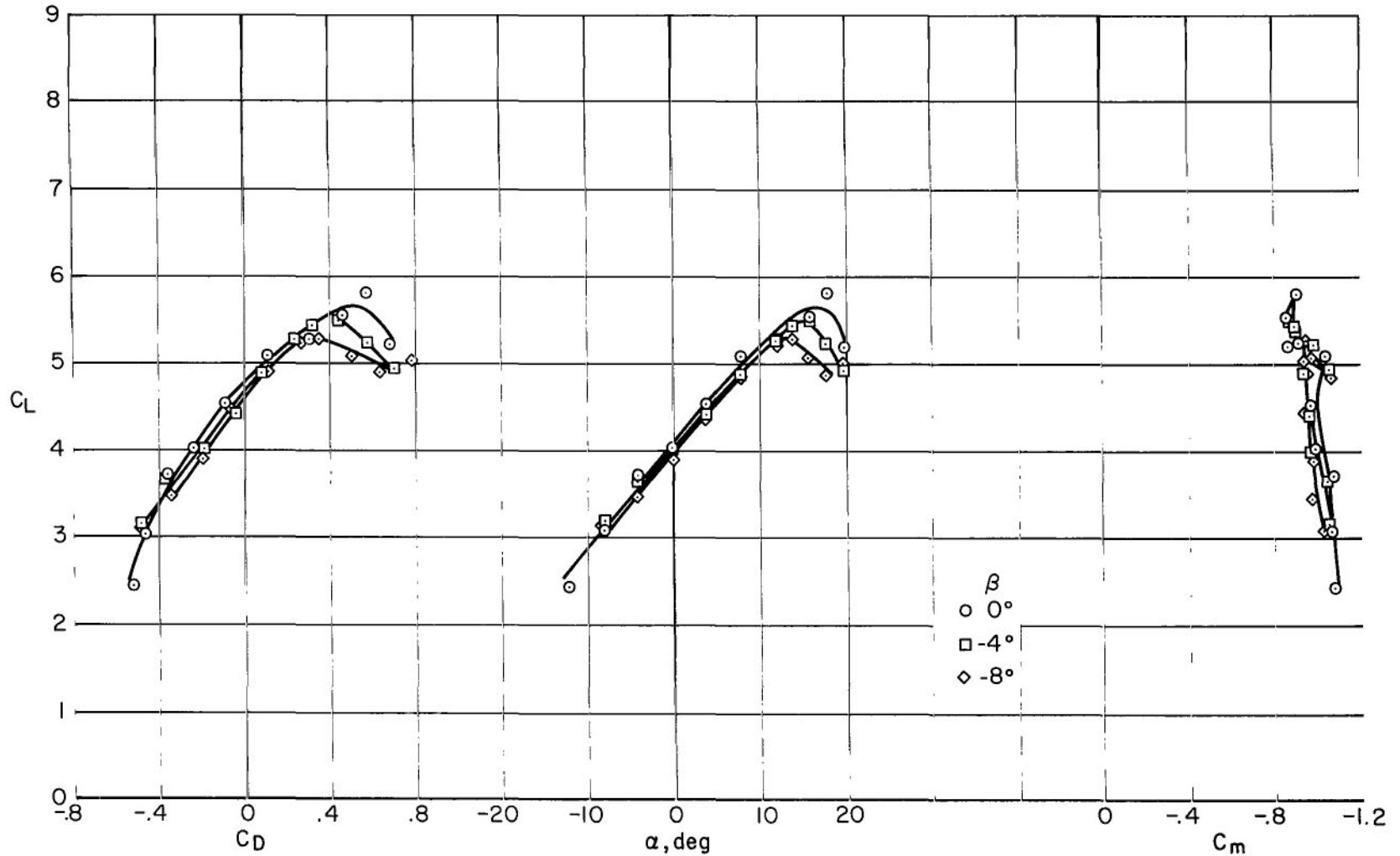
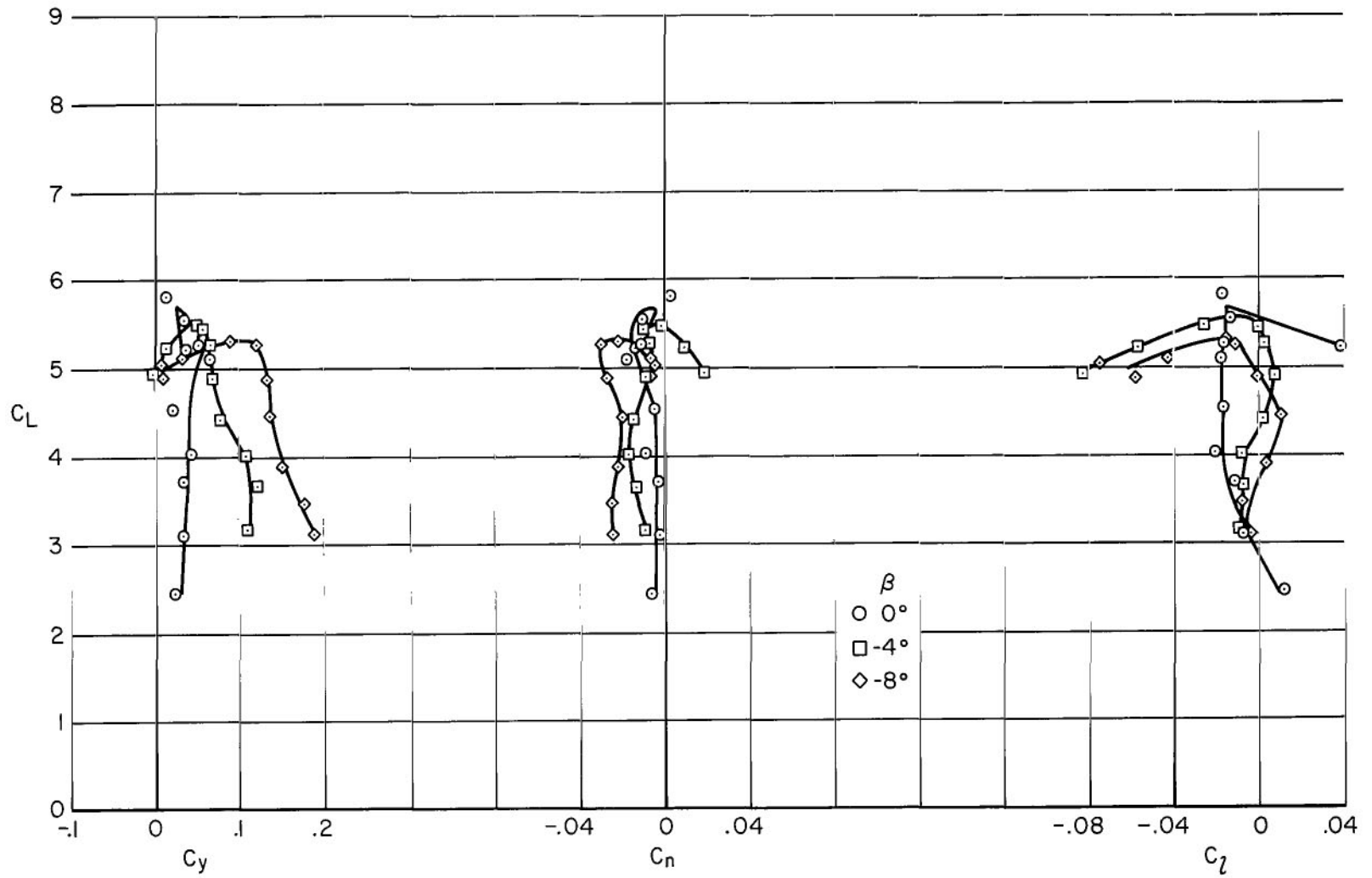
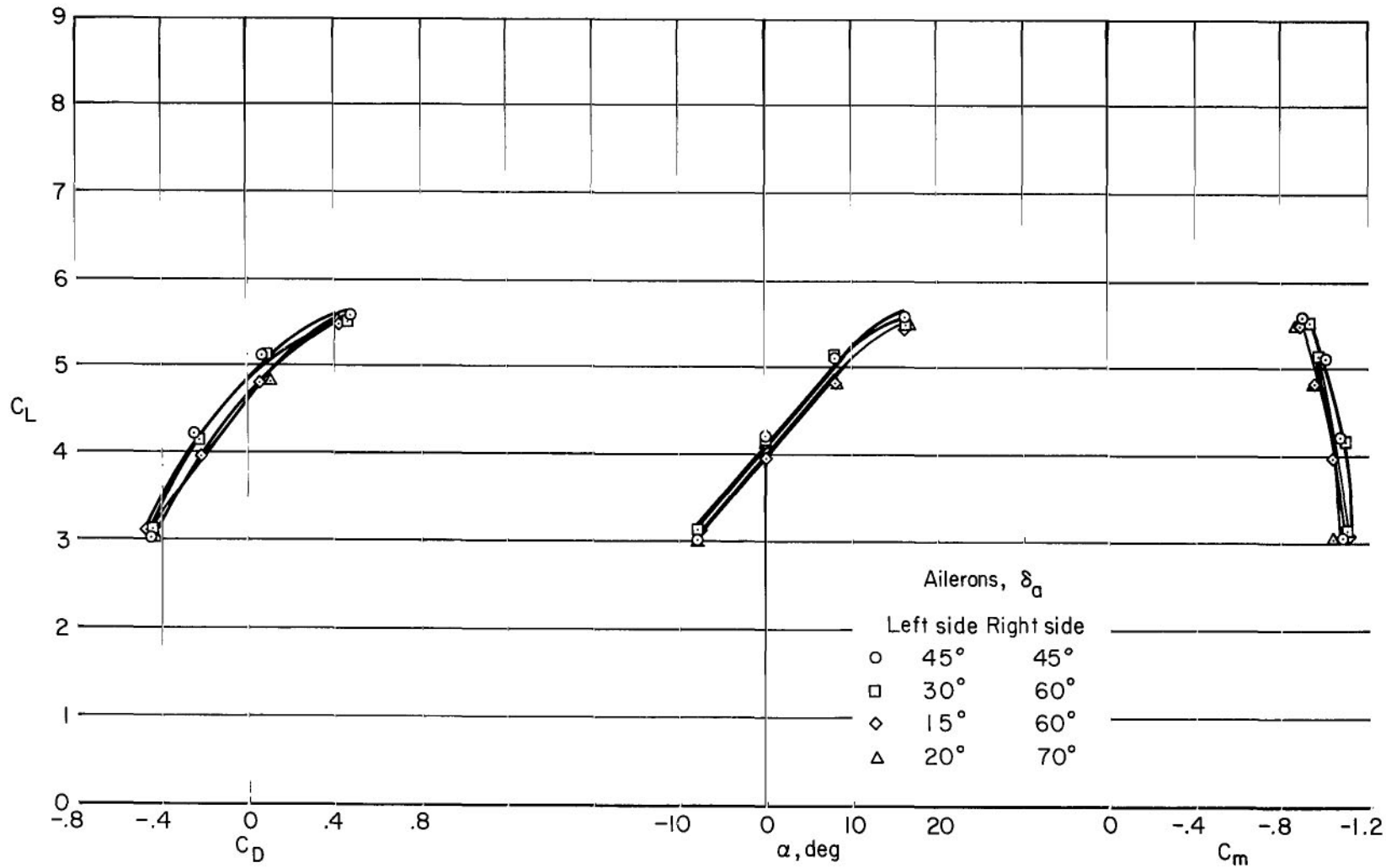
(a)  $C_L$  vs.  $C_D$ ,  $\alpha$  and  $C_m$ 

Figure 23.- Characteristics of the model with the vertical tail on as affected by yaw;  $\delta_f = 60^\circ$ ,  $\delta_a = 45^\circ$ ,  $C_J = 1.18$ ,  $C_{\mu_a} = 0.036$ ,  $C_{\mu_f} = 0$ , F, horizontal tail off.



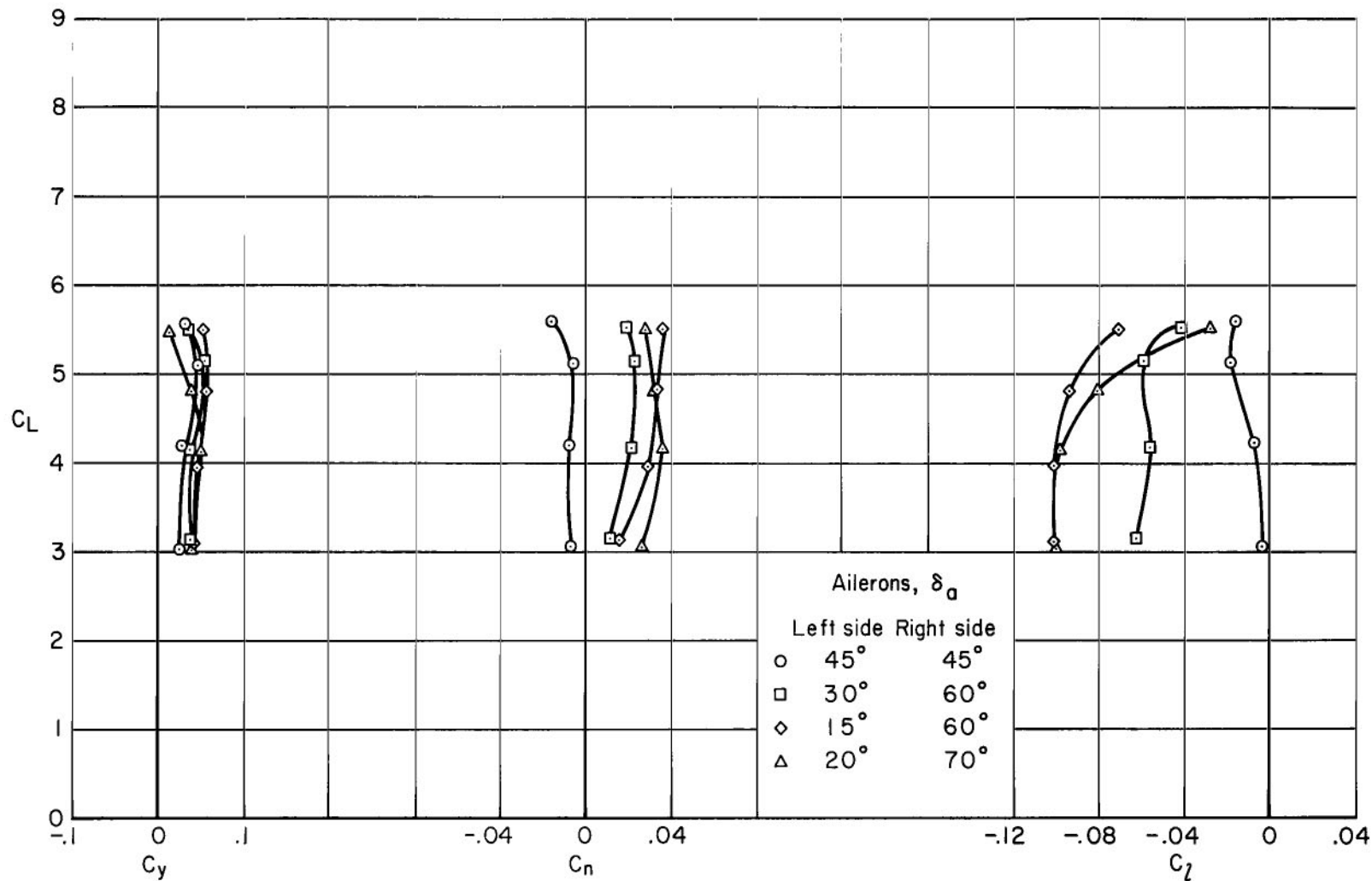
(b)  $C_L$  vs.  $C_y$ ,  $C_n$ , and  $C_l$

Figure 23.- Concluded.



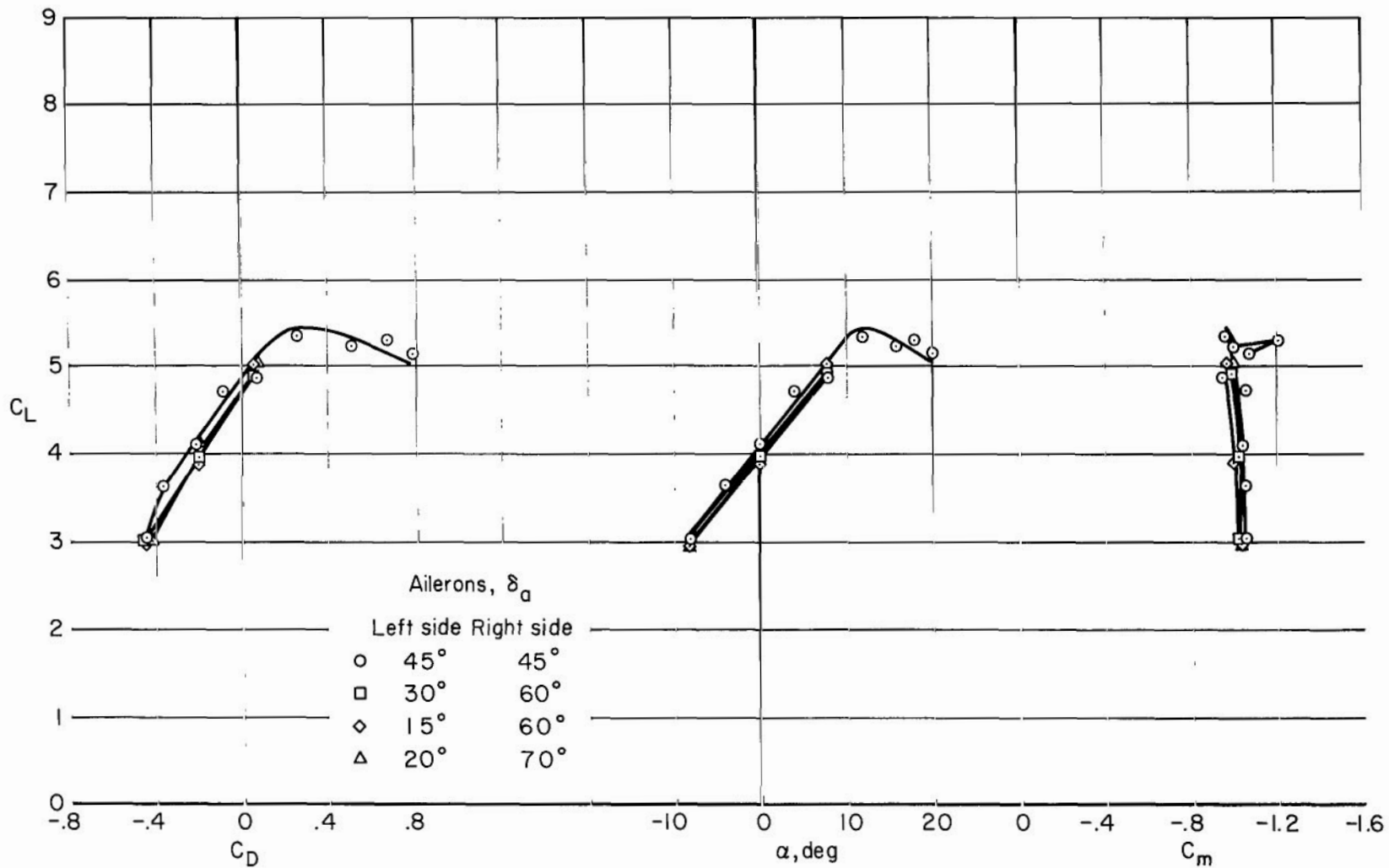
(a)  $C_L$  vs.  $C_D$ ,  $\alpha$ , and  $C_m$ ;  $\beta = 0^\circ$

Figure 24.- The effect of differential-aileron setting on the characteristics of the model with the vertical tail off;  $\delta_a = 60^\circ$ ,  $\delta_r = 45^\circ$ ,  $C_J = 1.21$ ,  $C_{\mu_a} = 0.036$ ,  $C_{\mu_r} = 0$ ,  $F$ , tail off.



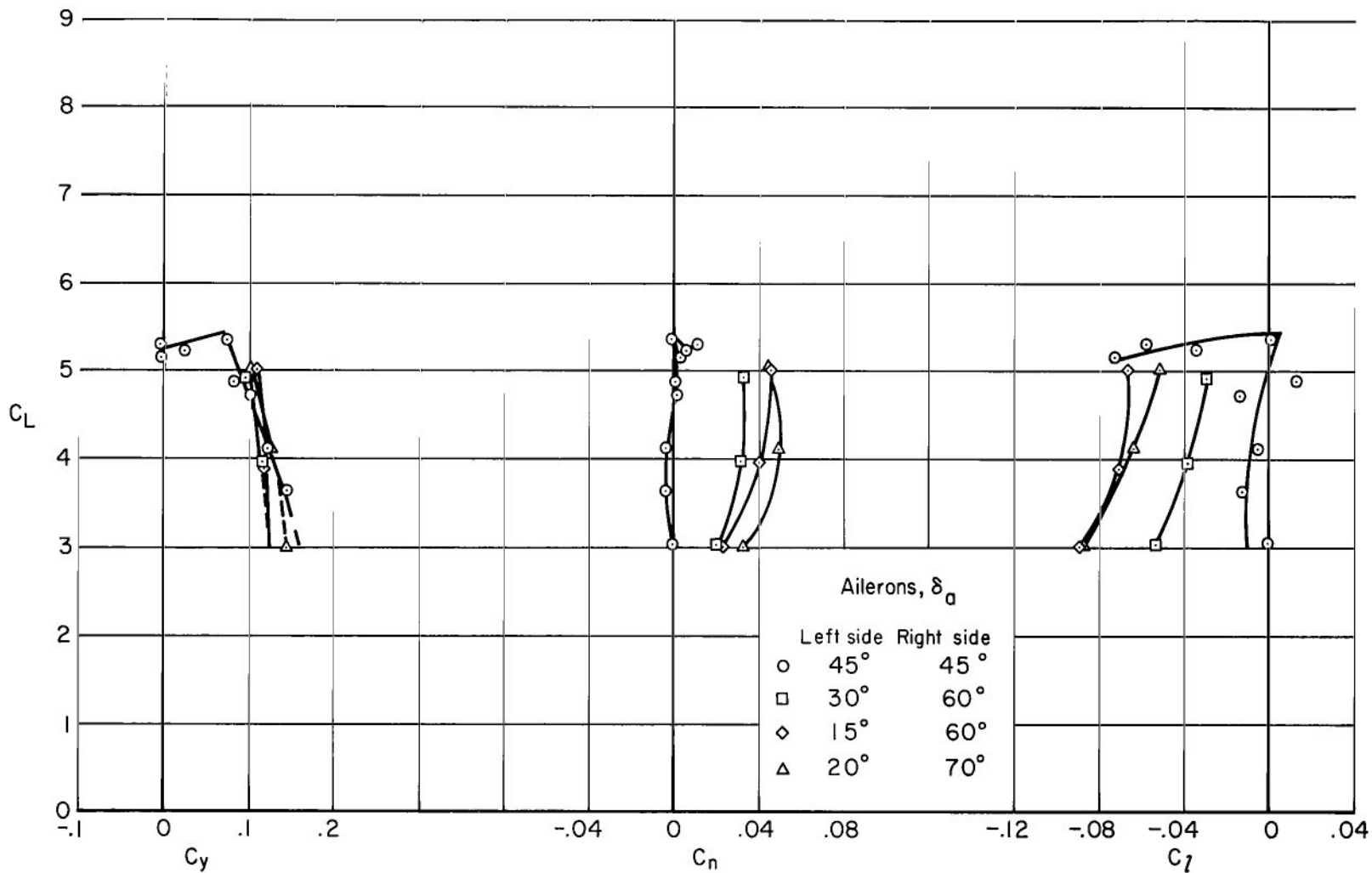
(b)  $C_L$  vs.  $C_y$ ,  $C_n$ ,  $C_l$ ;  $\beta = 0^\circ$

Figure 24.- Continued.



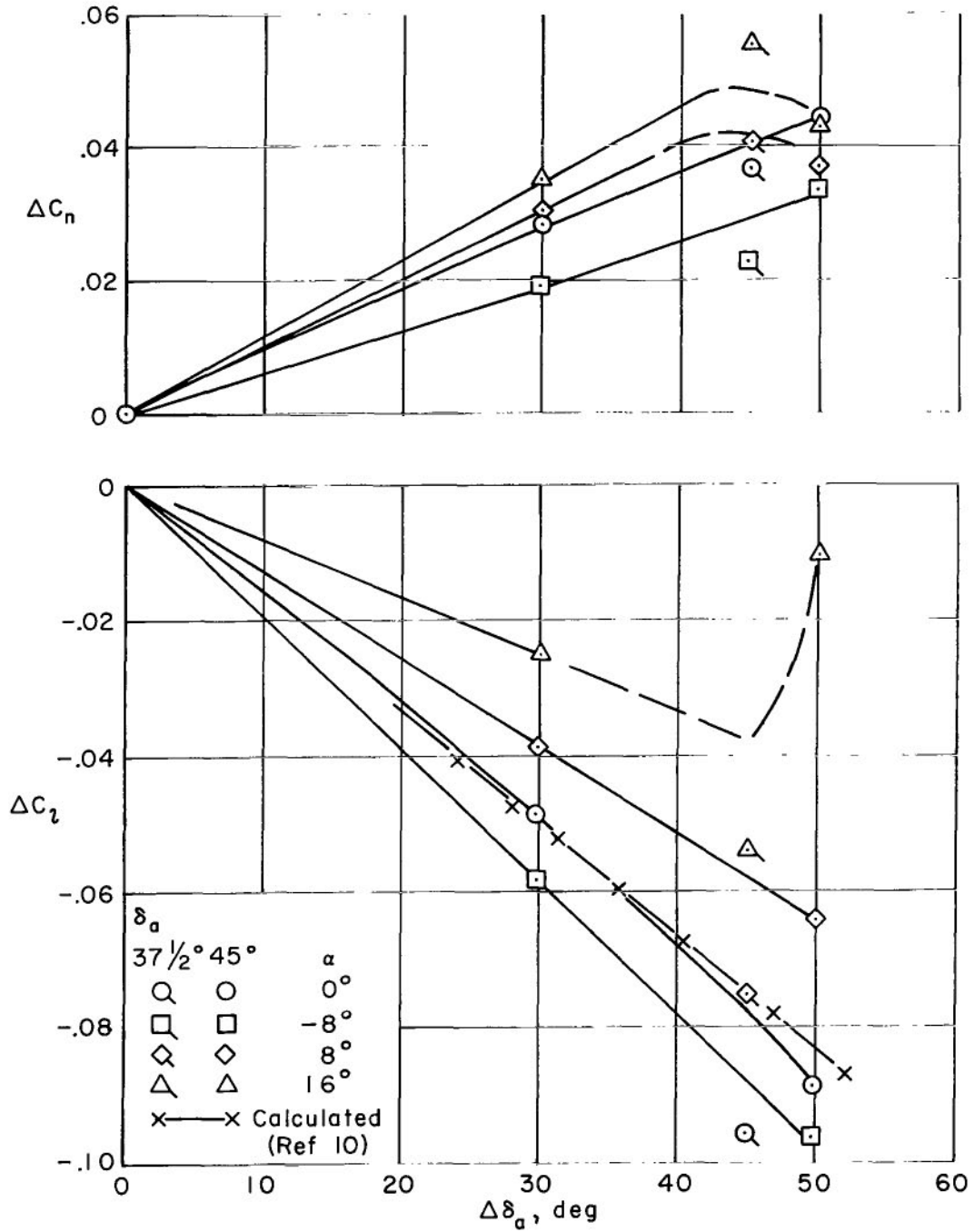
(c)  $C_L$  vs.  $C_D$ ,  $\alpha$  and  $C_m$ ;  $\beta = -8^\circ$

Figure 24.- Continued.



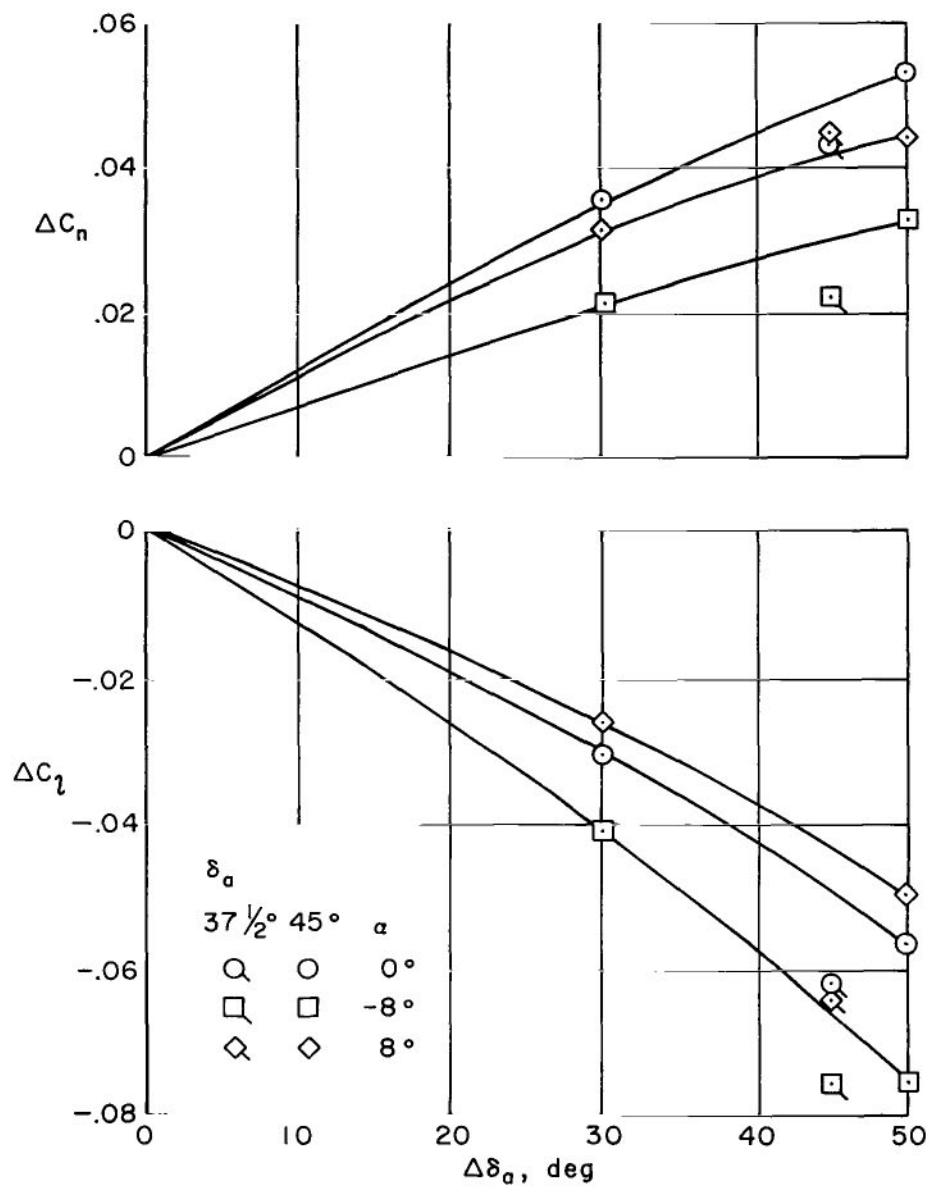
(d)  $C_L$  vs.  $C_y$ ,  $C_n$ , and  $C_l$ ;  $\beta = -8^\circ$

Figure 24.- Concluded.



(a)  $\beta = 0^\circ$

Figure 25.- Variation of increments in yawing and rolling moment with aileron differential deflection;  $\delta_F = 60^\circ$ ,  $\delta_a = 45^\circ$ ,  $C_J = 1.19$ ,  $C_{\mu_a} = 0.035$ ,  $C_{\mu_F} = 0$ , vertical tail off, F.



(b)  $\beta = -8^\circ$

Figure 25.- Concluded.

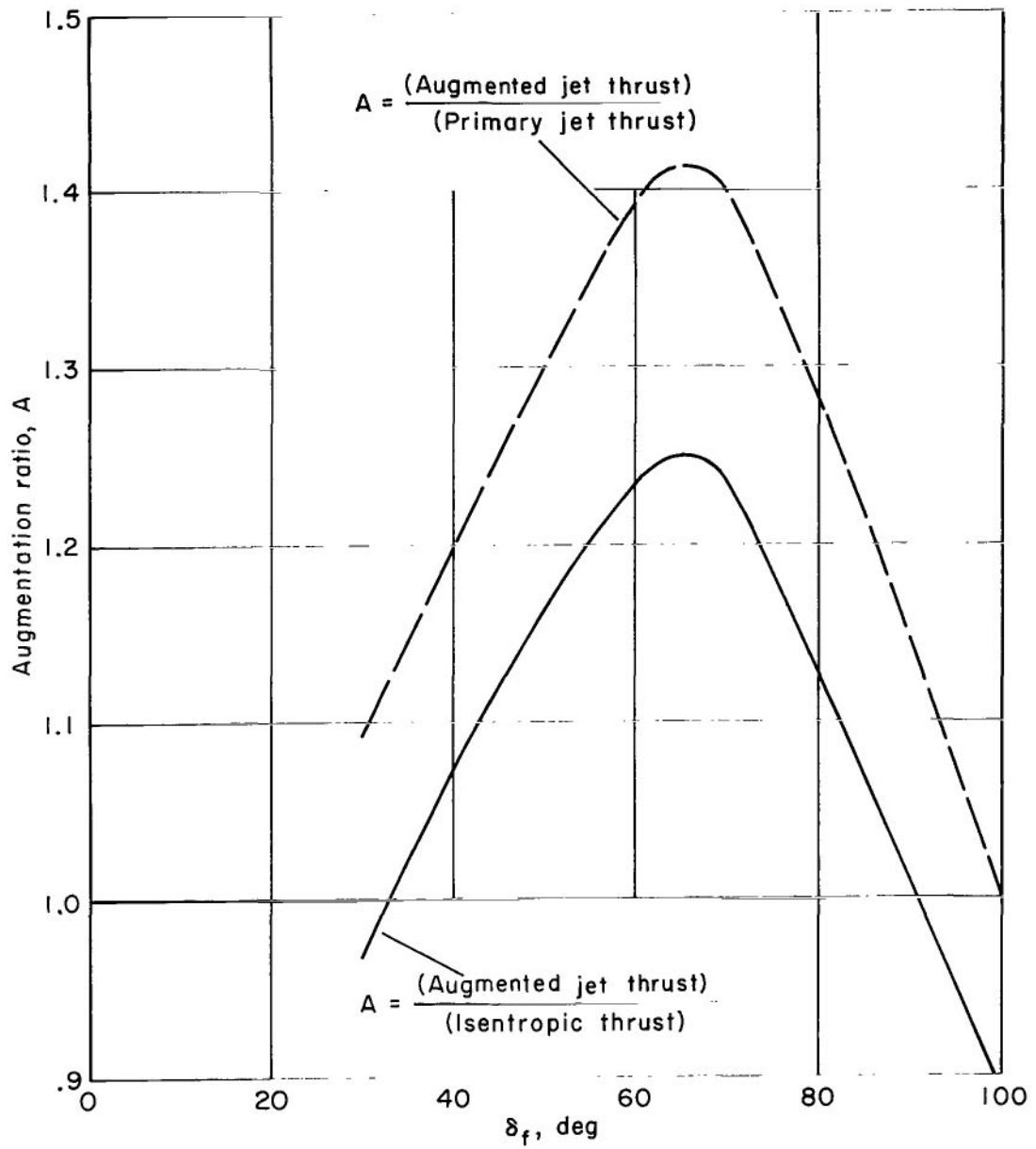


Figure 26.- Maximum augmentation ratio, jet angle, and optimum lower door position as functions of flap deflection.

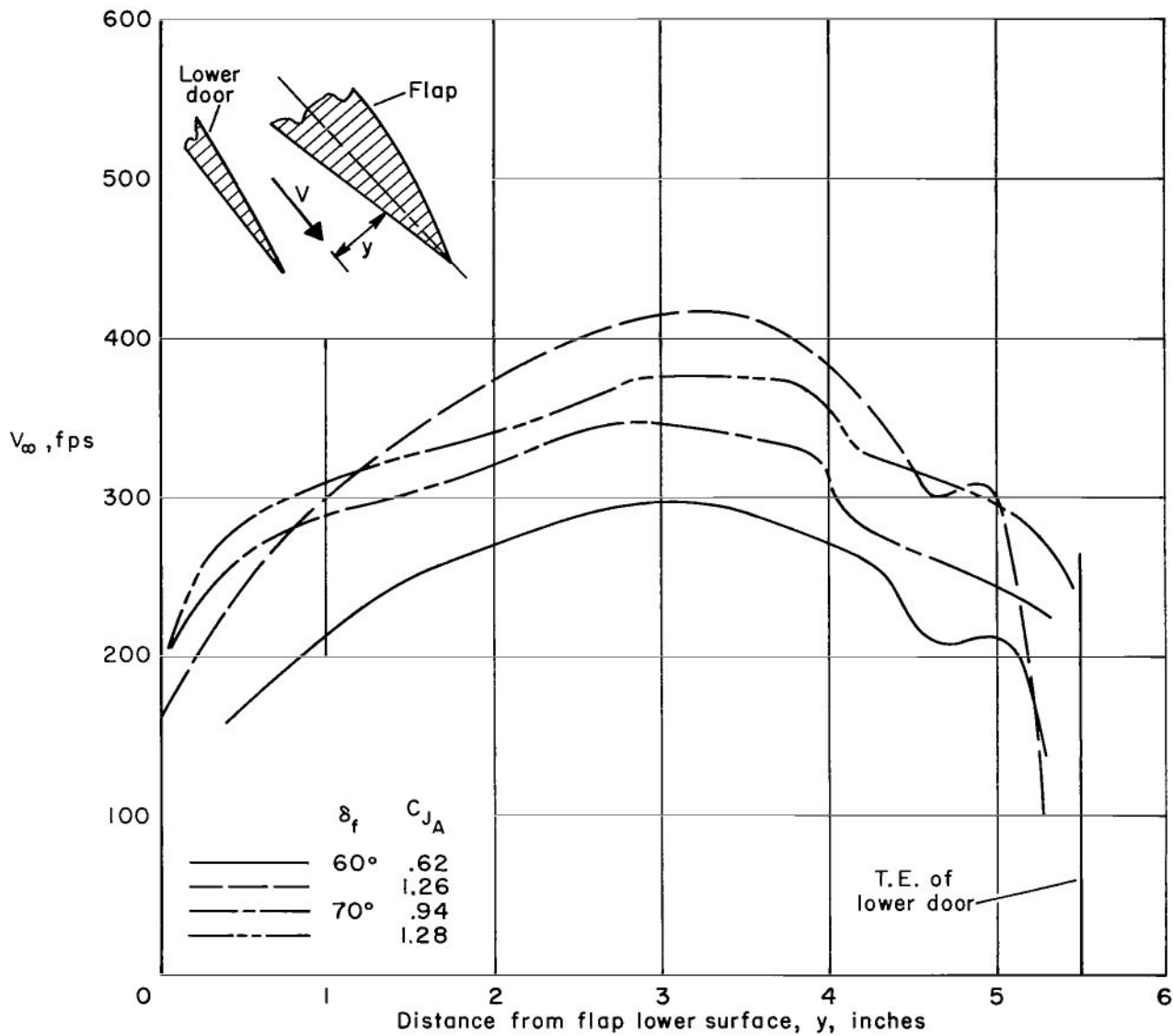
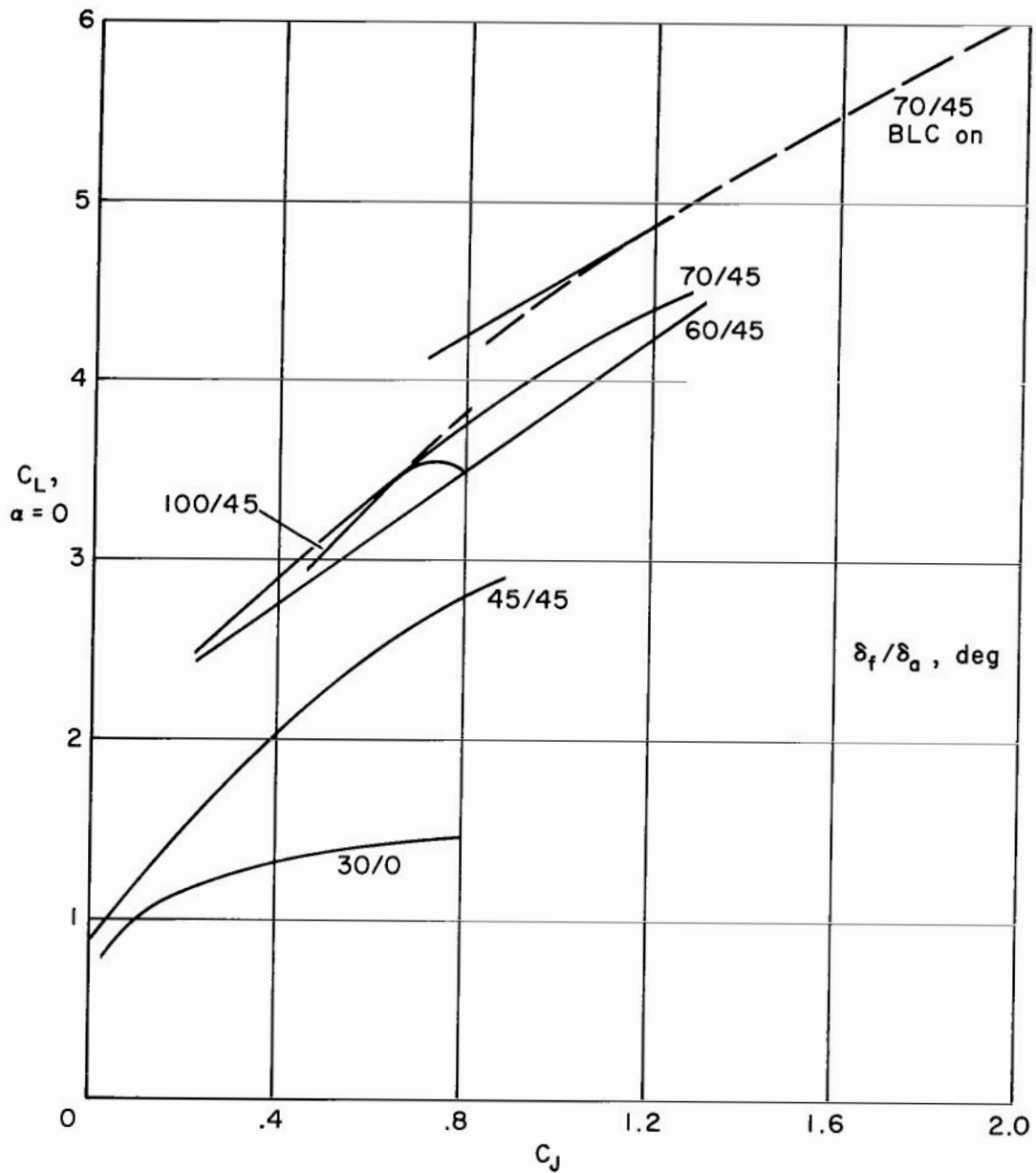
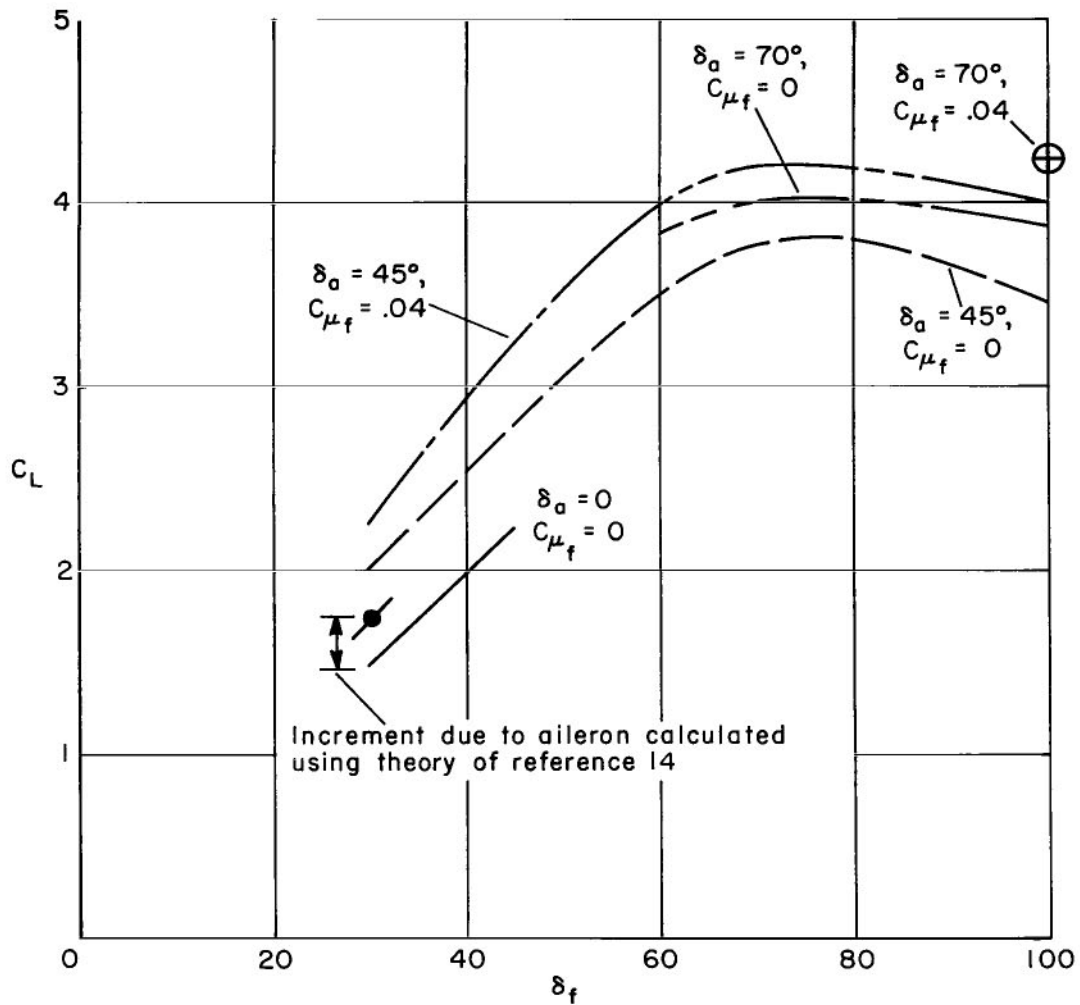


Figure 27.- Velocity distribution across the augmentor at  $\eta = 0.52$  for a free-stream dynamic pressure of 7.8 psf;  $\alpha = 0^\circ$ ,  $C_{\mu F} = 0$ .



(a)  $C_L$  vs.  $C_J$

Figure 28.- The variations of lift with jet coefficient and flap deflection for zero angle of attack.



(b)  $C_L$  vs.  $\delta_f$ ;  $C_J = 0.81$ .

Figure 28.- Concluded.

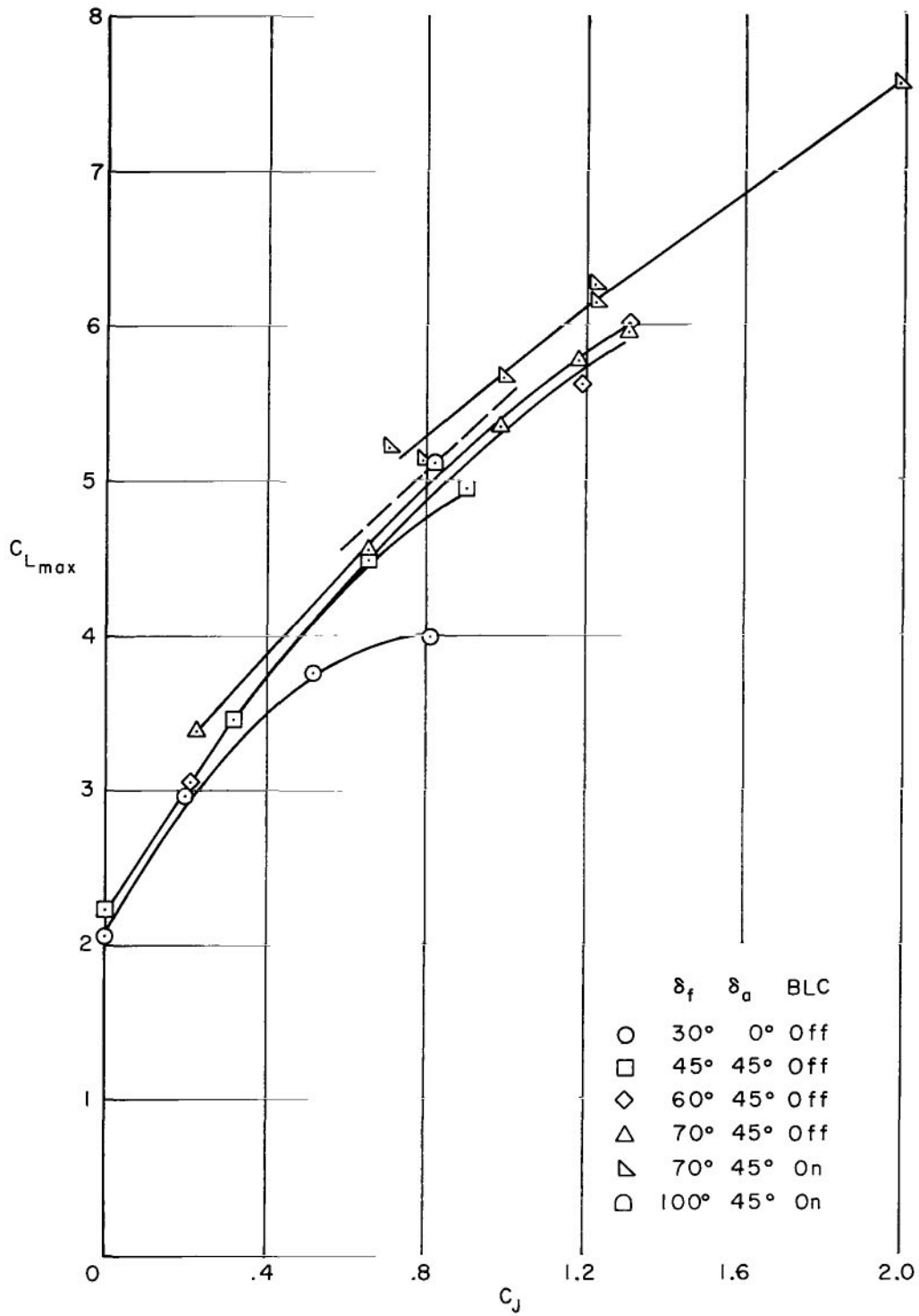
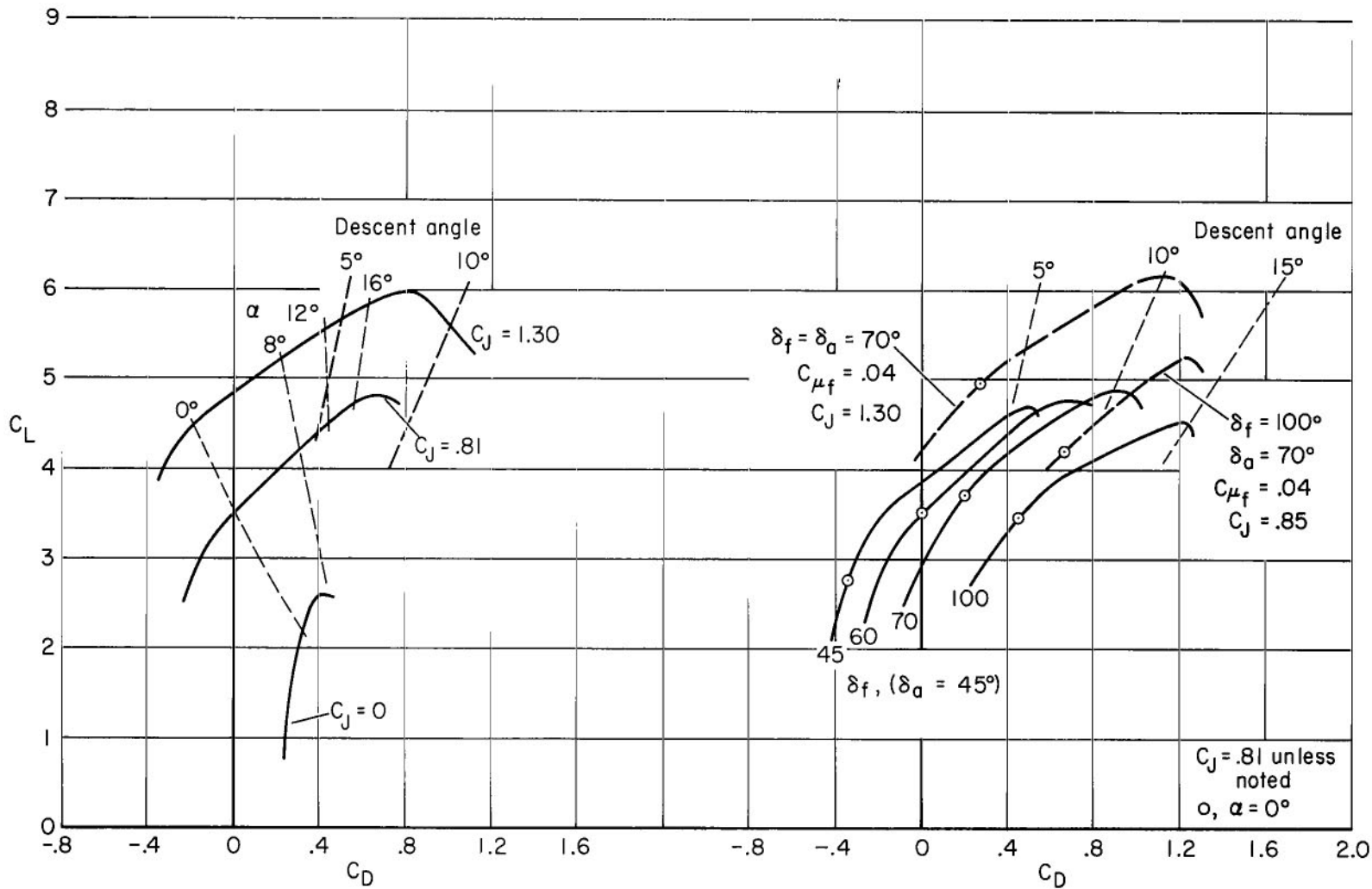


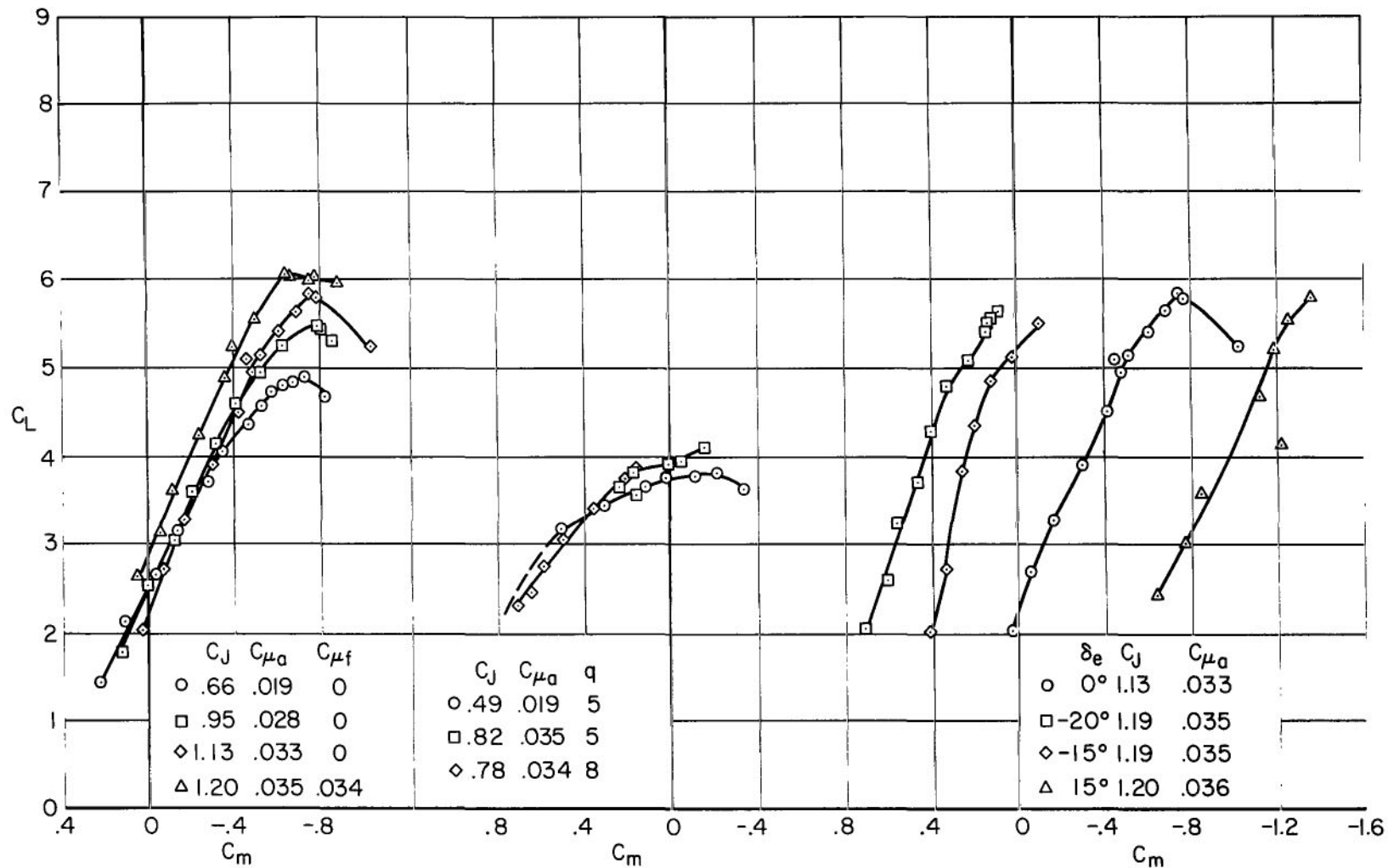
Figure 29.- The variation of maximum lift coefficient with jet coefficient; full-span leading-edge slats.



(a)  $\delta_f = 60^\circ$

(b) Effect of flap deflection.

Figure 30.- Summary of the drag polars as affected by jet coefficient and flap deflection.



(a) Effect of  $C_J$  and  $C_{\mu_f}$ ;  $\delta_f = 60^\circ$ ,  $\delta_a = 45^\circ$ ,  $i_t = 1^\circ$ ,  $\delta_f = 0^\circ$ .  
 (b) Effect of  $C_J$ ;  $\delta_f = 100^\circ$ ,  $\delta_a = 45^\circ$ ,  $i_t = 1^\circ$ ,  $\delta_e = -10^\circ$ ,  $C_{\mu_f} = 0$ .  
 (c) Effect of elevator;  $\delta_f = 60^\circ$ ,  $\delta_a = 45^\circ$ ,  $i_t = 1^\circ$ ,  $C_{\mu_f} = 0$ .

Figure 31.- Pitching-moment data for the model with tail on and corrected for wind-tunnel-wall effects; F.

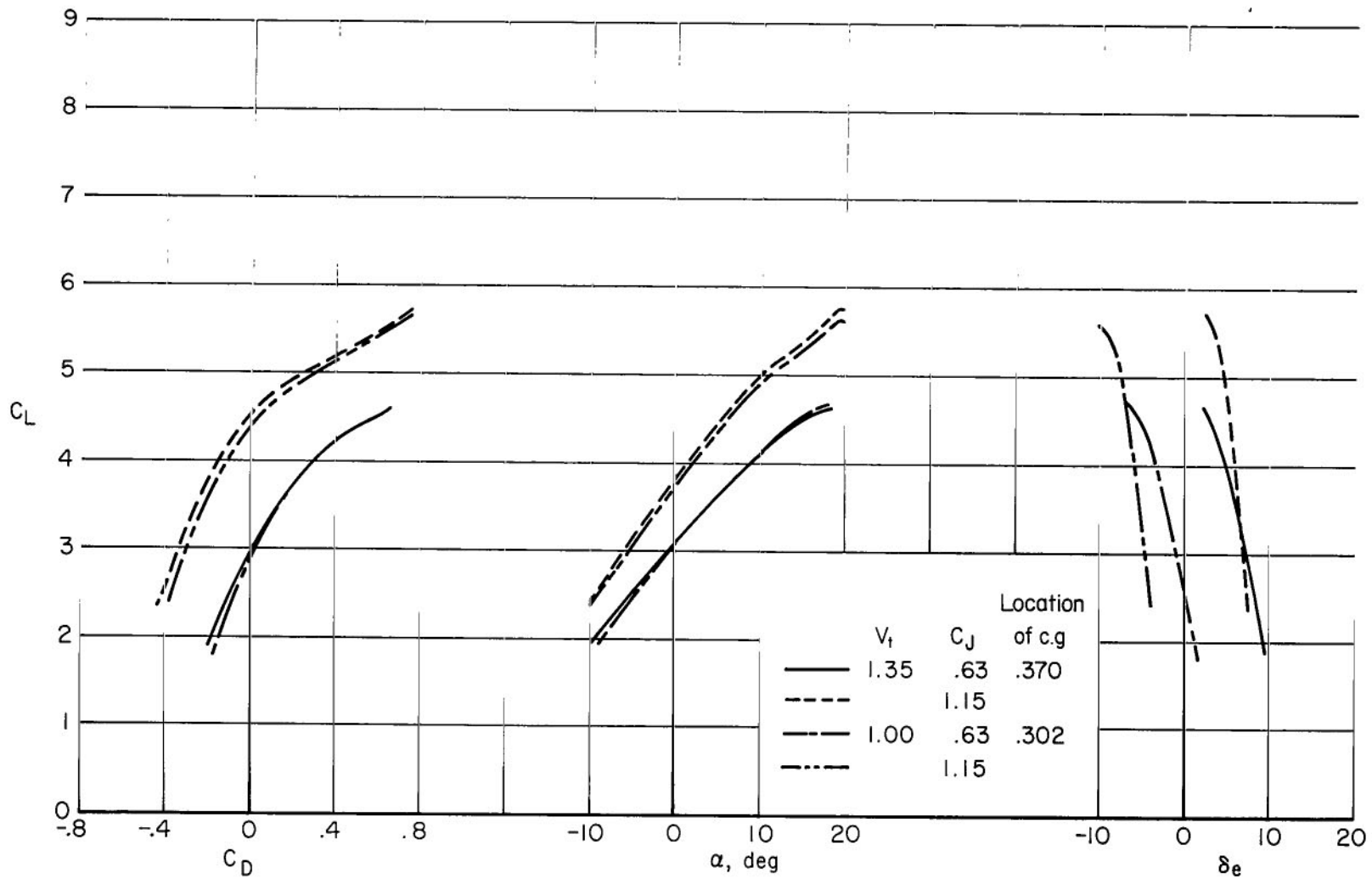
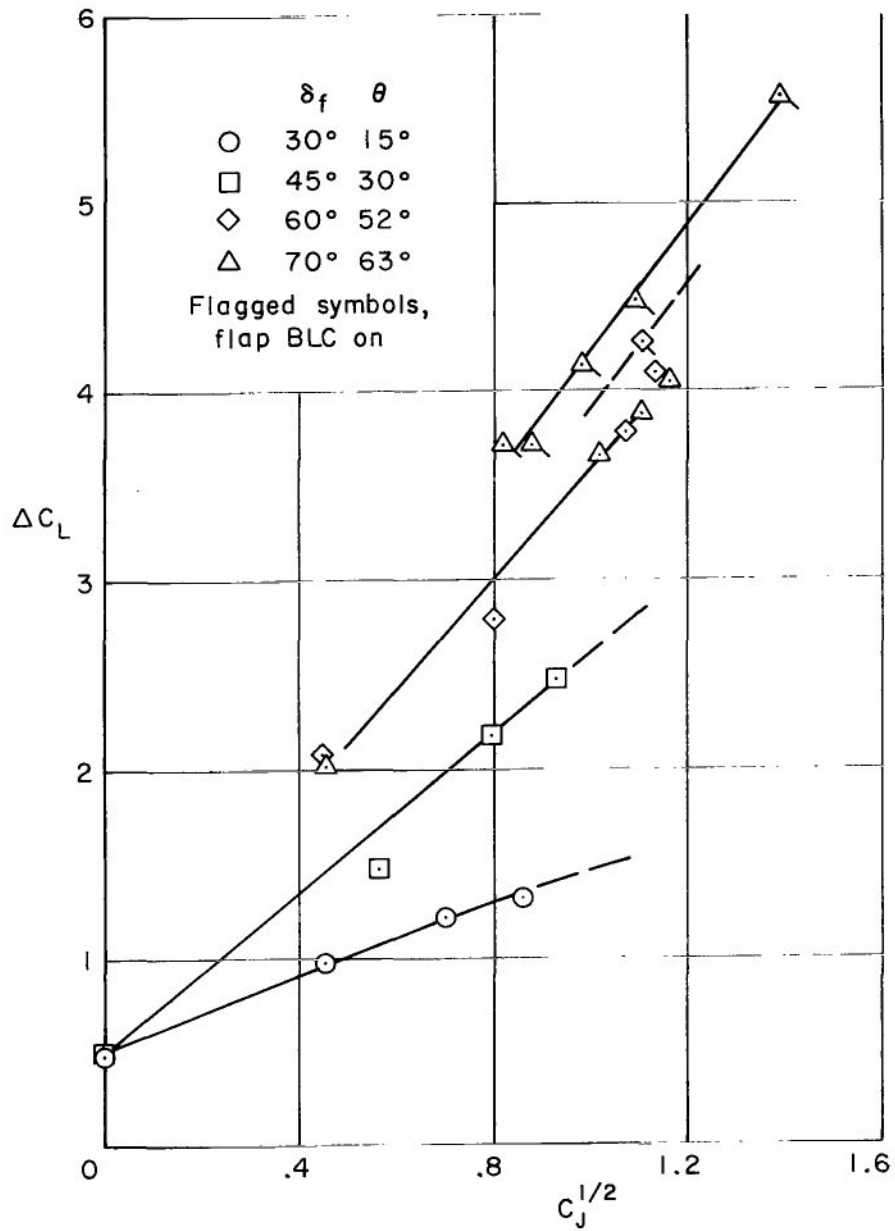
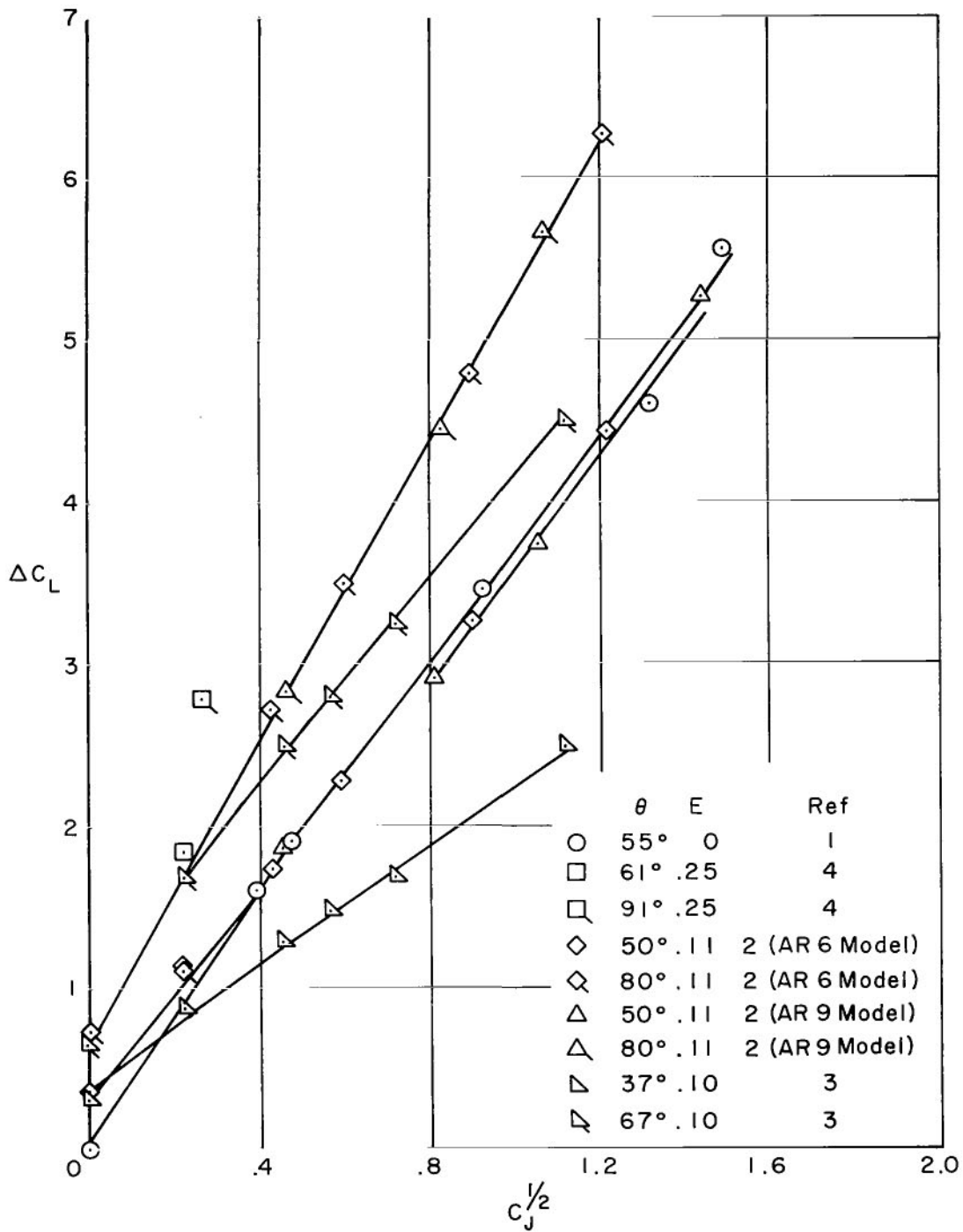


Figure 32.- Longitudinal trim characteristics for the model with a static margin of 5 percent;  
 $\delta_f = 60^\circ$ ,  $\delta_a = 45^\circ$ ,  $C_{\mu_f} = 0$ ,  $i_t = 1.0^\circ$ , F.



(a) Augmented-jet flap.

Figure 33.- Variations of flap lift increment with  $C_J^{1/2}$  for  $\alpha = 0^\circ$ .



(b) Jet flap models adjusted to the present model geometry.

Figure 33.- Concluded.

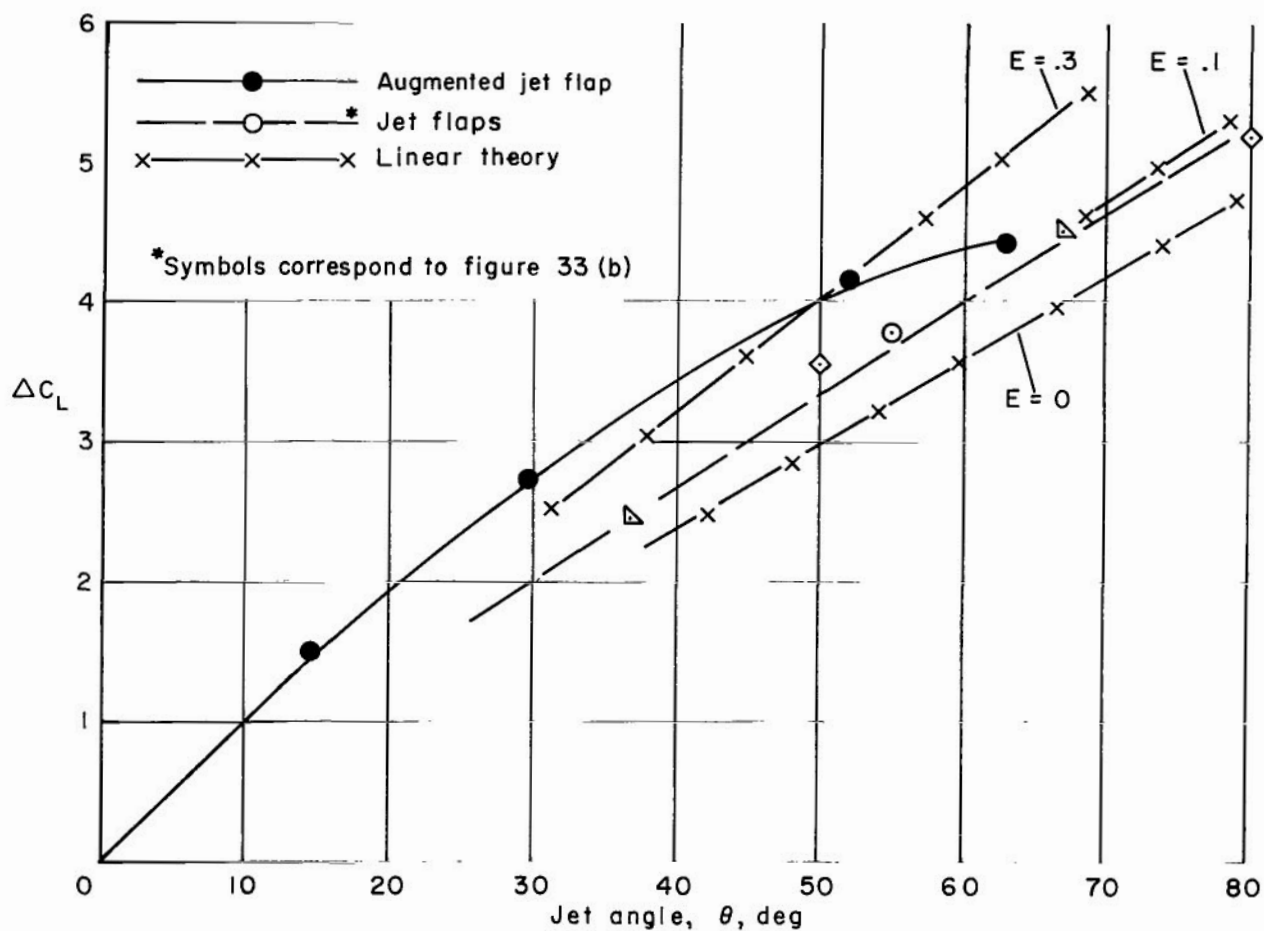


Figure 34.- Comparisons of the lift increments obtained with the augmented jet flap and basic jet flap configuration; values based on the present model geometry,  $C_J = 1.15$  based on jet reaction force.

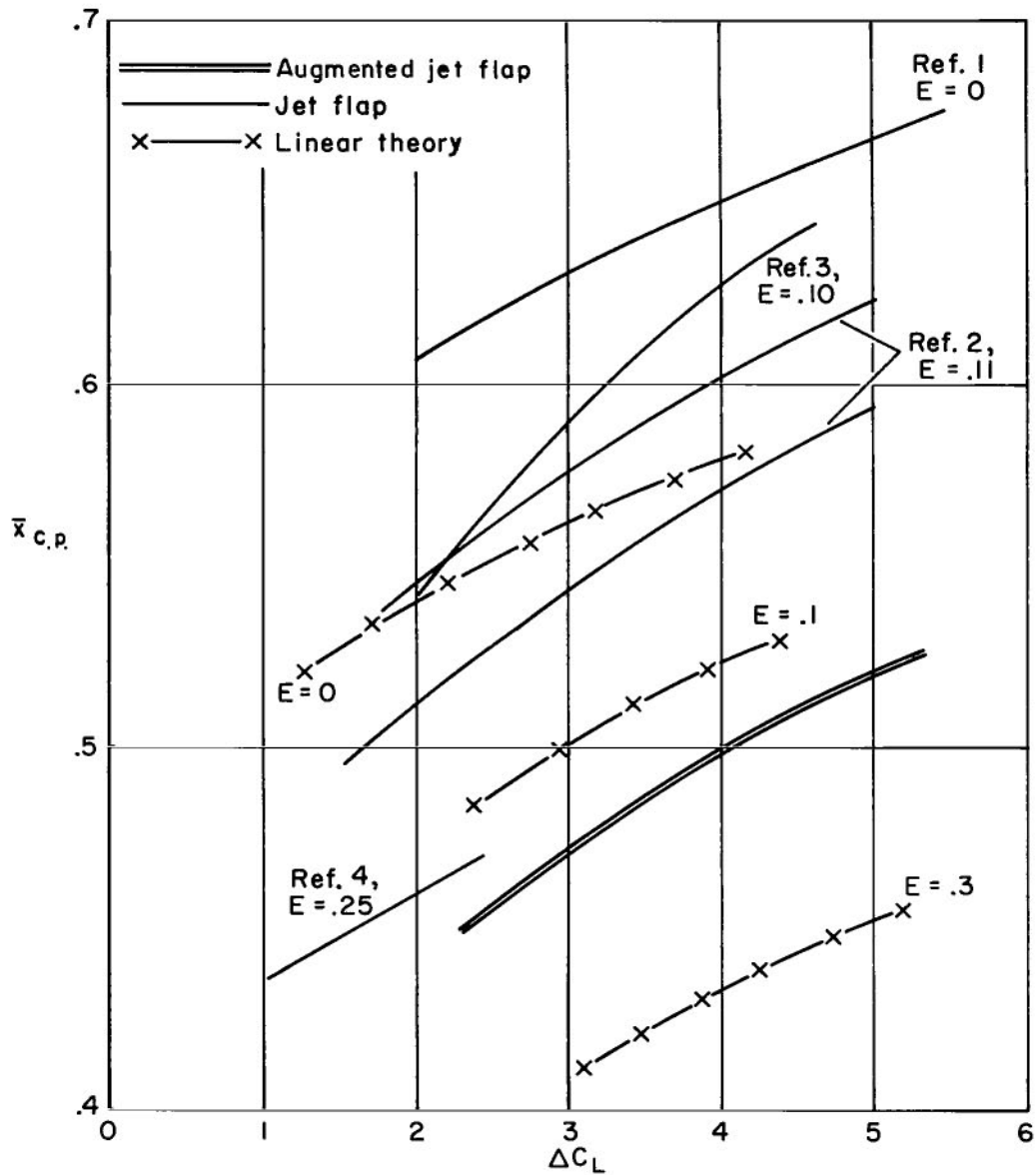


Figure 35.- Comparison of the center-of-pressure locations for the augmented jet flap and the jet flap;  $\alpha = 0^\circ$ ,  $\delta_f = 60^\circ$ .

FIRST CLASS MAIL

08U 001 26 51 3DS 68150 00903  
AIR FORCE WEAPONS LABORATORY/AFWL/  
KIRTLAND AIR FORCE BASE, NEW MEXICO 87117

ATT MISS MADELINE F. CANOVA, CHIEF TECHNICAL  
LIBRARY /W/ II /

MASTER: If Undeliverable (Section 15E  
Postal Manual) Do Not Return

*"The aeronautical and space activities of the United States shall be conducted so as to contribute . . . to the expansion of human knowledge of phenomena in the atmosphere and space. The Administration shall provide for the widest practicable and appropriate dissemination of information concerning its activities and the results thereof."*

— NATIONAL AERONAUTICS AND SPACE ACT OF 1958

## NASA SCIENTIFIC AND TECHNICAL PUBLICATIONS

**TECHNICAL REPORTS:** Scientific and technical information considered important, complete, and a lasting contribution to existing knowledge.

**TECHNICAL NOTES:** Information less broad in scope but nevertheless of importance as a contribution to existing knowledge.

**TECHNICAL MEMORANDUMS:** Information receiving limited distribution because of preliminary data, security classification, or other reasons.

**CONTRACTOR REPORTS:** Scientific and technical information generated under a NASA contract or grant and considered an important contribution to existing knowledge.

**TECHNICAL TRANSLATIONS:** Information published in a foreign language considered to merit NASA distribution in English.

**SPECIAL PUBLICATIONS:** Information derived from or of value to NASA activities. Publications include conference proceedings, monographs, data compilations, handbooks, sourcebooks, and special bibliographies.

**TECHNOLOGY UTILIZATION PUBLICATIONS:** Information on technology used by NASA that may be of particular interest in commercial and other non-aerospace applications. Publications include Tech Briefs, Technology Utilization Reports and Notes, and Technology Surveys.

*Details on the availability of these publications may be obtained from:*

SCIENTIFIC AND TECHNICAL INFORMATION DIVISION  
NATIONAL AERONAUTICS AND SPACE ADMINISTRATION  
Washington, D.C. 20546